Allosteric Logic of the *V. vulnificus* Adenine Riboswitch Resolved by Four-dimensional Chemical Mapping

Siqi Tian[1], Wipapat Kladwang[1], and Rhiju Das[1, 2, *]

[1]Department of Biochemistry, and [2]Department of Physics, Stanford University,
Stanford, California 94305, United States

* Corresponding Author. Phone: (650) 723 5976. E-mail: rhiju@stanford.edu

ABSTRACT

The structural logic that define the functions of gene regulatory RNA molecules may be radically different from classic models of allostery, but the relevant structural correlations have remained elusive in even intensively studied RNA model systems. Here, we present a four-dimensional expansion of chemical mapping called lock-mutate-map-rescue (LM^2R), which integrates multiple layers of mutation with nucleotide-resolution chemical mapping. This technique resolves the core mechanism of the adenine-responsive *V. vulnificus add* riboswitch including its gene expression platform, a paradigmatic system for which both Monod-Wyman-Changeux (MWC) conformational selection models and non-MWC alternatives have been proposed. To discriminate amongst these models, we locked each functionally important helix through designed mutations and assessed formation or depletion of other helices via high-throughput compensatory rescue experiments. These LM^2R measurements give strong support to the pre-existing correlations predicted by MWC models, disfavor alternative models, and reveal new structural heterogeneities that may be general across ligand-free riboswitches.

Keywords: riboswitch, allostery, conformational ensemble, compensatory mutagenesis, SHAPE, secondary structure, multidimensional chemical mapping.

INTRODUCTION

Conformational changes in RNA molecules are ubiquitous features of gene regulation in all living cells and viruses. Recent years have seen an explosion of discoveries of compact *cis*-acting mRNA elements that sense small molecules, proteins, and other RNAs and modulate transcriptional termination, ribosome recruitment, splicing, and other genetic events.[1-3] Beginning with classic work by Yanofsky and colleagues in the 1970s, these discoveries have been associated with elegant models of allostery in which each molecule interconverts between at least two conformational states.[4-6] In particular, the allostery is typically presumed to occur through Monod-Wyman-Changeux mechanisms (also called 'conformational selection' or 'population shift' models) [6-8]. In these pictures, ligand binding to an aptamer region of the RNA shifts a pre-existing equilibrium between strikingly different secondary structures, resulting in allosteric exposure or sequestration of another sequence-distal region harboring a ribosome binding site or other gene expression platform.[9-11] If these multiple structures could be determined in detail, they would each offer a potential new target for biological control and antibiotic development.[12]

Despite decades of work on RNA allostery, experiments directly testing the base pair correlations posited for specific systems have been difficult. A paradigmatic example is the *add* riboswitch, which has become a dominant model system for studying ligand-sensing riboswitches. This compact adenine-sensing element resides in the 5′ untranslated region (UTR) of the *add* adenosine deaminase mRNA of human pathogenic bacterium *Vibrio vulnificus*, and controls translation of the mRNA in response to adenine. Domains of this RNA have been subjected to nearly every *in vitro* biochemical and biophysical technique available, including time-resolved X-ray laser diffraction.[13-24] Almost all studies to date have assumed some variation of an MWC model of action.[15] Recently, however, a tour de force study, bringing together multidimensional NMR spectroscopy, NMR relaxation studies, designed model systems, and supporting measurements from stopped-flow and calorimetry techniques, revealed detailed single-nucleotide-resolution base pairing information and intriguing temperature dependences for the complex structural ensemble of the *add* riboswitch.[25] Although similar in some respects to previously proposed MWC models, the new model contradicted a standard MWC assumption[7-8, 26]: it proposes that, in the absence of adenine, riboswitches that sample the correct aptameric secondary structure do not also concomitantly open their ribosome binding sites and increase gene expression, as predicted by MWC conformational selection. Despite this fundamental distinction, the non-MWC model appears fully consistent with all available data, and it remains unclear what structural correlations, if any, underlie the allosteric logic of the *add* riboswitch. As

a reflection of current uncertainties in the system, the same group that first proposed an non-MWC model for the *add* RNA has recently revived the MWC framework to interpret newer single molecule measurements on the same system.[27]

To resolve the allosteric logic of the *add* riboswitch, we have developed a high-dimensional expansion of single-nucleotide-resolution chemical mapping (Figure 1). We previously showed that structural perturbations from mutating each nucleotide of an RNA could be read out at every other nucleotide through chemical mapping to give rich two-dimensional data sets and accurate blind predictions for RNAs with single, well-defined structures (mutate-and-map, M^2).[28-30] Expanding to three dimensions, testing compensating mutations at pairs of nucleotides through their effects on the reactivities of other nucleotides gave incisive evidence for specific base pairs (mutate-map-rescue, M^2R), again for molecules with single dominant structures.[31-32] Here, we expand the M^2R method to allow dissection of more complex ensembles involving numerous functionally important structures, taking advantage of a Bayesian framework and extensive simulations to connect experimental observables to underlying helix frequencies. By identifying 'lock' mutants that stabilize helices posited for each state, we infer how the presence of one helix enhances or suppresses the presence of other helices, through further rounds of M^2R on the mutant backgrounds (Figures 1A and B). This four-dimensional chemical mapping workflow (termed lock-mutate-map-rescue, LM^2R) resolves fundamental questions raised by the existing models of the *add* riboswitch and also exposes new ensemble properties that were not expected in prior models.

RESULTS

Inferring helix frequencies through quantitative compensatory rescue

Our key methodological innovation arose from attempts to more quantitatively analyze compensatory mutation experiments for RNA structure read out through chemical mapping (mutate-map-rescue, M^2R).[31-32] Briefly, if mutation of either side of a base pair (mutant A or mutant B) disrupts the reactivities at other nucleotides in the RNA, but the compensatory double mutation (mutant AB) restores the SHAPE reactivities to the wild type (WT) profile, these observations suggest that the two sites were base paired in the starting WT sequence. Our prior work assumed that such observed compensation would arise with negligible probability if the mutated nucleotides were not paired. To test this assumption and automate the protocol, we carried out simulations of these experiments and developed a quantitative 'rescue factor' metric that accurately recovered expert assessments from simulated and experimental data, including the

Tetrahymena ribozyme P4-P6 domain and a blind RNA-puzzle modeling challenge, the GIR1 lariat capping ribozyme (Methods & Supporting Results):

$$Rescue\ factor \equiv 1.0 - \frac{diff_{(WT,AB)}}{\max\left(diff_{(WT,A)}, diff_{(WT,B)}\right)} \quad , \qquad (1)$$

where the Euclidean difference *diff* between two SHAPE profiles *d* over probed nucleotides *i* = 1 to *N* is given by:

$$diff_{(A,B)} = \sqrt{\frac{1}{N}\sum_{i=1}^{N}(d_A - d_B)^2} \qquad (2)$$

These *in silico* tests confirmed that observation of strong rescue implies high helix frequency (Figure 1C) but unexpectedly also showed that modest rescue ratios could be informative. Values lower than one but greater than zero corresponded to 'partial' rescue, where the reactivities at some nucleotides revert to wild type (WT) values but others do not (Figure 1D, center). While individual base pair tests were noisy, averaging recue factors over tests on three or more base pairs gave values that showed a striking correlation with helix frequencies (Figure 1C). Furthermore, absence of rescue (rescue factor close to zero; Figure 1D, bottom) gave upper bounds on the helix frequency (Supporting Figure S1). To estimate uncertainties in these estimates, we used a Bayesian framework to derive posterior probabilities of each helix frequency given the observed rescue factor, calibrated based on these simulations. Below, we present cumulative distributions of these posterior probabilities in figures and tables (see also Supporting Figure S1); for ease of reading in the main text, we give simply median values of the helix frequency posterior probability distributions. We also developed a separate category-based classification to check that compensatory rescue of different base pairs within the same helix gave concordant results, and that automated analysis reproduced manual analysis (Supporting Results). These simulation and experimental studies suggested that compensatory rescue measurements, even ones that resulted in partial or no detectable rescue, could be used to estimate helix frequencies and uncertainties for those values, without relying on complex fits[16], though we sought more detailed tests, as described next.

The add riboswitch system

To test the applicability of M^2R helix frequency estimation to understanding complex RNA structural ensembles, we applied it to the paradigmatic *V. vulnificus add* adenine-sensing

riboswitch including its expression platform (Figure 2). On one hand, the NMR analysis of this system offered detailed data for validating or falsifying helix frequencies. On the other hand, that study and other analyses have revealed an unresolved but fundamental question in how the RNA's multiple structures give rise to function. There is currently no controversy about the riboswitch's adenine-bound state (termed *holo*; Figure 2A, right). Helices P1, P2, and P3 are formed in the 5´-UTR, defining an adenine binding aptamer at nucleotides 15-81, with a well-defined tertiary structure that has been determined through crystallography. Also, a linker including an additional hairpin (P5, nts 89–110) connects the aptamer to the Shine-Dalgarno sequence and AUG start codon (nts 112–122), which are open and available for ribosome recruitment. In the absence of adenine, all available models posit that the riboswitch forms a secondary structure ensemble dominated by a new P4 domain that pairs with the Shine-Dalgarno sequence and the AUG start codon (nts 112–122) with nucleotides that were originally part of P1 (nts 75–88, here called the 'switch region'[15], cross-hatched in Figure 2A, left). Concomitantly, the aptamer helices P1 and P2 are rearranged into an alternative structure. In keeping with the previous NMR study, these conformations with a rearranged adenine aptamer secondary structure are grouped into a state *apoB*. The major uncertainty regards what happens when adenine is not present but the RNA nevertheless samples a secondary structure poised to bind adenine, with P1, P2, and P3 formed. This state is termed *apoA*.

At 20–30 °C, several studies have estimated that the fraction of the riboswitch in the adenine-binding-ready *apoA* conformation occurs with a frequency of ~40% both *in vitro* and *in cellulo*.[13, 33] An MWC conformational selection model would assume that this thermally sampled state should have not only the same adenine aptamer secondary structure as adenine-bound *holo*, but also the same open Shine-Dalgarno conformation as the adenine-bound *holo*, without the P4 domain. That is, *apoA* should be ON, able to recruit ribosomes. A key prediction of the MWC conformational selection model is therefore an exact structural identity of the gene expression platform in the molecule's active configuration, whether sampled at thermal equilibrium (*apoA*) or stabilized by binding of ligands at the distal pocket (*holo*) (compare Figure 2A, center and right). (We note that the MWC model allows for local rearrangements in the aptamer binding pocket in going from *apoA* to *holo*, but these adenine-induced changes are not allowed to propagate to the gene expression platform, as the fixed stem P1 spatially separates the aptamer and the expression platform in either *apoA* and *holo*.)

At first glance, the NMR-informed portrait[25] is similar to the MWC conformational selection model, with high-population and low-population adenine-free states that display distinct structures incompatible and compatible with adenine binding (*apoB* and *apoA*), and a third adenine-bound state (*holo*) that is similar to the adenine-free *apoA*. However, the key feature[8] of the MWC conformational selection model is lost (Figure 2B). In the absence of ligand, the NMR measurements could not directly detect opening of the gene expression platform at low frequency in the absence of ligand, i.e., transient sampling of the ON conformation. While this lack of signal could be due to ambiguities in the NMR measurements, both ligand-free states *apoA* and *apoB* were interpreted to be OFF with respect to gene expression, in conflict with the MWC conformational selection model.[34] The new model, referred to as the 'non-MWC' model henceforth, suggests instead a mixed conformation for *apoA*, where a shortened P1, P2, and P3 form the adenine aptamer secondary structure but also some parts of the P4 domain (here denoted P4A and P4B) are retained, blocking the Shine-Dalgarno site, i.e., *apoA* should be mostly OFF. The non-MWC model does not explain how subsequent adenine binding to the aptamer of *apoA* might communicate through P1 to release the Shine-Dalgarno site and promote gene expression, raising the prospect of a radically different mechanism for allostery in RNA compared to classic MWC systems. Posed as a simple question, then: is apoA ON (MWC) or OFF (non-MWC)?

Before carrying out extensive mutagenesis and compensatory rescue experiments, we tested whether one-dimensional SHAPE profiling on the WT RNA might discriminate between MWC and non-MWC models (Figure 2 and SI Figure S3). In the absence of adenine, the *add* riboswitch SHAPE profile (Figure 2C) showed protections within the 'switch region', which is predicted to have pairings in both *apoA* and *apoB*, in both MWC and non-MWC models; other regions show variable levels of protection. Incubation with 5 mM adenine (Figure 2D) gave protections in the 5´-most aptamer region, consistent with formation of P1, P2, and P3, and RNA tertiary structure formation at and around the adenine binding pocket, as expected for the *holo* state. In addition, adenine-dependent increases in SHAPE reactivity in the expression platform, the Shine-Dalgarno ribosome binding site and the AUG codon (nts 112-122), supported the adenine-coupled opening of the expression platform that is the hallmark of riboswitch function (Figure 2D). Unexpectedly, in between these two regions, nucleotides 105-111 also modestly increased in SHAPE reactivity upon adenine binding, although, in both the MWC and non-MWC models, this segment is predicted to be sequestered into a P5 helix in all states (Figure 2). However, this observation can be accommodated into both the MWC and non-MWC models by assuming partial opening of P5

in the adenine-bound *holo* state (see Discussion, below) and therefore does not discriminate between the models.

Three-dimensional mutate-map-rescue recovers ensemble helix frequencies

We then tested if quantitative mutate-map-rescue (Figure 1) might confirm or contradict prior NMR results and enable discrimination between MWC and non-MWC models. We carried out M^2R method on the separate adenine-bound and adenine-free ensembles. Prior to rescue experiments, which involve double compensatory mutants, we systematically scanned single mutants of each nucleotide to its complement, followed by SHAPE profiling across the riboswitch, which gave the two-dimensional patterns in Figure 3. Automated analyses of these mutate-and-map (M^2) data to determine the dominant secondary structure and to infer an approximate structural ensemble supported both the MWC and non-MWC models but did not carry the precision to discriminate between them (Supporting Figure S4). Nevertheless, the M^2 data were suggestive. As expected for a multi-state RNA, several mutations produced dramatic perturbations across the SHAPE profile. Compared to the WT sequence, many of these mutants gave protections or enhancements in the 5´-most aptamer region of the riboswitch (nts 25-32) and concomitant exposures or protections (respectively) near the 3´ end of the riboswitch (nts 105-122), which included both the start codon and Shine-Dalgarno ribosome binding sequence (arrows, Figure 3A-B). Such correlations between structuring the aptameric region and opening the gene expression platform, even in the absence of ligand, qualitatively supported predictions of the MWC conformational selection model, but we sought stronger, quantitative tests through deeper mutational analysis.

Compensatory rescue experiments assessed helix frequencies in the presence and absence of adenine and quantitatively agreed with prior models (Figure 3E-F). First, in all prior models, the adenine-bound riboswitch (*holo*, Figure 2) was expected to display P1, P2, and P3 in the aptamer and P5. Indeed, in the presence of 5 mM adenine, SHAPE measurements for single and compensatory mutations targeting these helices and rescue factor analysis gave helix frequencies of 79%, 64%, 56% and 29%, respectively (Figure 3E,3G). Each of these cases showed visually striking rescue in their SHAPE profiles as mutations disrupted adenine binding, and compensatory mutations restored the adenine-bound profiles (Figure 3C, top ‘quartet’ of profiles); the lower helix frequency of P5 was consistent with its assumed partial opening, as noted with one-dimensional mapping. Measuring rescue factors for other tested helices, including P1B, P2B, P4A, P4B, and P4C predicted for the *apoB* state and numerous helices (P6, P7,

through P17; SI Figure S4) proposed to occur at low frequencies from M^2-guided modeling[16], gave no evidence for their presence. We derived upper bounds on these helices' frequencies of 16% or lower; in cumulative distributions of posterior probabilities, there was a clear separation from the high-frequency helices (Figure 3C, bottom quartet of profiles; Figures 3E-3G; SI Figure S5; and Table 1). In addition, we used a double-base-pair mutation scheme for M^2R, which induced stronger perturbations and rescuing effects, and supported the same pairings as above (SI Figure S6 and Table 2).

In addition to their predictions above for the adenine-bound state, all prior models of the *add* riboswitch expected the RNA to show a diverse set of helices in the absence of adenine, reflecting an admixture of *apoA* vs. *apoB*. Helices P3 and P5 are expected to be present at high frequencies, and both are detected by compensatory rescue experiments, with median helix frequencies of 73% and 75%, respectively (Figure 3F). In all prior models (Figure 2), other helices were predicted to be present at lower but significant frequencies. Compensatory rescue experiments recovered evidence for the *apoB*-specific helices P4A (48%), P1B (44%), and P2B (17%); the *apoA*-specific helices P1 (53%) and P2 (31%); and the *apoB* helices whose presence in *apoA* is under question, P4B (55%) and P4C (68%) (Figure 3D, 3F, 3H). As with the adenine-bound conditions, the double-base-pair M^2R results were consistent with the single-base-pair M^2R results (SI Figure S6). In addition, helices P6, P7, through P17 (SI Figure S5) again served as negative controls and gave low helix frequencies by compensatory rescue, as expected (pink cumulative distributions in Figure 3H; Table 1). In principle, the results for helices P4B and P4C could discriminate between the models under question (Figure 2A-B), as the non-MWC model predicts their frequencies to be close to 100%, while the MWC conformational selection model predicts their frequencies to be lower, in the same range as P4A (48%; compare yellow and blue cumulative distributions in Figure 3H). While the low helix frequency estimates favor the predictions from the MWC conformational selection model, remaining uncertainties in these values (broadness of probability distributions in Figure 3H; and Tables 1-2) precluded incisive discrimination between the models based purely on M^2R experiments with the WT *add* sequence, and we turned to the four-dimensional chemical mapping method that involves M^2R in mutational backgrounds that lock each riboswitch state.

Four-dimensional Lock-Mutate-Map-Rescue enables dissection of ensemble states

To stringently discriminate between the MWC and non-MWC models, we sought to measure the presence or absence of helices P4B and P4C in the *apoA* state, taking advantage of mutant backgrounds that 'lock' this state and the ability of quantitative compensatory rescue to estimate helix frequencies (lock-mutate-map-rescue, LM^2R). While our original single-mutant scan (Figure 3B and SI Figure S4) suggested several such mutants, we were concerned that their effects involved destabilizing the P4 domain and might bias our measurements towards favoring the MWC model. Instead, we took advantage of mutations outside P4 that stabilized P1 or P2, components of the aptamer secondary structure that define *apoA* in all available models. A number of double-base-pair compensatory mutants for P1 and P2 exhibited SHAPE profiles that agreed well with each other (Figure 4A), supporting their use as mutant backgrounds for isolating *apoA*. We noted that all of these *apoA*-stabilizing mutants exhibited increased reactivity in the expression platform region (nts 105-122) relative to the adenine-free WT RNA, at a level comparable to the adenine-bound WT RNA (Figure 4A); this observation already suggested that *apoA* is similar to *holo* in this region, favoring the MWC model over the non-MWC model. We also observed similarities in the gene expression platform between these adenine-free *apoA*-stabilizing mutants and adenine-bound WT RNA with other chemical modifiers (dimethyl sulfate, glyoxal, ribonuclease V1, terbium(III), and ultraviolet irradiation at 302 nm; SI Figure S7).

We selected two mutants for lock-mutate-map-rescue probing *apoA*: lock-P1 (A19C, U20G, A76C, U77G) and lock-P2 (U28G, A29C, U41G, G42C). As a consistency check, we confirmed that compensatory rescue gave a strong P1 helix frequency (72%) when P2 was locked. Similarly, compensatory rescue targeting P2 gave a significant helix frequency **(**42%**)** when P1 was locked (Figure 4C, SI Figure S8, and Table 2). As a further check, both models under question predicted the absence of P4A in *apoA*; indeed, in either the lock-P1 or lock-P2 background, we did not detect compensatory rescue targeting P4A, and could set an upper bound on its frequency of 4%. Finally, we tested the helix frequency of P4B, which was predicted to be absent (0%) in *apoA* by the MWC model and present (100%) in the non-MWC model (Figure 2A). We saw no evidence for compensatory rescue of P4B in either *apoA*-stabilizing background. Measurements in the lock-P1 background and in the lock-P2 background gave P4B helix frequencies of 4%, in both cases (Figure 4C; and compare blue and yellow curves in Figure 4E). Separate experiments on a variant MutP2 (A29C, A30G, U40C, U41G) used to stabilize *apoA* in prior studies[25] similarly gave no evidence for P4B (SI Figure S9, Table 3). Taken together, these measurements provided strong evidence against the non-MWC model and favor the MWC model.

To further dissect the adenine-free *add* riboswitch ensemble, we selected analogous mutant backgrounds that stabilized *apoB*, based on double-base-pair mutants used to stabilize P1B (U17G, C18G, G43C, G44C) and P4A (U77G, G78C, C119G, A120C) (Figure 4B). For the lock-P1B mutant, compensatory-rescue experiments confirmed the helices expected in *apoB* by both the MWC and non-MWC models (P2B, P4A, and P4B at 53%, 55%, and 80%, respectively; Figure 4F). Experiments with the lock-P4A mutant also gave the expected rescue for P4B (55%) but, unexpectedly, not for P1B or P2B (6% or 9%). The latter results suggest previously undetected conformational heterogeneity in the aptamer region in *apoB* (Figure 4D, Supporting Results). Further supporting the inability to trap *apoB* by locking any single helix, the reactivity profiles of lock-P4A and lock-P1B were distinct (Figure 4B).

As an independent test of the helix content in *apoA* vs. *apoB*, we carried out a 'flipped' lock-mutate-map-rescue experiment compared to the experiments above. Rather than locking P1 and P2 and assessing the presence of P4B, we locked P4B and assessed the presence of P1 and P2. In the MWC model (Figure 2A), a P4B-stabilizing mutant background should isolate *apoB*, and give no compensatory rescue for P1 and P2. In the non-MWC model (Figure 2B), where P4B is common to both the *apoA* and *apoB*, the P4B-stabilizing mutant background should give the same results as the WT RNA, and give partial compensatory rescue for P1 and P2. In fact, the P4B-stabilizing background (lock-P4B; U82G, C83G, G115C, A116C) gave a SHAPE profile better matching the *apoB*-stabilizers than the WT RNA sequence, favoring the MWC model over the non-MWC model. Furthermore, compensatory rescue experiments in the lock-P4B background showed no rescue for P1 and P2 (median helix frequencies estimated at 5% and 6%, respectively), again favoring the MWC model over the non-MWC model (SI Figure S10).

DISCUSSION

Four-dimensional chemical mapping for complex RNA ensembles

Complex secondary structure ensembles underlie many, and perhaps most, RNA regulatory elements. Understanding how a panoply of structures underlies the allosteric logic of these elements requires assessing not just the frequencies of different helices in the RNA structural ensemble but how the presence of one helix enhances or suppresses the frequency of others. Four-dimensional chemical mapping offers an experimental route to this information that is unique in its high throughput and use of standard equipment (capilly electrophoretic sequencers). The strategy (Figure 1) is to 'lock' one helix into place through mutations (dimension 1) and to then introduce mutations elsewhere (dimension 2). Perturbation of the chemical mapping profile at

other nucleotides (dimension 3) provides evidence of involvement by the mutated nucleotide in RNA structure, perhaps a second helix. If compensatory mutation of a candidate partner in the second helix (dimension 4) then gives no, partial, or complete rescue of the mapping profile, the frequency of the second helix can be inferred to be low, medium, or high, with uncertainties estimated from simulation. The current throughput of PCR assembly and capillary electrophoretic sequencing enables single-nucleotide-resolution mapping of many hundreds of variants per experiment at the signal-to-noise needed for this four-dimensional lock-mutate-map-rescue (LM^2R) workflow. With this throughput, dissection of the co-occurrence or exclusivity of variable helices underlying a 100 to 200 nucleotide RNA domain becomes feasible.

Resolving the core mechanism of a paradigmatic riboswitch

This work demonstrates application of four-dimensional chemical mapping to resolve a fundamental biochemical question. Applying the methodology to the *add* riboswitch from *V. vulnificus* gives the model shown in Figure 5, consistent with a Monod-Wyman-Changeux-like 'standard model' of allostery rather than a non-MWC revision proposed after detailed NMR experiments. The two models differed in one core aspect: how ligand sensing in an aptamer region is allosterically communicated to expose a ribosome binding site and turn on *add* mRNA gene expression (Figure 2). Early M^2 experiments showed that, even in the absence of adenine, mutations that gave protections in the 5′ region of the *add* riboswitch also gave exposures in the 3′ region including the ribosome binding site (Figure 3A). Furthermore, different mutants that locked the correct adenine secondary structure without adenine exhibited SHAPE data that were indistinguishable from the adenine-bound riboswitch in the gene expression platform and, more broadly, at all nucleotides downstream of the aptamer region (Figure 4A-B). The most incisive analysis came from LM^2R. In experiments locking P1 and P2, which are specific to the aptameric secondary structure, the rescue data give evidence against the formation of P4 helices that would sequester the ribosome binding site. In other words, the *add* gene expression platform is ON when the sequence-separate aptamer region is folded even in the absence of the adenine ligand (Figure 2; Figure 5, *apoA*). Conversely, LM^2R experiments locking P1B, P4A, or P4B turn the riboswitch OFF and give evidence against the formation of P1 and P2 helices.

These data favor anti-correlation between aptamer secondary structure formation and structures sequestering the ribosome binding site even without adenine binding, as predicted in the MWC conformational selection model, and disfavor a non-MWC revision that omits this coupling (compare Figure 2A and Figure 2B). Stated differently, allosteric communication of the aptameric

region and the gene expression platform is an intrinsic property of the folding landscape of the *add* riboswitch sequence that can be established without adenine. A simple conceptual understanding of this property involves considering a "switch region"[15] (nucleotides 75–81, Figure 5) that is able to form base pairs with nucleotides at the 5′ end of the RNA (anti-switch region) but is also able to form pairs (in P4A) with four nucleotides in the Shine-Dalgarno ribosome binding site at the 3′ end of the untranslated region (SD, Figure 5). Depending on whether the former or latter pairing is 'chosen' by the switch region, the RNA either closes the P1 helix of the aptamer secondary structure (P1) or closes the P4 domain that sequesters the ribosome binding site. As noted above, despite its similarity to MWC allosteric mechanisms for proteins, this model for the *add* riboswitch shows much more dramatic changes in structure than is typically seen in protein allostery, where conformational shifts typically preserve secondary structure [8, 26].

Comparison to prior data and proposals

The model in Figure 5 is consistent with all data collected in this study as well as all measurements on the *V. vulnificus add* riboswitch published to date. First, a number of prior studies applied techniques that do not directly read out base pairing but are sensitive to ligand binding and can quantify energetics and kinetics. Functional measurements *in vitro* and *in vivo*, use of fluorescent reporters, and single-molecule force experiments all have given *apoA* frequencies of ~40% at 20–30°C. [13-23, 33] Second, X-ray crystallographic studies have been limited to constructs with just the aptameric region[24, 35-42]; these structures all show P1, P2, and P3 helices, in accord with Figure 5. Third, the detailed NMR measurements that suggested the alternative *apoA* (Figure 2B) were also consistent with the *apoA* base pairings in the MWC model (Figure 2A): nuclear Overhauser effect (NOE) spectroscopy unambiguously established that pairings in both P1 and P4A occur in the absence of adenine, but could not infer whether these helices might co-occur or be mutually exclusive (Figure 2A-B). Fourth, analogous to our locking approach, the NMR study used a variant MutP2 (A29C, A30G, U40C, U41G) to stabilize the aptamer secondary structure. While our chemical mapping measurements suggest that this mutant only partially stabilizes P2 (SI Figure S5), both the NMR study and our LM^2R measurements detect P1 and no P4A in this background (SI Figure S9), supporting the MWC model in Figure 5. Fifth, our SHAPE and multi-probe chemical mapping data suggest partial opening of P5 in *apoA* and *holo* (Figure 2G-H), and our LM^2R analysis suggests only partial formation of P2 in *apoA* (Figure 3E) and partial formation of P2B in *apoB* (Figure 3F). These observations are again consistent with NMR studies which could unambiguously detect P5 and precisely measure

relative frequencies of, e.g., P2 vs. P2B, but could not establish these helices' absolute frequencies. Sixth, newer single molecule FRET measurements detect transient formation of the L2/L3 tertiary contact prior to adenine binding in *apoA* and stabilization upon adenine binding to *holo* [27]. These data are consistent with, and indeed were interpreted within, an MWC framework in which formation of the aptameric secondary structure occurs in concert with opening of the gene expression platform, even without adenine to shift the equilibrium in favor of the 'ON' state. Seventh, the prior detailed NMR analysis led to a compelling non-MWC model of riboswitch temperature robustness that involves compensating the improving affinity of the aptamer for adenine at colder temperatures by a pre-equilibrium that favored *apoB* over *apoA* at those temperatures. Although the precise predictions of the switching efficiencies of this model are affected by the interpretation of whether *apoA* is ON or OFF, approximately the same temperature compensation occurs in the MWC conformational selection model of Figure 5 (SI Figure S11).

There is now concordance across numerous measurements for an MWC model that posits strong secondary structure similarities between *apoA* and *holo*. We also propose herein that further heterogeneity is likely to be present in *apoB*, the 'OFF' state, as LM^2R measurements with different helix stabilizers gave different results for this state, suggesting incomplete correlation of the tested 'signature' helices (P1B and P4A). Numerous alternative secondary structures are possible for this state (see, e.g., SI Figure S4). The presence of these myriad helices, each at low population, would explain their detection difficulty with this and prior bulk equilibrium techniques but their appearance in single-molecule measurements.[19] Supporting this picture, higher-order M^2 analysis in single mutant backgrounds (SI Figure S12) isolate and confirm numerous alternative *apoB* structures. We note that there are no functional reasons for *apoB* to maintain a single secondary structure – it simply has to disallow adenine binding while keeping the gene expression platform closed in P4. Without selection for a pure single structure, we therefore suggest that *apoB* has remained structurally heterogeneous, and the exact populations of its helix pairings outside P4 may shift in different solution conditions and flanking sequences while still being consistent with riboswitch function. We further speculate that 'non-functional' states of other riboswitches and RNA gene regulatory modules may have highly heterogeneous structures and, indeed, this feature might explain why those states have been refractory to conventional structural biology approaches developed primarily to dissect protein structure/function. This picture also implies that antibiotics targeting any specific *apo* structure of the *add* and other riboswitches are unlikely to succeed, as single mutations that disrupt the

targeted structure while still maintaining the *apo* ensemble should be easy to find and would offer resistance.

General applicability of 4D RNA chemical mapping

The next challenge for understanding riboswitches and other *cis*-regulatory RNA elements is to test how the structural ensembles defined through *in vitro* studies are retained or altered by co-transcriptional effects, protein binding, helicases, crowding, noise due to low numbers of molecules, and other complexities of these molecules' native biological environments.[32, 43] Amongst available biochemical and biophysical techniques, chemical mapping methods read out by sequencing have unusual promise in delivering single-nucleotide-resolution structural information in such environments. As techniques improve to edit genomes across organisms and to amplify and measure chemical mapping signals *in cellulo*, the lock-mutate-map-rescue approach developed here offers the possibility of dissecting complex structural ensembles for these shape-shifting molecules.

ACKNOWLEDGMENTS

We thank M. Ali, S. Doniach, and C. VanLang for early discussions and experiments on the *add* riboswitch. We thank Drs. H. Schwalbe and B. Fürtig for personal communication regarding temperature compensation and NMR analysis and sharing a manuscript before publication. We acknowledge financial support from NIH R01 GM102519 (to R.D.).

METHODS

RNA Synthesis and Construct Design

Double-stranded DNA templates were prepared by PCR assembly of DNA oligomers with maximum length of 60 nt ordered from IDT (Integrated DNA Technologies). DNA templates contain a 20-nt T7 RNA polymerase promoter sequence (TTCTAATACGACTCACTATA) on the 5´ end and a 20-nt Tail2 sequence (AAAGAAACAACAACAACAAC) on the 3´ end. The sequence of interest is flanked by one hairpin with single-stranded buffering region on each end.[44] The primer assembly scheme and plate orders for all constructs were automatically designed by Primerize-2D.[45]

PCR reactions, including 100 pmol of terminal primers and 1 pmol of internal primers were carried out as previously described. PCR products were purified using Ampure XP magnetic beads (Agencourt) on a 96-well microplate format following manufacturer's instructions. DNA

concentrations were measured on a Nanodrop 1000 spectrophotometer (Thermo Scientific). *In vitro* transcription reactions were described previously, followed by similar purification (using Ampure XP beads with externally added 10% PEG-8000) and quantification steps.

Chemical Modification

M^2, M^2R and LM^2R chemical mapping were carried out in 96-well format as described previously [29, 31]. Prior to chemical modification, 1.2 pmol of RNA was heated to 90 °C for 2 min and cooled on ice for 2 min to remove secondary structure heterogeneity, then folded for 20 min at 37 °C in 15 µL of 10 mM $MgCl_2$, 50 mM Na-HEPES pH 8.0 (with or without 5 mM adenine). RNA was modified by adding 5 µL of freshly made SHAPE reagent, 5 mg/mL 1M7 (1-methyl-7-nitroisatoic anhydride) dissolved in anhydrous DMSO. Modification reactions were incubated at room temperature for 12 min and then quenched by 5 µl of 0.5 M Na-MES pH 6.0. Quenches also included 1 µL of poly(dT) magnetic beads (Ambion) and 0.065 pmol of FAM-labeled Tail2-A20 primer for reverse transcription. Samples were separated using magnetic stands, washed thoroughly with 70% ethanol, and air-dried. Beads were resuspended in 5.0 µL reverse transcription mix with SuperScript III (Thermo Fisher), then incubated at 48 °C for 30 min. RNAs were degraded by adding 5 µL 0.4 M NaOH and incubating at 90 °C for 3 min. Solutions were cooled down on ice then neutralized with 3 µL acid quench (1.4 M NaCl, 0.6 M HCl, and 1.3 M Na-acetate). Fluorescent labeled cDNA was recovered by magnetic bead separation, rinsed 70% ethanol, and air-dried. The beads were resuspended in 10 µL Hi-Di formamide (Applied Biosystems) with 0.0625 µL ROX-350 ladder (Applied Biosystems) and eluted for 20 min. The eluants were loaded onto capillary electrophoresis sequencers (ABI3100 or ABI3730).

Multi-probe chemical mapping was performed with procedures similar to SHAPE chemical mapping, with variations in the modification and quench steps. Specific preparations were as follows: 1% dimethyl sulfate (DMS), mixing 1 µL 10.5 M DMS into 9 µL ethanol, and then 90 µL doubly deionized water (ddH_2O); 0.4% glyoxalin, dilution to 1/100x of 8.8 M glyoxal; RNase V1, serial dilution to 1/1000x in storage buffer (50% glycerol, 50 mM Tris-HCl pH 7.4, 100 mM NaCl, 0.1 mM EDTA); Terbium(III), 4 mM $TbCl_3$ in ddH_2O; FMN, 2 mM flavin mononucleotide in ddH_2O. Volumes of 5 µL of these modifier stocks were added to folded RNA solution for 12 min, except for UV treatment, in which samples were exposed directly under a hand-held 302-nm UV lamp for 3 min. FMN phot oxidation reactions were placed on a visible-light box during the entire 12 min reaction. Modifications were quenched by 5 µL of 2-mercaptoethanol for 1M7,

DMS, glyoxal and RNase V1; 72 mM EDTA for Terbium(III); or ddH_2O (and removal of light source) for 'no mod' controls, FMN, and UV.

CE Data Processing

The Hit RACE 2.0 software was used to analyze CE (capillary electrophoresis) data.[46-48] Electrophoretic traces were aligned and baseline subtracted using linear and non-linear alignment routines as previously described.[44] Sequence assignment was accomplished semi-automatically with human supervision. Band intensities were obtained by fitting profiles to Gaussian peaks and integrating. Normalization, correction for signal attenuation, and background subtraction were enabled by inclusion of referencing hairpin loop residues (GAGUA) at both 5′ and 3′ ends, 10x dilution replicates, and no-modification controls. Briefly, true values for saturated peaks were obtained from 10x dilutions. Signal attenuation was corrected from 5′ to 3′ ends based on the relative reactivity between 5′ and 3′ referencing hairpin loop intensities.[44] Reactivities of SHAPE profiles were normalized against GAGUA, while other modifiers in multi-probe mapping were normalized to subsets of GAGUA which are reactive to that particular modifier.

Data Deposition

All chemical mapping datasets, including M^2, M^2R, LM^2R and multi-probe mapping, have been deposited at the RNA Mapping Database (http://rmdb.stanford.edu)[49] under the following accession codes: ADD140_1M7_0001, ADD140_1M7_0002, ADD140_1M7_0003, ADD140_1M7_0004, ADD140_1M7_0005, ADD140_1M7_0006, ADD140_1M7_0007, ADD140_1M7_0008, ADD140_1M7_0009, ADD140_1M7_0010, ADD140_1M7_0011, ADD140_1M7_0012, ADD140_1M7_0013, ADD140_1M7_0014, ADD140_RSQ_0001, ADD140_RSQ_0002, ADD140_RSQ_0003, ADD140_RSQ_0004, ADD140_LCK_0001, ADD140_LCK_0002, ADD140_LCK_0003, ADD140_LCK_0004, ADD140_LCK_0005, ADD140_LCK_0006, ADD71_STD_0001, ADD128_STD_0001, ADD140_STD_0001, ADD140_DCP_0001, ADD140_DCP_0002, RNAPZ5_RSQ_0001, TRP4P6_RSQ_0001, 16SFWJ_RSQ_0001.

LEGENDS

Table 1. Helix frequency estimate results for single base-pair M^2R

Median helix frequencies from Rfam simulations are reported along with 90% confidence range from the same bin. The rescue factor for each helix is averaged across all tested base pairs.

Table 2. Helix frequency estimate results for double base-pair M^2R.

Median helix frequencies from Rfam simulations are reported along with 90% confidence range from the same bin. The rescue factor for each helix is averaged across all tested base pairs.

Table 3. Helix frequency estimate results for LM^2R constructs and MutP2 from previous study.

Median helix frequencies from Rfam simulations are reported along with 90% confidence range from the same bin. The rescue factor for each helix is averaged across all tested base pairs.

Figure 1. Schematic of four-dimensional chemical mapping for RNA structural ensembles, the lock-mutate-map-rescue (LM^2R) method.

(A) Secondary structure ensemble is dissected by locking one helix in place by double base-pair mutations (green circles). The co-existence of a helix in question (cyan line) is then tested by single base-pair mutations (red circles) M^2R in the locked ensemble.

(B) Base-pairing probability plot and example quartet of LM^2R result. Positions of locked mutations and M^2R pair are marked by horizontal and vertical lines. The helix frequency estimate is colored in gray scale. An example SHAPE profile quartet shows the perturbations and rescue effects.

(C) Correlation of observed rescue factor against helix frequency for helices predicted with length longer than 2-bp from 325 Rfam families mutated and folded *in silico*. Each data point represents a helix whose rescue factor and simulated helix frequency has been averaged across all its base-pairs. Helices are colored by their length. The rescue factor estimates the extent of similarity restored in a double mutant's reactivity compared to WT (wild type), scaled by perturbations observed in single mutants.

(B) In silico M^2R quartets illustrating full compensatory rescue (high rescue factor), partial rescue (mid rescue factor) and no rescue (low rescue factor).

Figure 2. MWC and non-MWC model of *add* riboswitch.

(A-B) In both models, *apoB* state (left) is OFF (Shine-Dalgarno sequence and start codon sequestered) and also incompetent for ligand binding due to the aptamer's rearrangement. The ligand-bound state *holo* (right) is ON with Shine-Dalgarno sequence and AUG codon (gene

expression platform) exposed. The *apoA* state (center), defined as the conformations with an aptamer fold ready for ligand binding, differ in the two models. In the Monod-Wyman-Changeux model (*A*), *apoA* is assumed to be ON, with a similar expression platform to *holo*, while in the non-MWC model proposed in an NMR study (*B*), the *apoA* state is proposed to be OFF, with the expression platform sequestered into helices P4B and P4C. *(C-D)* One-dimensional SHAPE reactivity of *add* construct (nts 13-140) in the absence or presence of ligand 5 mM adenine. (*A-D*) Locations of helices in the MWC and non-MWC models are marked as follows: For the aptamer domain, OFF-state helices are P1B and P2B (blue); ON-state helices are P1 and P2 (gold). For the expression platform, OFF-state helices are P4A-C (blue). Helices P3 and P5 (brown) are shared across all models. The switch region, anti-switch region, Shine-Dalgarno sequence and AUG codon are labeled by the same patterns in *(A-D)*.

Figure 3. Mutate-map-rescue (M^2R) evaluates ensemble helix frequency in 5 mM adenine (A,C,E,G) and no adenine (B,D,F,H).
(A-B) Mutate-and-map (M^2) datasets of *add* riboswitch. Mutants that show anti-correlation of SHAPE reactivity pattern in the aptamer domain and expression platform are marked by the orange arrows. *(C-D)* Representative *in vitro* M^2R quartets of helices P1 and P4A. In each quartet, four SHAPE profiles are shown from left (5´) to right (3´): WT, mutant A, mutant B, and compensatory double mutant AB. Flanking sequences used for SHAPE reactivity normalization are not shown. *(E-F)* Base-pairing probability plot of single base-pair M^2R on *add* riboswitch. Expected helix frequencies (100% *holo* for 5 mM adenine; 60% *apoB* + 40% *apoA* for no adenine) are shown in the bottom-left half, and helix-wise estimates by M^2R are shown in the top-right half. *(G,H)* Cumulative distributions of posterior probabilities of each helix frequency, given measured rescue factors.

Figure 4. Lock-mutate-map-rescue (LM^2R) dissects helix frequency in locked ensemble.
(A-B) One-dimensional SHAPE reactivity of lock-P1, lock-P2, lock-P4A and lock-P1B constructs compared to WT in the absence of ligand adenine. Targeting the *apoA* state, lock-P1 and lock-P2 exhibited similar SHAPE reactivity profiles (except for partial opening in P2 region of lock-P1), and show higher reactivity in the expression platform compared to WT. Targeting the *apoB* state, lock-P4A and lock-P1B also exhibited similar reactivity patterns (except for partial opening in P1B region and more stringent protection of the expression platform in lock-P4A) and gave lower reactivities in the expression platform compared to WT.

(C) Base-pairing probability plot of LM^2R tests in lock-P1 and lock-P2 constructs. Compensatory rescue in either lock background recover high frequencies for helices P1 and P2 but not for P4A and P4B.
(D) Base-pairing probability plot of LM^2R tests in lock-P4A and lock-P1B constructs. Compensatory rescue experiments for P4A and P4B give high helix frequency in either lock background but not for P1 and P2. In lock-P4A, helices P1B and P2B have low helix frequency as well, suggesting heterogeneity in aptamer domain folding in the absence of ligand. Helices locked in place are highlighted by green boxes; helices not tested herein are in dashed boxes.
(E,F) Cumulative distributions of posterior probabilities of each helix frequency, given measured rescue factors, in each of the four locked-helix backgrounds.

Figure 5. Current model for the *add* structural ensemble.
The proposed model favors the MWC model of allostery. Sampling of the aptamer secondary structure in the absence of ligand (*apoA*) correlates with opening of the P4 domain and gene expression, analogous to ligand-bound *holo*. The ligand-free *apoB* state sequesters the Shine-Dalgarno sequence and AUG codon in the P4 domain, precluding gene expression. Our measurements and other studies are consistent with additional alternative structures in the *apoB* state (dashed blue lines) and stabilization of the aptamer through coupled tertiary contacts upon adenine binding in the *holo* state (solid yellow lines).

REFERENCES

1. Henkin, T. M., Riboswitch RNAs: Using RNA to sense cellular metabolism. *Genes Dev.* **2008,** *22* (24), 3383-3390.
2. Nudler, E.; Mironov, A. S., The riboswitch control of bacterial metabolism. *Trends Biochem. Sci.* **2004,** *29* (1), 11-17.
3. Gesteland, R. F.; Cech, T.; Atkins, J. F., *The RNA world : The nature of modern RNA suggests a prebiotic RNA world*. 3rd ed.; Cold Spring Harbor Laboratory Press: Cold Spring Harbor, N.Y., 2006; p xxiii, 768 p.
4. Yanofsky, C., Transcription Attenuation: Once Viewed as a Novel Regulatory Strategy. *Journal of Bacteriology* **2000,** *182* (1), 1-8.
5. Gutiérrez-Preciado, A.; Henkin, T. M.; Grundy, F. J.; Yanofsky, C.; Merino, E., Biochemical Features and Functional Implications of the RNA-Based T-Box Regulatory Mechanism. *Microbiology and Molecular Biology Reviews* **2009,** *73* (1), 36-61.
6. Monod, J.; Wyman, J.; Changeux, J.-P., On the nature of allosteric transitions: A plausible model. *Journal of Molecular Biology* **1965,** *12* (1), 88-118.
7. Gunasekaran, K.; Ma, B.; Nussinov, R., Is allostery an intrinsic property of all dynamic proteins? *Proteins* **2004,** *57* (3), 433-43.
8. Changeux, J. P.; Edelstein, S. J., Allosteric mechanisms of signal transduction. *Science* **2005,** *308* (5727), 1424-8.

9. Fernández-Luna, M. T.; Miranda-Ríos, J., Riboswitch folding: One at a time and step by step. *RNA Biol.* **2008,** *5* (1), 20-23.
10. Gilbert, S. D.; Batey, R. T., Riboswitches: Fold and function. *Chem. Biol.* **2006,** *13* (8), 805-807.
11. Breaker, R. R., Riboswitches and the RNA world. *Cold Spring Harb. Perspect. Biol.* **2012,** *4* (2), a003566.
12. Jones, C. P.; Ferre-D'Amare, A. R., Long-Range Interactions in Riboswitch Control of Gene Expression. *Annu Rev Biophys* **2017,** *46*, 455-481.
13. Lemay, J.-F.; Desnoyers, G.; Blouin, S.; Heppell, B.; Bastet, L.; St-Pierre, P.; Massé, E.; Lafontaine, D. A., Comparative study between transcriptionally- and translationally-acting adenine riboswitches reveals key differences in riboswitch regulatory mechanisms. *PLoS Genet.* **2011,** *7* (1), e1001278.
14. Mandal, M.; Breaker, R. R., Adenine riboswitches and gene activation by disruption of a transcription terminator. *Nat. Struct. Mol. Biol.* **2004,** *11* (1), 29-35.
15. Batey, R. T., Structure and mechanism of purine binding riboswitches. *Q. Rev. Biophys.* **2012,** *45* (3), 345-381.
16. Cordero, P.; Das, R., Rich structure landscapes in both natural and artificial RNAs revealed by mutate-and-map analysis. *PLoS Comput. Biol.* **2015,** *11* (11), e1004473.
17. Stoddard, C. D.; Widmann, J.; Trausch, J. J.; Marcano-Velázquez, J. G.; Knight, R.; Batey, R. T., Nucleotides adjacent to the ligand-binding pocket are linked to activity tuning in the purine riboswitch. *J. Mol. Biol.* **2013,** *425* (10), 1596-1611.
18. Rieder, R.; Lang, K.; Graber, D.; Micura, R., Ligand-induced folding of the adenosine deaminase A-riboswitch and implications on riboswitch translational control. *ChemBioChem* **2007,** *8* (8), 896-902.
19. Neupane, K.; Yu, H.; Foster, D. A. N.; Wang, F.; Woodside, M. T., Single-molecule force spectroscopy of the add adenine riboswitch relates folding to regulatory mechanism. *Nucleic Acids Res.* **2011,** *39* (17), 7677-7687.
20. Lemay, J.-F.; Penedo, J. C.; Tremblay, R.; Lilley, D. M. J.; Lafontaine, Daniel A., Folding of the adenine riboswitch. *Chem. Biol.* **2006,** *13* (8), 857-868.
21. Greenleaf, W. J.; Frieda, K. L.; Foster, D. A. N.; Woodside, M. T.; Block, S. M., Direct observation of hierarchical folding in single riboswitch aptamers. *Science* **2008,** *319* (5863), 630-633.
22. Wickiser, J. K.; Cheah, M. T.; Breaker, R. R.; Crothers, D. M., The kinetics of ligand binding by an adenine-sensing riboswitch. *Biochemistry* **2005,** *44* (40), 13404-13414.
23. Lemay, J.-F.; Lafontaine, D. A., Core requirements of the adenine riboswitch aptamer for ligand binding. *RNA* **2007,** *13* (3), 339-350.
24. Stagno, J. R.; Liu, Y.; Bhandari, Y. R.; Conrad, C. E.; Panja, S.; Swain, M.; Fan, L.; Nelson, G.; Li, C.; Wendel, D. R.; White, T. A.; Coe, J. D.; Wiedorn, M. O.; Knoska, J.; Oberthuer, D.; Tuckey, R. A.; Yu, P.; Dyba, M.; Tarasov, S. G.; Weierstall, U.; Grant, T. D.; Schwieters, C. D.; Zhang, J.; Ferre-D'Amare, A. R.; Fromme, P.; Draper, D. E.; Liang, M.; Hunter, M. S.; Boutet, S.; Tan, K.; Zuo, X.; Ji, X.; Barty, A.; Zatsepin, N. A.; Chapman, H. N.; Spence, J. C.; Woodson, S. A.; Wang, Y. X., Structures of riboswitch RNA reaction states by mix-and-inject XFEL serial crystallography. *Nature* **2017,** *541* (7636), 242-246.
25. Reining, A.; Nozinovic, S.; Schlepckow, K.; Buhr, F.; Furtig, B.; Schwalbe, H., Three-state mechanism couples ligand and temperature sensing in riboswitches. *Nature* **2013,** *499* (7458), 355-359.
26. Eaton, W. A.; Henry, E. R.; Hofrichter, J.; Mozzarelli, A., Is cooperative oxygen binding by hemoglobin really understood? *Nat Struct Mol Biol* **1999,** *6* (4), 351-358.
27. Warhaut, S.; Mertinkus, K. R.; Hollthaler, P.; Furtig, B.; Heilemann, M.; Hengesbach, M.; Schwalbe, H., Ligand-modulated folding of the full-length adenine riboswitch probed by NMR and single-molecule FRET spectroscopy. *Nucleic Acids Res* **2017**.
28. Kladwang, W.; Cordero, P.; Das, R., A mutate-and-map strategy accurately infers the base pairs of a 35-nucleotide model RNA. *RNA* **2011,** *17* (3), 522-534.
29. Kladwang, W.; VanLang, C. C.; Cordero, P.; Das, R., A two-dimensional mutate-and-map strategy for non-coding RNA structure. *Nat. Chem.* **2011,** *3* (12), 954-962.
30. Miao, Z.; Adamiak, R. W.; Blanchet, M.-F.; Boniecki, M.; Bujnicki, J. M.; Chen, S.-J.; Cheng, C.; Chojnowski, G.; Chou, F.-C.; Cordero, P.; Cruz, J. A.; Ferré-D'amaré, A. R.; Das, R.; Ding, F.; Dokholyan, N. V.; Dunin-Horkawicz, S.; Kladwang, W.; Krokhotin, A.; Lach, G.; Magnus, M.; Major, F.; Mann, T. H.; Masquida, B.; Matelska, D.; Meyer, M.; Peselis, A.; Popenda, M.; Purzycka, K. J.; Serganov, A.; Stasiewicz, J.; Szachniuk, M.; Tandon, A.; Tian, S.; Wang, J.; Xiao, Y.; Xu, X.; Zhang, J.; Zhao, P.; Zok,

T.; Westhof, E., RNA-Puzzles round II: Assessment of RNA structure prediction programs applied to three large RNA structures. *RNA* **2015,** *21* (6), 1066-1084.
31. Tian, S.; Cordero, P.; Kladwang, W.; Das, R., High-throughput mutate-map-rescue evaluates SHAPE-directed RNA structure and uncovers excited states. *RNA* **2014,** *20* (11), 1815-26.
32. Tian, S.; Das, R., RNA structure through multidimensional chemical mapping. *Q. Rev. Biophys.* **2016,** *49* (e7), 1-30.
33. Reining, A.; Nozinovic, S.; Schlepckow, K.; Buhr, F.; Furtig, B.; Schwalbe, H., Three-state mechanism couples ligand and temperature sensing in riboswitches. *Nature* **2013,** *499* (7458), 355-9.
34. Furtig, B.; Nozinovic, S.; Reining, A.; Schwalbe, H., Multiple conformational states of riboswitches fine-tune gene regulation. *Current opinion in structural biology* **2015,** *30*, 112-24.
35. Stoddard, C. D.; Widmann, J.; Trausch, J. J.; Marcano-Velázquez, J. G.; Knight, R.; Batey, R. T., Nucleotides Adjacent to the Ligand-Binding Pocket are Linked to Activity Tuning in the Purine Riboswitch. *Journal of Molecular Biology* **2013,** *425* (10), 1596-1611.
36. Zhang, J.; Ferré-D'Amaré, Adrian R., Dramatic Improvement of Crystals of Large RNAs by Cation Replacement and Dehydration. *Structure* **2014,** *22* (9), 1363-1371.
37. Gilbert, S. D.; Reyes, F. E.; Edwards, A. L.; Batey, R. T., Adaptive Ligand Binding by the Purine Riboswitch in the Recognition of Guanine and Adenine Analogs. *Structure* **2009,** *17* (6), 857-868.
38. Edwards, A. L.; Batey, R. T., A Structural Basis for the Recognition of 2′ -Deoxyguanosine by the Purine Riboswitch. *Journal of Molecular Biology* **2009,** *385* (3), 938-948.
39. Serganov, A.; Yuan, Y.-R.; Pikovskaya, O.; Polonskaia, A.; Malinina, L.; Phan, A. T.; Hobartner, C.; Micura, R.; Breaker, R. R.; Patel, D. J., Structural Basis for Discriminative Regulation of Gene Expression by Adenine- and Guanine-Sensing mRNAs. *Chemistry & Biology* **2004,** *11* (12), 1729-1741.
40. Daldrop, P.; Reyes, Francis E.; Robinson, David A.; Hammond, Colin M.; Lilley, David M.; Batey, Robert T.; Brenk, R., Novel Ligands for a Purine Riboswitch Discovered by RNA-Ligand Docking. *Chemistry & Biology* **2011,** *18* (3), 324-335.
41. Delfosse, V.; Bouchard, P.; Bonneau, E.; Dagenais, P.; Lemay, J.-F.; Lafontaine, D. A.; Legault, P., Riboswitch structure: an internal residue mimicking the purine ligand. *Nucleic Acids Research* **2010,** *38* (6), 2057-2068.
42. Gilbert, S. D.; Love, C. E.; Edwards, A. L.; Batey, R. T., Mutational Analysis of the Purine Riboswitch Aptamer Domain. *Biochemistry* **2007,** *46* (46), 13297-13309.
43. Leamy, K. A.; Assmann, S. M.; Mathews, D. H.; Bevilacqua, P. C., Bridging the gap between in vitro and in vivo RNA folding. *Q Rev Biophys* **2016,** *49*, e10.
44. Kladwang, W.; Mann, T. H.; Becka, A.; Tian, S.; Kim, H.; Yoon, S.; Das, R., Standardization of RNA chemical mapping experiments. *Biochemistry* **2014,** *53* (19), 3063-3065.
45. Tian, S.; Das, R., Primerize-2D: automated primer design for RNA multidimensional chemical mapping. *Bioinformatics* **2017**.
46. Kim, H.; Cordero, P.; Das, R.; Yoon, S., HiTRACE-Web: An online tool for robust analysis of high-throughput capillary electrophoresis. *Nucleic Acids Res.* **2013,** *41* (W1), W492-W498.
47. Yoon, S.; Kim, J.; Hum, J.; Kim, H.; Park, S.; Kladwang, W.; Das, R., HiTRACE: High-throughput robust analysis for capillary electrophoresis. *Bioinformatics* **2011,** *27* (13), 1798-1805.
48. Lee, S.; Kim, H.; Tian, S.; Lee, T.; Yoon, S.; Das, R., Automated band annotation for RNA structure probing experiments with numerous capillary electrophoresis profiles. *Bioinformatics* **2015,** *31* (17), 2808-2815.
49. Cordero, P.; Lucks, J. B.; Das, R., An RNA Mapping DataBase for curating RNA structure mapping experiments. *Bioinformatics* **2012,** *28* (22), 3006-3008.

single base-pair M2R	(-) add		(+) add	
p1	**53%**	(35% - 62%)	**79%**	(72% - 91%)
p2	**31%**	(4% - 58%)	**64%**	(58% - 72%)
p3	**73%**	(66% - 91%)	**56%**	(40% - 68%)
p5	**75%**	(58% - 87%)	**29%**	(14% - 55%)
p1b	**44%**	(14% - 55%)	**3%**	(2% - 9%)
p2b	**17%**	(2% - 55%)	**17%**	(2% - 55%)
p4a	**48%**	(11% - 66%)	**4%**	(2% - 26%)
p4b	**55%**	(28% - 67%)	**4%**	(2% - 26%)
p4c	**68%**	(58% - 80%)	**4%**	(2% - 23%)
p6	**6%**	(3% - 19%)	**5%**	(2% - 16%)
p8	**9%**	(3% - 32%)	**4%**	(2% - 26%)
p9	**12%**	(2% - 31%)	**3%**	(2% - 15%)
p10	**3%**	(1% - 10%)	**3%**	(1% - 14%)
p11	**12%**	(3% - 31%)	**16%**	(3% - 29%)
p12	**10%**	(2% - 37%)	**6%**	(2% - 27%)
p13	**9%**	(3% - 32%)	**4%**	(2% - 26%)
p14	**4%**	(1% - 23%)	**4%**	(2% - 15%)
p15	**12%**	(3% - 31%)	**36%**	(12% - 51%)
p16	**14%**	(2% - 38%)	**8%**	(3% - 31%)
p17	**4%**	(2% - 26%)	**4%**	(2% - 16%)

Table 1

double base-pair M2R	(-) add		(+) add	
p1	**5%**	(2% - 14%)	**82%**	(73% - 91%)
p2	**6%**	(2% - 14%)	**84%**	(79% - 97%)
p3	**64%**	(58% - 72%)	**84%**	(79% - 97%)
p5	**71%**	(54% - 87%)	**6%**	(2% - 26%)
p1b	**3%**	(2% - 9%)	**3%**	(2% - 15%)
p2b	**4%**	(1% - 23%)	**10%**	(2% - 37%)
p4a	**9%**	(3% - 32%)	**4%**	(2% - 13%)
p4b	**42%**	(9% - 61%)	**5%**	(2% - 19%)
p4c	**10%**	(2% - 37%)	**3%**	(1% - 14%)
p6	**8%**	(2% - 24%)	**6%**	(3% - 19%)
p13	**4%**	(2% - 12%)	**8%**	(2% - 30%)

Table 2

LM2R			
Lock P1	p2	**42%**	(21% - 69%)
	p4b	**4%**	(2% - 12%)
Lock P2	p1	**76%**	(66% - 88%)
	p4a	**4%**	(2% - 16%)
	p4b	**4%**	(2% - 12%)
Lock P4A	p1b	**9%**	(2% - 19%)
	p2b	**6%**	(2% - 27%)
	p2	**6%**	(2% - 14%)
	p4b	**55%**	(28% - 67%)
Lock P1B	p2b	**53%**	(5% - 75%)
	p4a	**55%**	(28% - 67%)
	p4b	**80%**	(30% - 88%)
	p3	**82%**	(69% - 93%)
Lock P4B	p1b	**8%**	(3% - 31%)
	p2b	**4%**	(1% - 23%)
	p1	**5%**	(2% - 14%)
	p2	**6%**	(2% - 14%)
	p4a	**47%**	(7% - 75%)
Mut P2	p1	**30%**	(1% - 62%)
	p4a	**8%**	(1% - 41%)
	p4b	**13%**	(2% - 56%)

Table 3

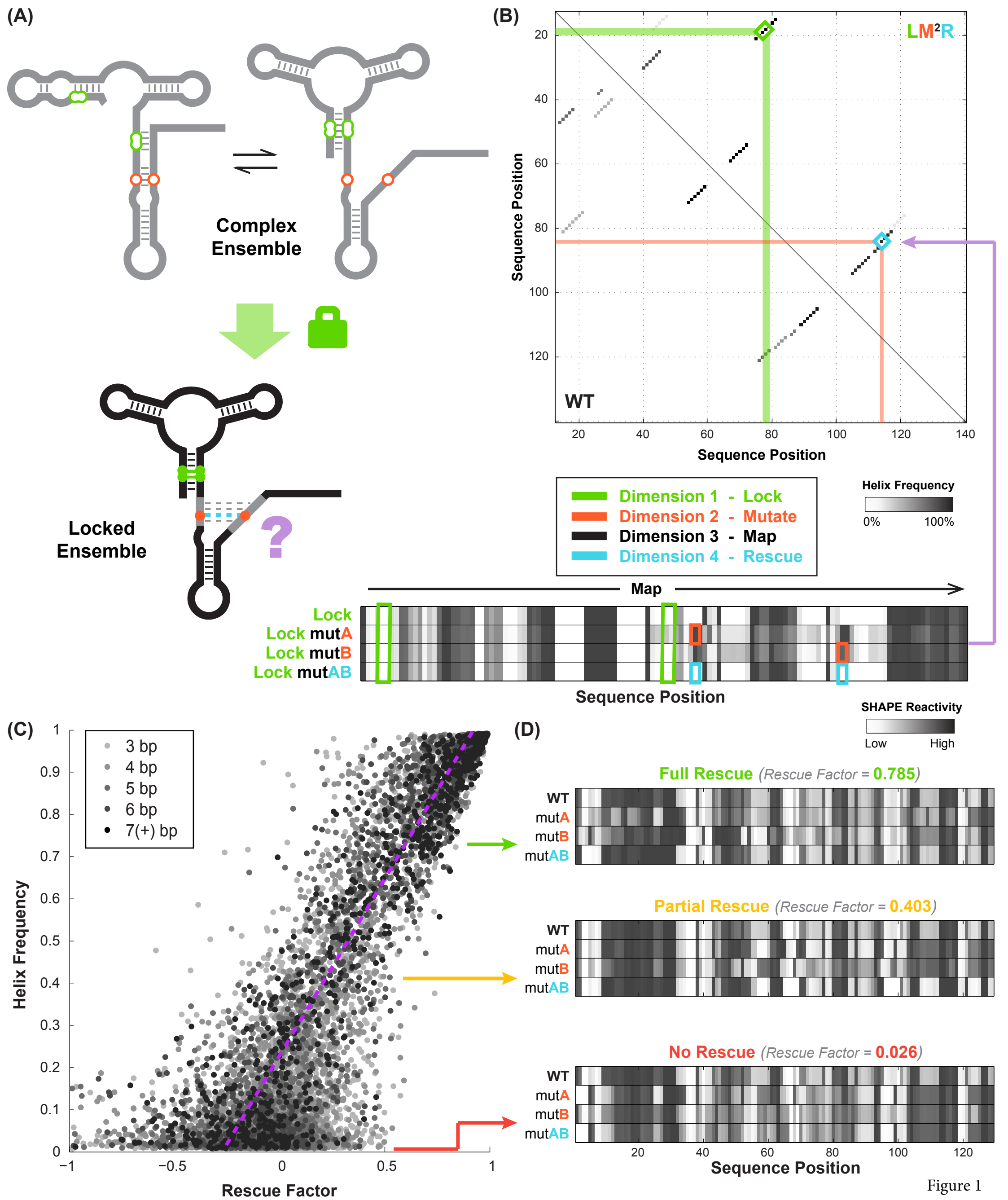
(A)
Complex Ensemble
Locked Ensemble
?
(B)
LM²R
WT
Sequence Position
Sequence Position
Dimension 1 - Lock
Dimension 2 - Mutate
Dimension 3 - Map
Dimension 4 - Rescue
Helix Frequency
0%
100%
Map
Lock
Lock mutA
Lock mutB
Lock mutAB
Sequence Position
SHAPE Reactivity
Low
High
(C)
3 bp
4 bp
5 bp
6 bp
7(+) bp
Helix Frequency
Rescue Factor
(D)
Full Rescue (Rescue Factor = 0.785)
Partial Rescue (Rescue Factor = 0.403)
No Rescue (Rescue Factor = 0.026)
WT
mutA
mutB
mutAB
Sequence Position

Figure 1

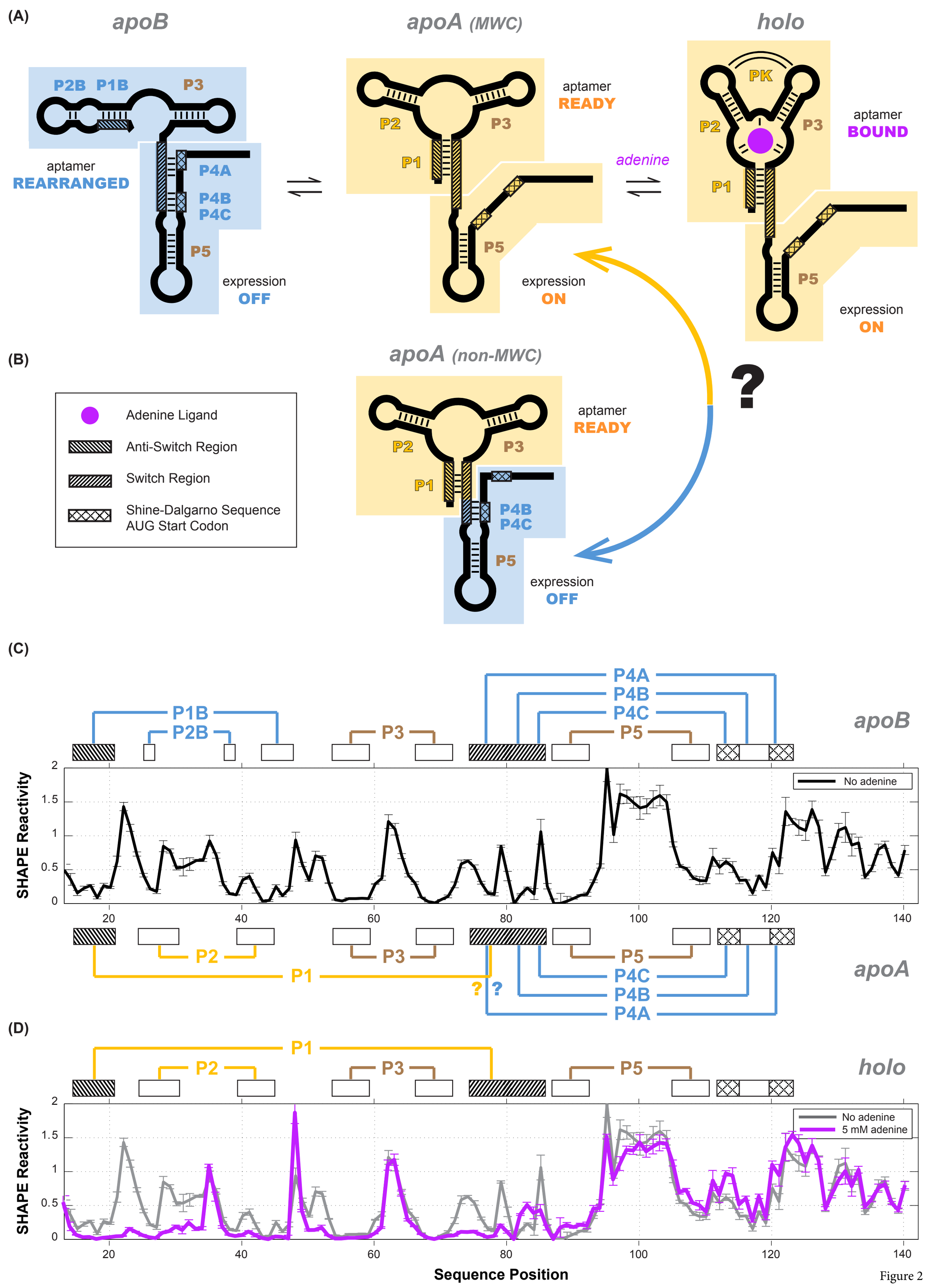
(A)
apoB
apoA (MWC)
holo
P2B P1B
P3
aptamer
REARRANGED
P4A
P4B
P4C
P5
expression
OFF
P2
P3
P1
aptamer
READY
P5
expression
ON
adenine
PK
P2
P3
P1
aptamer
BOUND
P5
expression
ON
?
(B)
apoA (non-MWC)
Adenine Ligand
Anti-Switch Region
Switch Region
Shine-Dalgarno Sequence
AUG Start Codon
P2
P3
P1
aptamer
READY
P4B
P4C
P5
expression
OFF
(C)
P4A
P4B
P4C
P1B
P2B
P3
P5
apoB
SHAPE Reactivity
No adenine
P2
P3
P5
P1
P4C
P4B
P4A
? ?
apoA
(D)
P1
P2
P3
P5
holo
SHAPE Reactivity
No adenine
5 mM adenine
Sequence Position

Figure 2

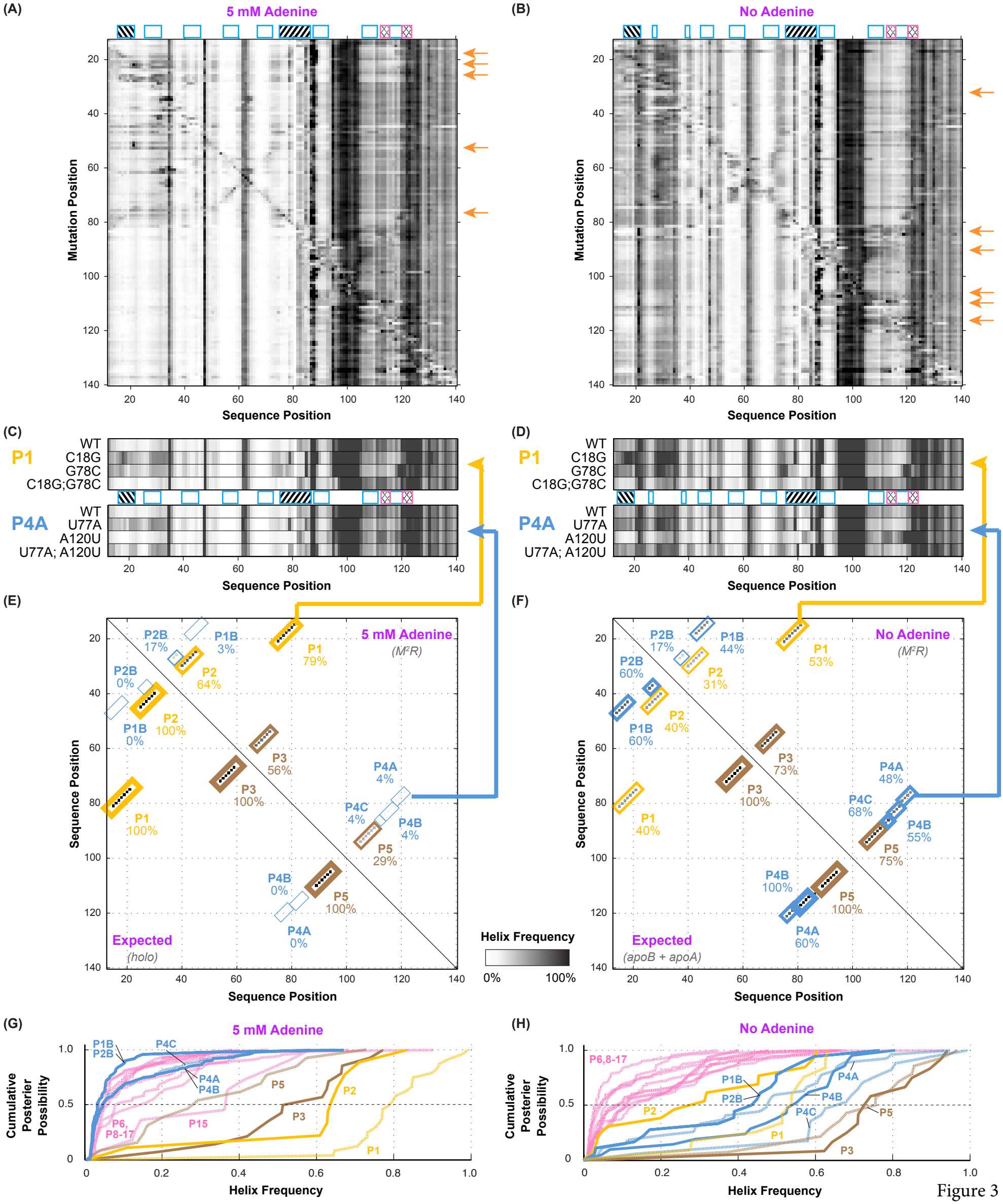
(A)
5 mM Adenine
Mutation Position
Sequence Position
(B)
No Adenine
Mutation Position
Sequence Position
(C)
P1
WT
C18G
G78C
C18G;G78C
P4A
WT
U77A
A120U
U77A; A120U
Sequence Position
(D)
P1
WT
C18G
G78C
C18G;G78C
P4A
WT
U77A
A120U
U77A; A120U
Sequence Position
(E)
5 mM Adenine
(M²R)
P2B 17%
P1B 3%
P1 79%
P2 64%
P2B 0%
P2 100%
P1B 0%
P3 56%
P3 100%
P4A 4%
P4C 4%
P4B 4%
P5 29%
P1 100%
P4B 0%
P5 100%
P4A 0%
Expected
(holo)
Sequence Position
Sequence Position
(F)
No Adenine
(M²R)
P2B 17%
P1B 44%
P1 53%
P2B 60%
P2 31%
P2 40%
P1B 60%
P3 73%
P3 100%
P4A 48%
P4C 68%
P4B 55%
P5 75%
P1 40%
P4B 100%
P5 100%
P4A 60%
Expected
(apoB + apoA)
Sequence Position
Sequence Position
Helix Frequency
0%
100%
(G)
5 mM Adenine
Cumulative Posterier Possibility
P1B
P2B
P4C
P4A
P4B
P5
P2
P3
P6, P8-17
P15
P1
Helix Frequency
(H)
No Adenine
Cumulative Posterier Possibility
P6,8-17
P1B
P2B
P4A
P4B
P4C
P2
P5
P1
P3
Helix Frequency

Figure 3

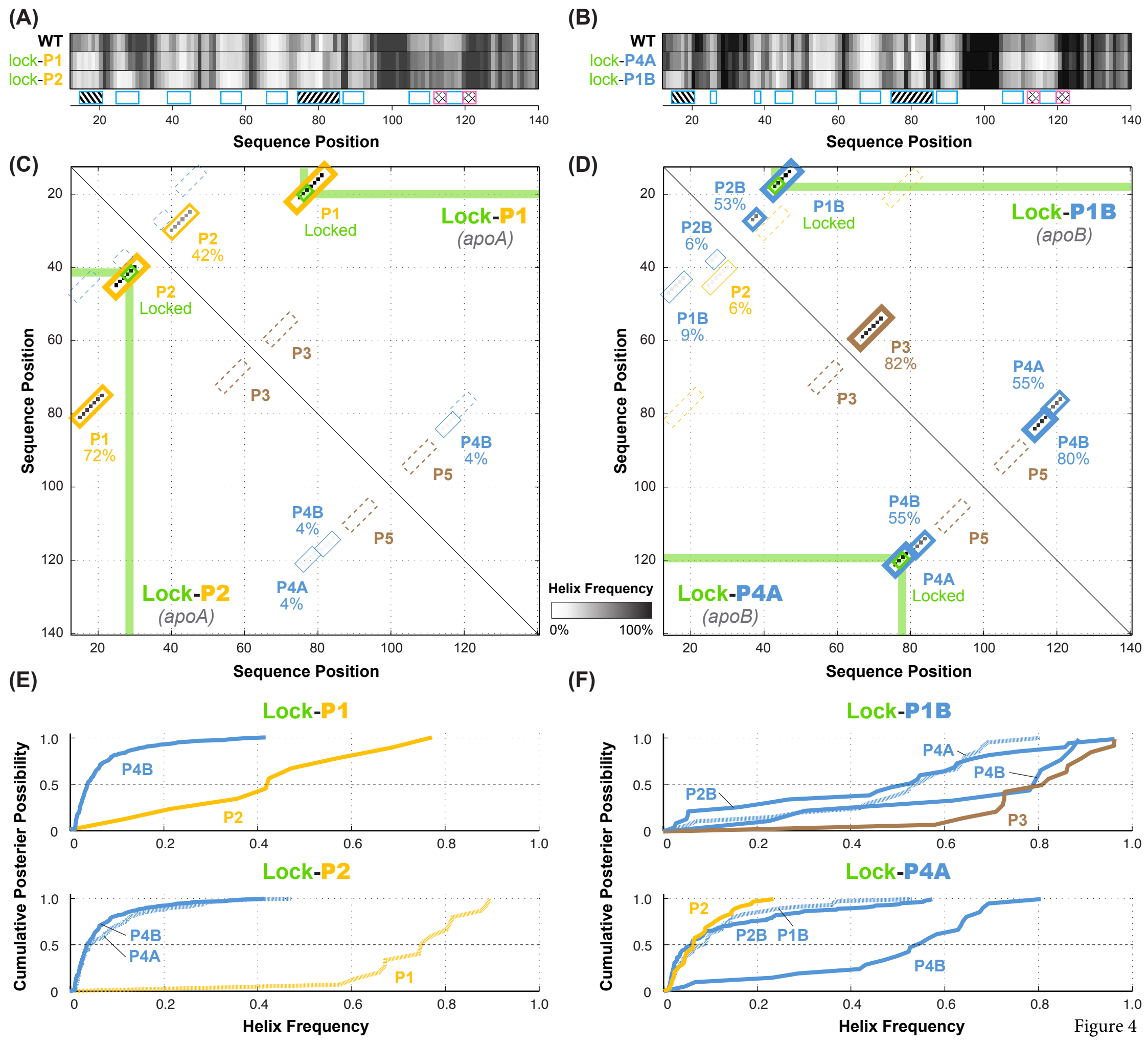
(A)
WT
lock-P1
lock-P2
Sequence Position
(B)
WT
lock-P4A
lock-P1B
Sequence Position
(C)
Lock-P1
(apoA)
P1
Locked
P2
42%
P2
Locked
P3
P3
P1
72%
P4B
4%
P5
P4B
4%
P5
P4A
4%
Lock-P2
(apoA)
Sequence Position
Sequence Position
Helix Frequency
0%
100%
(D)
P2B
53%
P1B
Locked
Lock-P1B
(apoB)
P2B
6%
P2
6%
P1B
9%
P3
82%
P3
P4A
55%
P4B
80%
P5
P4B
55%
P5
P4A
Locked
Lock-P4A
(apoB)
Sequence Position
Sequence Position
(E)
Lock-P1
P4B
P2
Lock-P2
P4B
P4A
P1
Cumulative Posterior Possibility
Helix Frequency
(F)
Lock-P1B
P4A
P4B
P2B
P3
Lock-P4A
P2
P2B
P1B
P4B
Cumulative Posterior Possibility
Helix Frequency

Figure 4

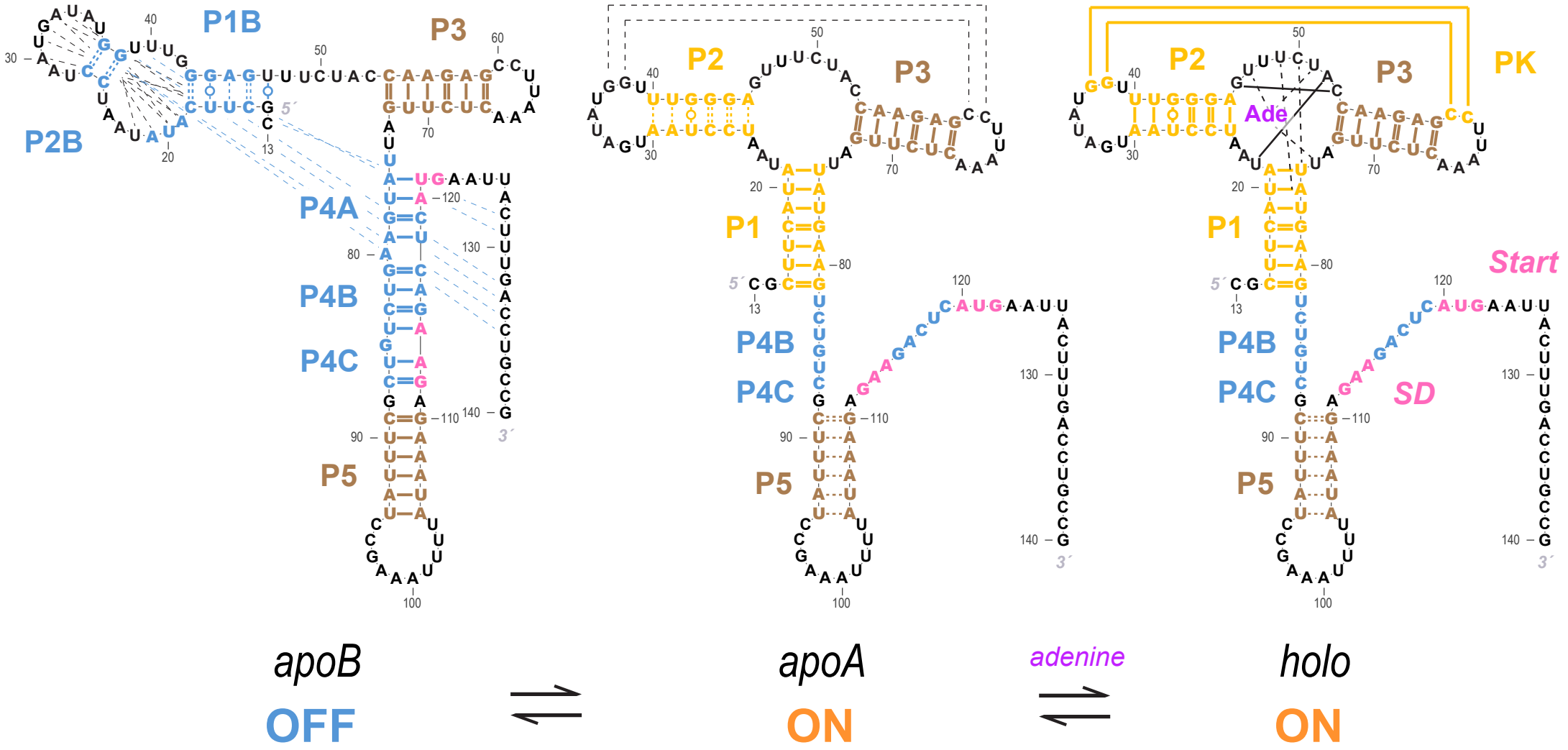
P1B
P3
P2B
P4A
P4B
P4C
P5
P2
P1
PK
Ade
Start
SD
apoB
OFF
apoA
ON
adenine
holo
ON

Figure 5

Supplemental Information for "Allosteric Logic of the *V. vulnificus* Adenine Riboswitch Resolved by Four-dimensional Chemical Mapping"

Siqi Tian[1], Wipapat Kladwang[1], and Rhiju Das[1, 2, *]

[1]Department of Biochemistry, and [2]Department of Physics, Stanford University,
Stanford, California 94305, United States

* Corresponding Author

This Supplemental Information document contains the following sections:

Supporting Results 2
Mutate-Map-Rescue (M^2R) – Application Generality and Automated Classification 2
Current Limitations of M^2R and Classifier 3
Adenine riboswitch construct design 4
Multi-probe chemical mapping tests partitioning predicted by the MWC model 4
Supporting Methods 5
In silico Partition, Autoscore Classifier and Rfam Sampling 5
Structural Equilibrium Fitting 6
SI Figures 8
Supporting References 11

Supporting Results

Mutate-Map-Rescue (M^2R) – Application Generality and Automated Classification

Before interrogating *add* riboswitch ensembles, we sought a method that would enable rapid and unbiased readout of helix frequencies. Our prior work on mutate-map-rescue (M^2R) tested RNA structures by disrupting a base pair by single mutation, and testing whether compensatory double mutations restore such perturbations, but relied on manual inspection to assess rescue, and focused on a single model system, a four-way junction domain of *E. coli* 16S rRNA.[1] We first sought to assess the generality of M^2R approach by applying it to other RNA elements. First, we deployed M^2R on the lariat-capping GIR1 ribozyme,[2] to test helix P5 from crystallographic model against its alternative version (alt-P5), which was predicted by our M^2-based model with a 2-register shift (Figure 2B). For each base pair tested, we compared the SHAPE profiles of WT (wild type), 2 single mutants, and the double mutant (rescue) in a 'quartet'. With the local perturbations caused by single mutants in the P5/alt-P5 region, double mutants based on the P5 successfully restored the SHAPE profile to WT, while double mutants based on the alt-P5 failed to rescue. Thus, M^2R provided evidence for the P5 helix but not the register-shifted alt-P5, consistent with the crystallographic structure of the ribozyme. In addition, we applied M^2R on the P4-P6 domain of the *Tetrahymena* ribozyme[3] to test for presence of crystallographic P5c against an alternative suggested by mutate-and-map analysis (SI Figure S1). Finally, M^2R-validated secondary structure models were confirmed experimentally on two RNA domains by functional assays *in vitro* or *in cellulo*: a human *HoxA9* mRNA IRES (internal ribosomal entry site) domain [4] and a stem loop domain from Influenza A virus [5].

In order to evaluate the accuracy of M^2R on a larger scale, we turned to *in silico* simulation to generate a much greater number of RNA test cases. Specifically, we asked: do M^2R-validated base pairs have high base-pairing probability (BPP) *in silico*? To answer this question, we sought to automate the calling of M^2R result with an automated classifier that would evaluate M^2R data with results matching human inspection, and this study eventually led to the definition of the 'rescue factor' applied to the adenine riboswitch. Our first scoring function took into account the following two factors: 1) the amount of perturbation seen in each of the two single mutants, compared to wild type profiles; and 2) the similarity (rescuing effect) between double mutant and WT. We captured the latter effect through a rescue factor metric:

$$\frac{diff_{(WT,AB)}}{\max\left(diff_{(WT,A)}, diff_{(WT,B)}\right)}$$

where

$$diff_{(A,B)} = \sqrt{\frac{1}{N}\sum_{i=1}^{N}(d_A - d_B)^2}$$

and d_A and d_B are vectors of normalized SHAPE profiles, with the same length of N (see Supporting Methods for further details). The classifier returned a result from three categories: Validated, Falsified, or Uncertain; the last one was assigned for cases that either 1) single mutants failed to introduce discernible perturbations, or 2) the rescuing effect was 'half-way' and hard to assign. After training with the *in vitro* M^2R data on the GIR1, P4-P6, and IRES measurements as well as *in silico* simulated counterparts, we obtained a classifier that recovered human expert calls (SI Figure S2).

Next, we simulated M^2R *in silico* on 325 RNA families from the Rfam database[6] whose lengths were in range between 100 and 250 nt. More than 37,000 base pairs were tested from helices that were longer than 2 bp and with predicted base pairing probability (BPP) greater than 1%. SI Figure S13 shows the BPP distribution of the 4-category classification. These results confirmed that the Validated and Falsified categories corresponded to base pairs with high and low BPP. Unexpectedly, we also observed a quantitative correlation between the *in silico* predicted BPP and the 'rescue factor' metric that underlies our classification, even for base pairs that appear with BPP frequencies between 0.3 and 0.7 (Figure 2A). Furthermore, for helices of longer length, this relationship became more well-defined. We reasoned that this correlation would enable estimation of BPP based on helix length and the 'rescue factor' metrics measured and averaged over all the base pairs for a given helix (SI Figure S13), and that this quantitative metric would be more informative than a qualitative 4-category classification. Further support for using the 'rescue factor' to estimate a posterior probability for tested helix frequencies arose from our studies on the adenine riboswitch with and without adenine, which could be compared to 'gold standard' helix frequency estimates from NMR analysis, as described in the main text.

Current Limitations of M^2R and Classifier

We trained an automated classifier based on previous M^2R *in vitro* data combined with *in silico* simulations. The classifier was later independently tested on *add* single-base-pair M^2R, double-base-pair M^2R, and LM^2R datasets, showing agreement with calling by an expert human referee (S.T.) (Figure 3A). Moreover, the BPP distribution of the simulated *in silico* counterparts for *add* riboswitch follows the same trend as Rfam tests (SI Figure S14), in agreement with its generality. The performance of such a simple classifier was acceptable and supported our heuristic for the rescue factor (SI Figure S13). Our preliminary attempt on 4-category classification gave conservative conclusions for M^2R quartets, with 'Partially Validated' as weaker cases for incomplete compensatory rescue. For final analyses, we chose to

present final rescue factors and corresponding helix frequencies (see, e.g., main text Figures 3 and 4); the classifier based on the rescue factor gives a more qualitative picture of the results, but allows simple visual checks that for each helix, different base pairs tested for compensatory rescue give concordant 'calls' for the frequency of the helix (Figure S14).

Adenine riboswitch construct design

We performed the M^2R pipeline on a 128-nt *add* riboswitch construct, which has 15 extra nucleotides on the 3′ end into the coding sequence compared to a 112-nt one used in a recent study.[7] We chose this longer *add* version after reproducing prior work in our laboratory[8-9] finding that the sequence context has an effect on the folding landscape of this riboswitch (SI Figure S5A). Although the 112-nt construct showed weak ligand-responsive chemical reactivity changes in the SD region under the salt conditions used in NMR [9], it does not show noticeable switching under our in vitro solution conditions. The extended construct gives chemical reactivity changes under all conditions tested. Besides M^2 (SI Figure S5B-C), we performed single-base-pair M2R on the *add* riboswitch (Figure 3, SI Figure S6).

Multi-probe chemical mapping tests partitioning predicted by the MWC model

As discussed in the main text introduction, the MWC model requires that, even in the absence of adenine ligand, the *add* riboswitch samples two states: *apoA* and *apoB*, that have secondary structures compatible and incompatible with aptamer adenine binding, respectively, and that these states are more likely or less likely, respectively, to have free ribosome binding sites. We tested this model with the aid of the lock-P1 and lock-P4A mutants, which isolated the *apoA* and *apoB* states, respectively, and chemical mapping to monitor the riboswitch structural ensemble at nucleotide resolution. To stringently test the prediction, we expanded our chemical mapping protocol to include five additional modifiers beyond SHAPE: DMS (dimethyl sulfate) [10], glyoxal [11], RNase V1 [12], terbium(III) [13-14], and ultraviolet irradiation at 302 nm [15], giving a total number of 1920 measurements measured in three sequences that would test a two-state partitioning. As expected from the model of *apoA* vs. *apoB*, these multiple modifier profiles varied significantly between the lock-P1 and lock-P4A mutants, especially in the expression platform regions (see, e.g., nts 98-112). Nevertheless, as predicted from the MWC model, a simple linear combination of the profiles, assuming 48% of the *apoA* state and 52% of the *apoB* state recovered the data measured for the adenine-free wild type riboswitch within experimental errors, except at nucleotides 79-81 (SI Figure 7A-B). We note that there was only one parameter optimized in this fit; scaling of each data profile was carried out based on well-defined flanking hairpins as normalization standards [16]. These values for the *apoA* vs. *apoB* state frequencies agree within errors with helix frequencies measured above in compensatory rescue experiments as well as with the prior NMR experiment at similar temperature (40%

apoA at 30 °C) [17]. However, the discrepancies at nucleotides 79-81 were reproducible, suggesting that there are additional secondary structures, potentially many at low frequencies, beyond those detected here in the ligand-free ensembles.

Supporting Methods

In silico Partition, Autoscore Classifier and Rfam Sampling

In silico RNA SHAPE profiles were simulated using the `partition` executable from the RNAstructure package version 5.6 [18-19]. The resulting pair-wise probability matrices was projected into a one-dimensional vector to get per-residue base pairing probabilities (BPP). For M^2R quartet simulations, the targeted base pair was mutated to G-C or C-G pairs (i.e., the 'Stable' library from Primerize-2D [20]). Flanking sequences (5´ or 3´) were not included for simulation.

The autoscore classifier utilizes a 'ratio' metric for classification. Normalized SHAPE profiles are used as input. First, the difference between two SHAPE profiles are calculated by:

$$diff_{(A,B)} = \sqrt{\frac{1}{N}\sum_{i=1}^{N}(d_A - d_B)^2}$$

Where d_A and d_B are vectors of normalized SHAPE reactivity values, with the same length of N.

For a given quartet of SHAPE profiles (WT, A, B, AB), we first determined whether there was pronounced perturbation introduced by either single mutants (A and B) by calculating:

$$max\left(diff_{(WT,A)}, diff_{(WT,B)}\right) \qquad (1)$$

If the value of (1) is less than a *CUTOFF*, the Uncertain class is assigned. Otherwise, continue to determine the amount of rescuing effect by the double mutant (AB):

$$\frac{diff_{(WT,AB)}}{\max\left(diff_{(WT,A)}, diff_{(WT,B)}\right)} \qquad (2)$$

[2] defines the 'ratio' metric, i.e., the ratio between the distance of AB to WT and the maximum distance of A or B to WT. If the value of [2] is less than *LOW*, the Validated class is assigned due to the relatively small residual of difference of AB to WT compared to single mutants. If the value of (2) is greater than *HIGH*, the Falsified class is assigned. For values of (2) between *LOW* and *HIGH*, the Partial class is assigned, which captures cases that show incomplete rescue or a mixed result.

The classifier was trained on *in silico* and *in vitro* data of GIR1, P4P6, 16S-FWJ, HoxA9 [4] and PSL2 (Hagey et al., manuscript in preparation), a total of 324 quartets. Data were cropped to the region of interest (i.e., excluding the flanking sequences); *in silico* simulated reactivity profiles were used directly, while *in vitro* data were attenuation-corrected and normalized by internal standards [16]. For each quarter, a manual score in 1 of the 4 categories was available from expert inspection (by S.T.). The set of parameters *CUTOFF* (0.1), *LOW* (0.4), and *HIGH* (0.7) were then determined by grid search, optimizing for recovery of the expert assessments. The classifier was then tested on *in silico* and *in vitro* data for the *add* riboswitch using the chosen parameters. Both training and test data compose of Falsified vs. Validated cases in a ~2.8:1 ratio.

RNA families with length between 100 and 250 nt were screened from the Rfam database (http://rfam.xfam.org/) 11.0 FASTA file [21]. A sequence from each family was randomly picked as representative, and its *in silico* BPP matrix was simulated. Base pairing positions to be tested by M^2R were selected from this BPP matrix, for BPP values greater than or equal to 1%, and in helices that are 3 bp or longer. For each helix, the averaged 'ratio' metric and BPP across all simulated M^2R quartets in the helix were calculated. Collectively, all simulated Rfam helices were visualized by first grouping the 'ratio' values into bins with width of 0.05, and then on boxplots of their BPP distribution within each bin. Intervals of 95% confidence are shown as black whiskers representing the 2.5 – 97.5 percentile of each bin, and boxes representing quartiles. Helix-wise average 'ratio' for helices with *in vitro* M2R data were similarly calculated. The *in vitro* BPP for those helices are assigned as: for GIR1 and P4P6, 1.0 or 0 based on their existence in crystallographic structures; for 16S-FWJ, 1.0, 0.8, 0.2 or 0 based on the prior M^2R results [22]. *In vitro* BPP of *add* helices *in vitro* were estimated by the median Rfam BPP of the 'ratio' bin the query helix falls into.

Structural Equilibrium Fitting

Equilibrium fractions of each state were determined by assuming that lock-P1 and lock-P4A stabilizers completely stabilize the corresponding structure – their reactivity profiles therefore represent the

reactivity profile for each state. The reactivities of lock-P1 and lock-P4A were taken to fit the WT reactivity by χ^2 score, which is calculated as follows:

$$\chi^2 = \sum_i \frac{(d_{WT} - d_{PRED})^2}{\sigma_{WT}^2 + \sigma_{PRED}^2}$$

$$d_{PRED} = \alpha \cdot d_{apoA} + (1 - \alpha) \cdot d_{apoB}$$

$$\sigma_{PRED}^2 = \alpha^2 \cdot \sigma_{apoA}^2 + (1 - \alpha)^2 \cdot \sigma_{apoB}^2$$

Where d_{WT}, d_{apoA}, and d_{apoB} are mean SHAPE reactivity profiles of WT, lock-P1, and lock-P4A, and σ_{WT}, σ_{apoA}, and σ_{apoB} are errors (standard deviation) of d_{WT}, d_{apoA}, and d_{apoB}. The parameter α is the fraction of the *apoA* state, ranging from 0 to 1. χ^2 is summed over all or a subset of nucleotide positions i as specified below. χ^2 scores are plotted against α, and the α value with minimum χ^2 is taken as the best fit. To prevent a single nucleotide position from dominating the fit by their extreme values, nucleotides 95 (SHAPE), 66 (DMS), and 85 (glyoxal) were excluded.

SI Figures

Figure S1. Correlation between rescue factor and helix frequency from Rfam simulation.
(A) Boxplot of all helices. The purple lines mark median, open boxes cover 25 and 75 percentile, cyan whiskers show 5 and 95 percentile, and gray plus signs label outliers. Rescue factor numbers are colored in red, yellow, or green, partitioned by 0.3 and 0.7.
(B) Boxplot of helices by their length: 3, 4, 5, 6, and ≥ 7 base-pairs.

Figure S2. M^2R quartets and helices tested for P4-P6 and GIR1.
(A) M^2R quartets of P4-P6 domain testing P5C, alt-P5C, and P6. Rescue factor for each quartet is given in the title and colored as in Figure S1.
(B-C) Secondary structures of P4-P6 and GIR1 highlighting tested helices.
(D) M^2R quartets of GIR1 ribozyme testing P5, alt-P5, P4, and pk2-5.

Figure S3. One-dimensional SHAPE profiles of *add* riboswitch constructs with different lengths.
Three different constructs were probed by SHAPE (1M7): *(top)* a 71-nt aptamer only construct (nts 13-83); *(middle)* a 113-nt construct (nts 13-125) including the expression platform, matching the previous NMR study; *(bottom)* a 128-nt construct (nts 13-140) further including the first 15 nt of the coding region. Reactivities are normalized based on GAGUA penta-loop reference hairpins (not shown). The 113-nt construct did not show significant switching for the Shine-Dalgarno sequence (nts 112-114) or AUG start codon (nts 120-122). See also reference.[8] The ligand-dependent reactivity changes in the aptamer domain are shared across all three constructs.

Figure S4. Candidate alternative helices from REEFFIT analyses. *(A)* Helices modeled to be in the adenine riboswitch based on M^2 data with and without adenine, using prior analysis assuming a dominant secondary structure. To estimate uncertainties, simulated data replicates were prepared by bootstrapping, and percentages give fraction of the simulations in which each helix was inferred to be in the dominant secondary structure. While not recovering the actual helix frequencies in the solution ensemble, this initial analysis revealed the sheer number of possible helices that needed to be considered in modeling the ensemble, particularly for the adenine-free state. *(B)* Helices P6, P8-13 were identified and tested by single base-pair M^2R. The presented structures are illustrating the helices only, and do not imply co-existence in the same structure. Helix name P7 was skipped to avoid naming conflict with a previous REEFFIT investigation[9].

Figure S5. All 188 single base-pair M^2R quartets for *add* riboswitch. Helices P1 (7 bp), P2 (6 bp), P3 (6 bp), P5 (6 bp), P1B (5 bp), P2B (2 bp), P4A (4 bp), P4B (4 bp), P4C (2 bp), P6 (5 bp), P8 (4 bp), P9 (5 bp), P10 (3 bp), P11 (9 bp), P12 (3 bp), P13 (4 bp), P14 (3 bp), P15 (7 bp), P16 (5 bp), and P17 (4 bp) were tested for both no adenine and 5 mM adenine conditions. Rescue factor for each quartet is given in the title and colored as in Figure S1.

Figure S6. All 82 double base-pair M^2R quartets for *add* riboswitch. Helices P1, P2, P3, P5, P1B, P2B, P4A, P4B, P4C, P6, and P13 were tested for both no adenine and 5 mM adenine conditions. MutP2 from previous study is also included. Rescue factor for each quartet is given in the title and colored as in Figure S1. Picked stabilizers for P1, P2, P4A, P1B, and P4B are labeled by green lock symbol.

Figure S7. Multi-probe chemical mapping of stabilizers and linear fitting of P1 and P4A
(A) Five-modifier (SHAPE, 1M7, glyoxal, terbium (III), UV 302 nm) reactivity profile for lock-P1 and lock-P4A constructs. χ^2 score-based linear fitting yields *apoA* state as 48% (SHAPE), 58% (DMS), 46% (glyoxal), 52% (terbium (III)) and 68% (UV 302 nm) in population. Some uncertainty remains in the UV shadowing data normalization for a quantitative fitting.
(B) Comparison of fitted SHAPE reactivity profile to observed WT. Reactivity profiles of lock-P1 (gold) and lock-P4A (blue) are plotted. The fitted profile resolves reactivity differences in the expression platform and resembles WT.
(C) Comparison of lock-P1 and lock-P2 profiles in the absence or presence of ligand to observed WT profile in the presence of 5 mM adenine. Lock-P1 and lock-P2 mutants show agreement in the expression platform reactivity with WT, even under no ligand condition.

Figure S8. All 82 single base-pair LM^2R quartets for *add* riboswitch. Helices P2 and P4B are tested by lock-P1 stabilizer; helices P1, P4A, and P4B are tested by lock-P2 stabilizer; helices P2, P1B, P2B, and P4B are tested by lock-P4A stabilizer; helices P2B, P4A, P4B, and P3 are tested by lock-P1B stabilizer; helices P1, P2, P1B, P2B, and P4A are tested by lock-P4B stabilizer; all under no adenine condition. Rescue factor for each quartet is given in the title and colored as in Figure S1.

Figure S9. All 15 single base-pair LM^2R quartets for *add* riboswitch with the MutP2 construct. Helices P1, P4A, and P4B were tested under no adenine condition. Rescue factor for each quartet is given in the title and colored as in Figure S1.

Figure S10. LM^{2}R stabilizer lock-P4B and helix frequency for *apoA* state.
(A) 1D SHAPE profiles for lock-P1, lock-P2, lock-P4A, lock-P1B, and lock-P4B stabilizers under both no adenine and 5 mM adenine conditions, with boxes showing successful stabilization resulting in protections from SHAPE, respectively.
(B) Base-pairing probability plot of LM^{2}R test on lock-P4B construct and expected *apoA* state from the non-MWC model. Helix P4A gives high helix frequency, while P1 and P2 exhibit no evidence. Helices P1B and P2B have low helix frequency as well, suggesting heterogeneity in aptamer domain folding in the absence of ligand. Helix locked in place is highlighted by green box; helices not tested by LM^{2}R are in dashed boxes.

Figure S11. Simulation of temperature dependence on switching efficiency. Thermodynamic parameters used are: ΔH_{Kpre} = 52 kJ·mol^{-1}, ΔS_{Kpre} = 167 J·mol^{-1}·K^{-1}, ΔH_{Kd} = 238 kJ·mol^{-1}, ΔS_{Kd} = 110 J·mol^{-1}·K^{-1}. Ligand concentrations: $[L_{low}]$ = 0.01 μM; $[L_{high}]$ = 1.0 μM for *(top)* panels and $[L_{low}]$ = 1.5 μM for *(bottom)* heatmaps. The *(top)* population linear plots used *[RNA]* = 1.5 nM; while *(bottom)* temperature vs. [RNA] heatmap simulated *[RNA]* = 0 – 100 nM for T = 0 – 40 °C. Parameters were derived from prior study reviewing the temperature compensation model.[23]

Figure S12. Higher-order M^2 on selected single mutant backgrounds. Single mutants *(A)* A109U, *(B)* G78C, *(C)* A116U, *(D)* G44C, *(E)* G37C, and *(F)* G81C were selected from a clustering analysis of WT M^2 data. A comparison of their 1D SHAPE profile to WT under both no adenine and 5 mM adenine conditions are shown along with complete M^2 datasets. *(G)* Secondary structures inferred for these single mutants are quite diverse, particularly for the adenine-free state (percentage values give bootstrapping confidence that those helices are present in the dominant secondary structure). The presence of these alternative structures would explain deviations of main text LM^{2}R results for *apoB*-locking backgrounds (Figures 4 and 5) from expectations derived from a single *apoB* secondary structure (Figure 5).

Figure S13. Performance of 4-bin auto-score classifier. Histogram of *in silico (A)* training data (16S-FWJ, P4P6, GIR1, Hox, PB2; total of 162 quartets), *(B)* test data (*add* single and double base-pair M^{2}R; total of 242 quartets), and (*C)* Rfam family (total of 62484 quartets) simulations are shown by their classification, and grouped by the *in silico* predicted base-pairing probability (BPP).

Figure S14. Base-pair-wise classification of M^{2}R and LM^{2}R quartets by the 4-bin auto-score. Table summary of 4-bin classification by human expert and automatic algorithm on *in vitro (A)* single base-pair

M^2R, *(B)* double base-pair M^2R, and *(C)* LM^2R and MutP2 are shown. Each symbol represents one quartet testing a single base-pair (or 2 adjacent base-pairs in *(B)*).

Supporting References

1. Tian, S.; Das, R., RNA structure through multidimensional chemical mapping. *Q. Rev. Biophys.* **2016,** *49* (e7), 1-30.
2. Meyer, M.; Nielsen, H.; Oliéric, V.; Roblin, P.; Johansen, S. D.; Westhof, E.; Masquida, B., Speciation of a group I intron into a lariat capping ribozyme. *Proceedings of the National Academy of Sciences of the United States of America* **2014,** *111* (21), 7659-7664.
3. Cate, J. H.; Gooding, A. R.; Podell, E.; Zhou, K.; Golden, B. L.; Kundrot, C. E.; Cech, T. R.; Doudna, J. A., Crystal structure of a group I ribozyme domain: Principles of RNA packing. *Science* **1996,** *273* (5282), 1678-1685.
4. Xue, S.; Tian, S.; Fujii, K.; Kladwang, W.; Das, R.; Barna, M., RNA regulons in Hox 5´ UTRs confer ribosome specificity to gene regulation. *Nature* **2014,** *517* (7532), 33-38.
5. Hagey, R.; Tian, S.; Pham, E.; Elazar, M.; Kladwang, W.; Taubenberger, J.; Das, R.; Glenn, J., A novel RNA secondary structural element modulates Influenza A virus packaging. **2017**, submitted.
6. Burge, S. W.; Daub, J.; Eberhardt, R.; Tate, J.; Barquist, L.; Nawrocki, E. P.; Eddy, S. R.; Gardner, P. P.; Bateman, A., Rfam 11.0: 10 years of RNA families. *Nucleic Acids Research* **2013,** *41* (D1), D226-D232.
7. Reining, A.; Nozinovic, S.; Schlepckow, K.; Buhr, F.; Furtig, B.; Schwalbe, H., Three-state mechanism couples ligand and temperature sensing in riboswitches. *Nature* **2013,** *499* (7458), 355-359.
8. Ali, M. Conformational transitions in RNA probed in riboswitch systems. Stanford University, 2011.
9. Cordero, P.; Das, R., Rich structure landscapes in both natural and artificial RNAs revealed by mutate-and-map analysis. *PLoS Comput. Biol.* **2015,** *11* (11), e1004473.
10. Cordero, P.; Kladwang, W.; VanLang, C. C.; Das, R., Quantitative dimethyl sulfate mapping for automated RNA secondary structure inference. *Biochemistry* **2012,** *51* (36), 7037-7039.
11. Banerjee, A. R.; Jaeger, J. A.; Turner, D. H., Thermal unfolding of a group I ribozyme: The low-temperature transition is primarily disruption of tertiary structure. *Biochemistry* **1993,** *32* (1), 153-163.
12. Zou, C.; Ouyang, Z., Joint modeling of RNase footprint sequencing profiles for genome-wide inference of RNA structure. *Nucleic Acids Res.* **2015,** *43* (19), 9187-9197.
13. Hargittai, M. R.; Musier-Forsyth, K., Use of terbium as a probe of tRNA tertiary structure and folding. *RNA* **2000,** *6* (11), 1672-1680.
14. Harris, D. A.; Walter, N. G., Probing RNA structure and metal-binding sites using terbium(III) footprinting. *Curr. Protoc. Nucleic Acid Chem.* **2003,** *13* (6.8).
15. Kladwang, W.; Hum, J.; Das, R., Ultraviolet shadowing of RNA can cause significant chemical damage in seconds. *Sci. Rep.* **2012,** *2*, 517.
16. Kladwang, W.; Mann, T. H.; Becka, A.; Tian, S.; Kim, H.; Yoon, S.; Das, R., Standardization of RNA chemical mapping experiments. *Biochemistry* **2014,** *53* (19), 3063-3065.
17. Reining, A.; Nozinovic, S.; Schlepckow, K.; Buhr, F.; Furtig, B.; Schwalbe, H., Three-state mechanism couples ligand and temperature sensing in riboswitches. *Nature* **2013,** *499* (7458), 355-9.
18. Mathews, D. H.; Disney, M. D.; Childs, J. L.; Schroeder, S. J.; Zuker, M.; Turner, D. H., Incorporating chemical modification constraints into a dynamic programming algorithm for prediction of RNA secondary structure. *Proc. Natl. Acad. Sci. USA* **2004,** *101* (19), 7287-7292.
19. Reuter, J.; Mathews, D., RNAstructure: Software for RNA secondary structure prediction and analysis. *BMC Bioinform.* **2010,** *11* (1), 129.
20. Tian, S.; Das, R., Primerize-2D: Automated primer design for RNA multidimensional chemical mapping. *Bioinformatics, in press* **2016**.

21. Burge, S. W.; Daub, J.; Eberhardt, R.; Tate, J.; Barquist, L.; Nawrocki, E. P.; Eddy, S. R.; Gardner, P. P.; Bateman, A., Rfam 11.0: 10 years of RNA families. *Nucleic Acids Res*. **2013,** *41* (D1), D226-D232.
22. Tian, S.; Cordero, P.; Kladwang, W.; Das, R., High-throughput mutate-map-rescue evaluates SHAPE-directed RNA structure and uncovers excited states. *RNA* **2014,** *20* (11), 1815-26.
23. Fürtig, B.; Nozinovic, S.; Reining, A.; Schwalbe, H., Multiple conformational states of riboswitches fine-tune gene regulation. *Curr. Opin. Struct. Biol.* **2015,** *30*, 112-124.

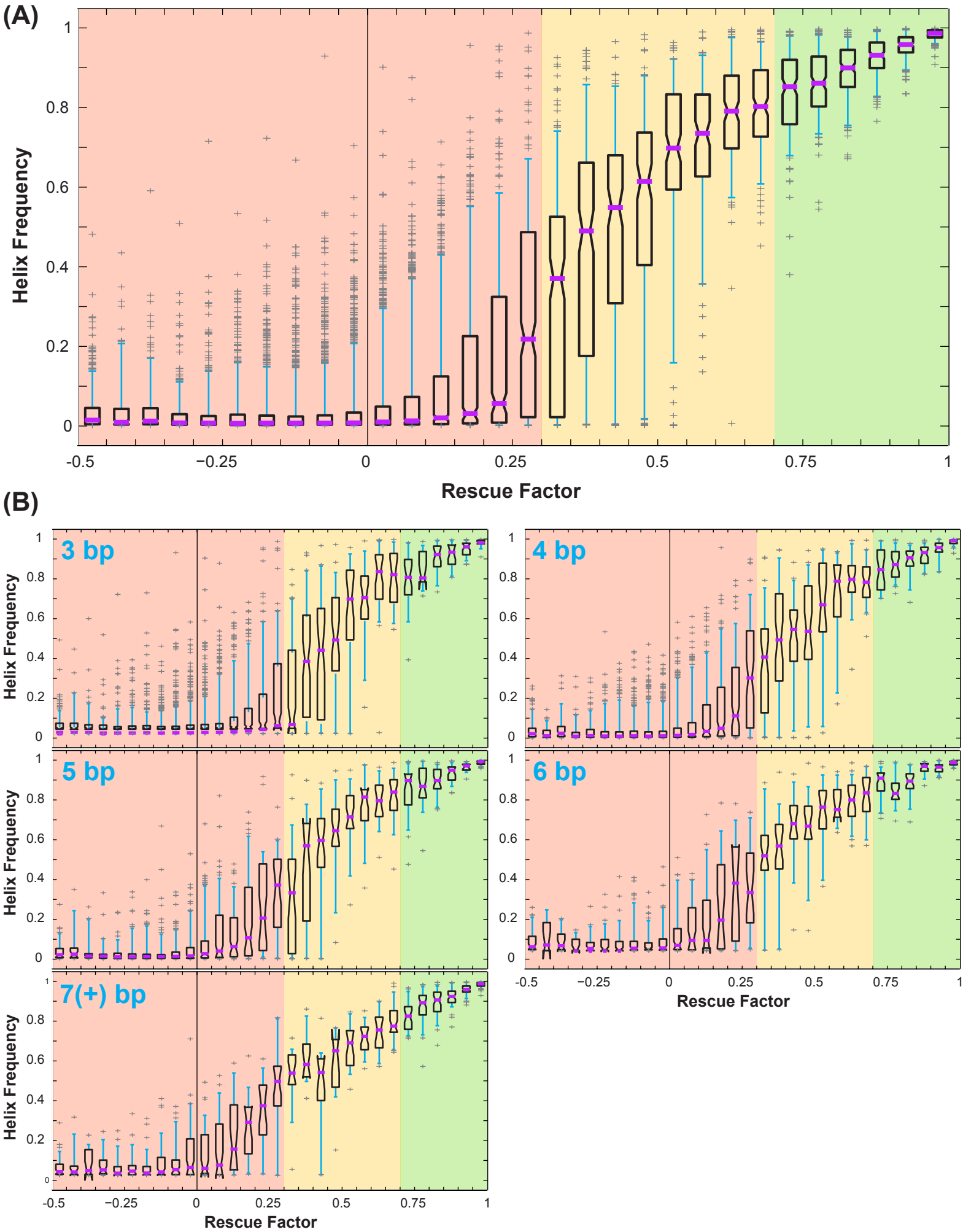
(A)
Helix Frequency
Rescue Factor
(B)
3 bp
4 bp
5 bp
6 bp
7(+) bp
Helix Frequency
Rescue Factor

SI Figure S1

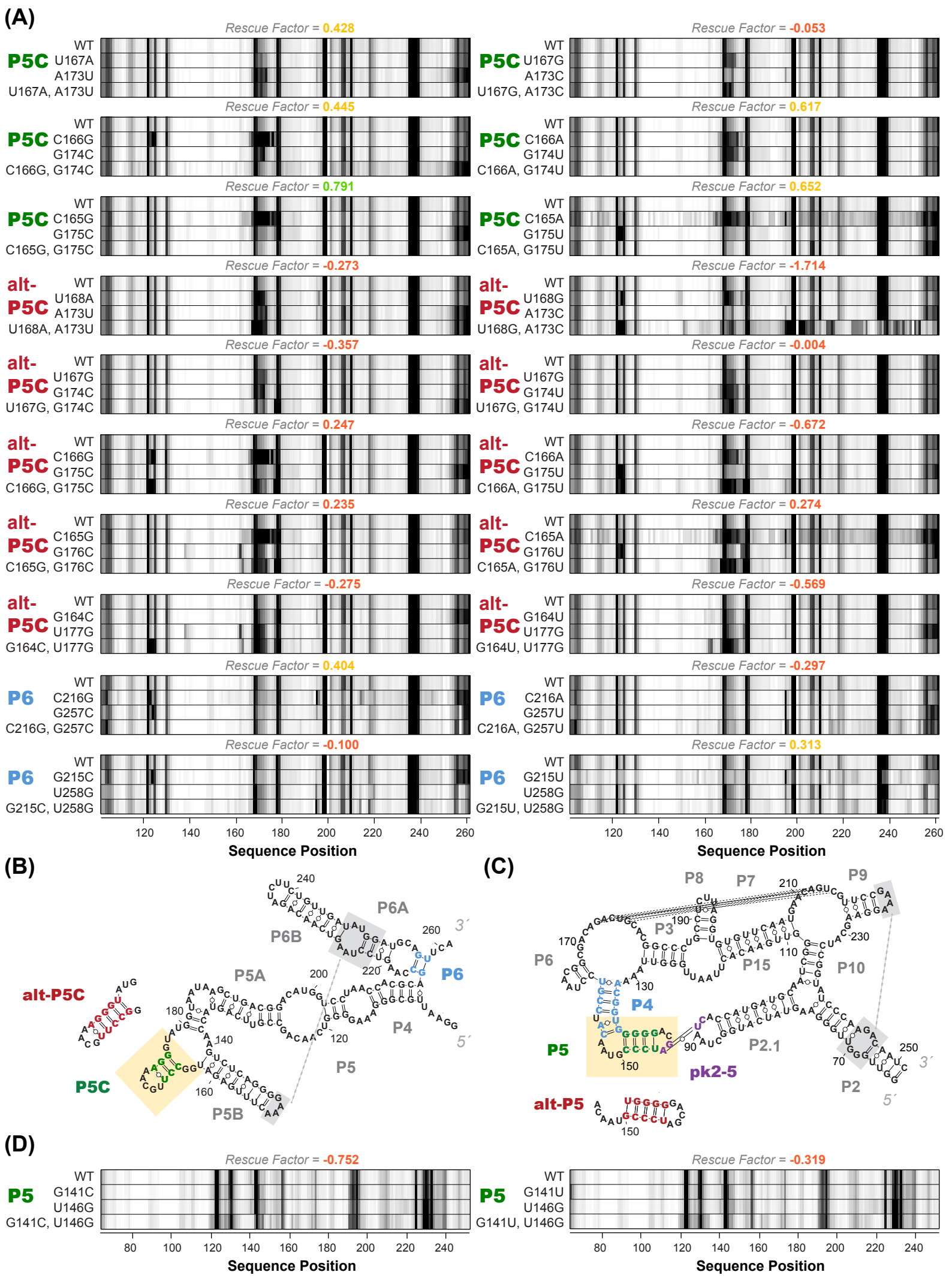
(A)
Rescue Factor = 0.428
P5C WT U167A A173U U167A, A173U
Rescue Factor = -0.053
P5C WT U167G A173C U167G, A173C
Rescue Factor = 0.445
P5C WT C166G G174C C166G, G174C
Rescue Factor = 0.617
P5C WT C166A G174U C166A, G174U
Rescue Factor = 0.791
P5C WT C165G G175C C165G, G175C
Rescue Factor = 0.652
P5C WT C165A G175U C165A, G175U
Rescue Factor = -0.273
alt-P5C WT U168A A173U U168A, A173U
Rescue Factor = -1.714
alt-P5C WT U168G A173C U168G, A173C
Rescue Factor = -0.357
alt-P5C WT U167G G174C U167G, G174C
Rescue Factor = -0.004
alt-P5C WT U167G G174U U167G, G174U
Rescue Factor = 0.247
alt-P5C WT C166G G175C C166G, G175C
Rescue Factor = -0.672
alt-P5C WT C166A G175U C166A, G175U
Rescue Factor = 0.235
alt-P5C WT C165G G176C C165G, G176C
Rescue Factor = 0.274
alt-P5C WT C165A G176U C165A, G176U
Rescue Factor = -0.275
alt-P5C WT G164C U177G G164C, U177G
Rescue Factor = -0.569
alt-P5C WT G164U U177G G164U, U177G
Rescue Factor = 0.404
P6 WT C216G G257C C216G, G257C
Rescue Factor = -0.297
P6 WT C216A G257U C216A, G257U
Rescue Factor = -0.100
P6 WT G215C U258G G215C, U258G
Rescue Factor = 0.313
P6 WT G215U U258G G215U, U258G
120 140 160 180 200 220 240 260
Sequence Position
(B)
alt-P5C
P5C
P5A
P5B
P5
P6A
P6B
P6
P4
3´
5´
(C)
P8
P7
P9
P3
P6
P15
P10
P4
P5
P2.1
pk2-5
P2
alt-P5
3´
5´
(D)
Rescue Factor = -0.752
P5 WT G141C U146G G141C, U146G
Rescue Factor = -0.319
P5 WT G141U U146G G141U, U146G
80 100 120 140 160 180 200 220 240
Sequence Position

SI Figure S2

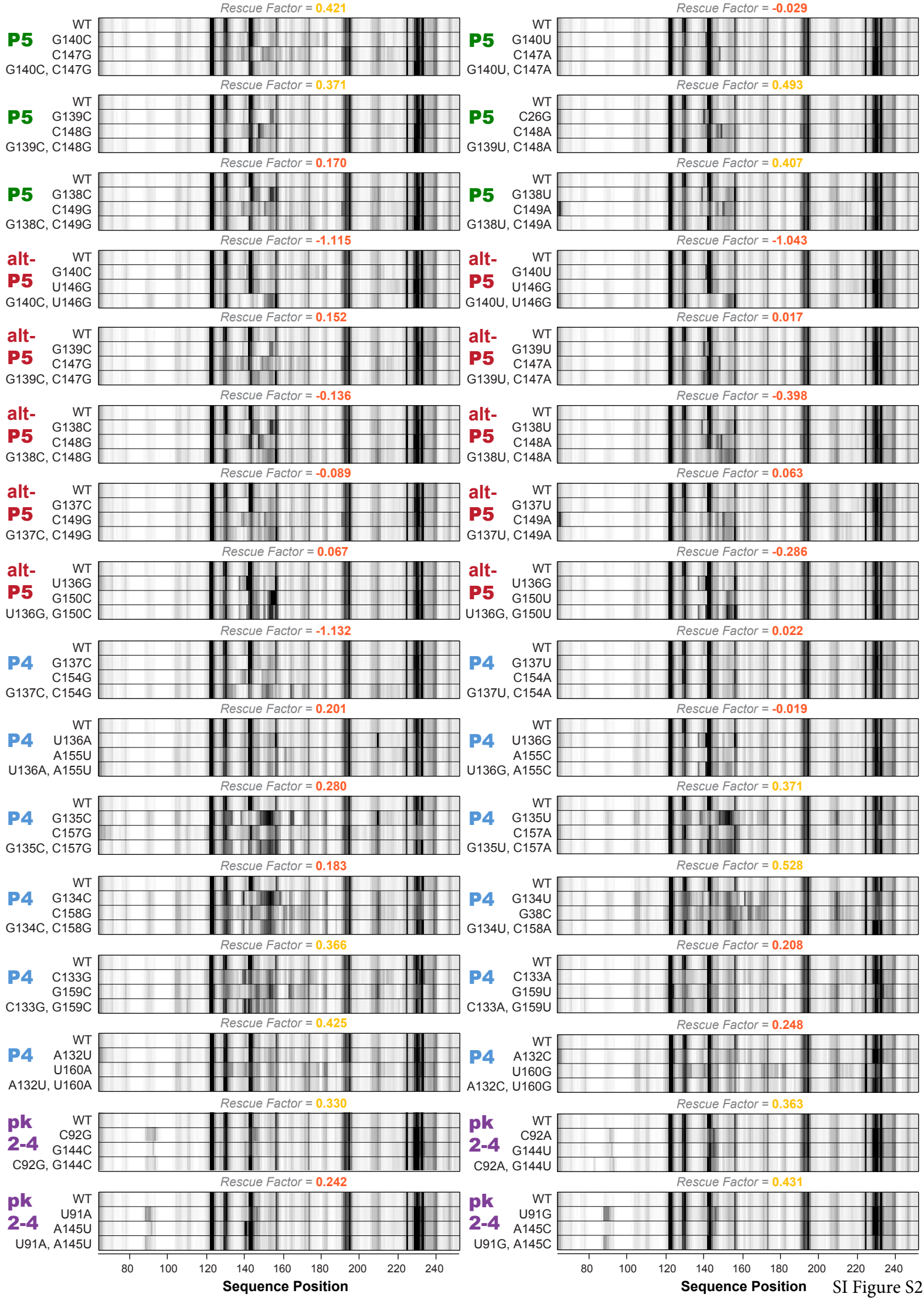
Rescue Factor = 0.421
P5
WT
G140C
C147G
G140C, C147G
Rescue Factor = -0.029
P5
WT
G140U
C147A
G140U, C147A
Rescue Factor = 0.371
P5
WT
G139C
C148G
G139C, C148G
Rescue Factor = 0.493
P5
WT
C26G
C148A
G139U, C148A
Rescue Factor = 0.170
P5
WT
G138C
C149G
G138C, C149G
Rescue Factor = 0.407
P5
WT
G138U
C149A
G138U, C149A
Rescue Factor = -1.115
alt-P5
WT
G140C
U146G
G140C, U146G
Rescue Factor = -1.043
alt-P5
WT
G140U
U146G
G140U, U146G
Rescue Factor = 0.152
alt-P5
WT
G139C
C147G
G139C, C147G
Rescue Factor = 0.017
alt-P5
WT
G139U
C147A
G139U, C147A
Rescue Factor = -0.136
alt-P5
WT
G138C
C148G
G138C, C148G
Rescue Factor = -0.398
alt-P5
WT
G138U
C148A
G138U, C148A
Rescue Factor = -0.089
alt-P5
WT
G137C
C149G
G137C, C149G
Rescue Factor = 0.063
alt-P5
WT
G137U
C149A
G137U, C149A
Rescue Factor = 0.067
alt-P5
WT
U136G
G150C
U136G, G150C
Rescue Factor = -0.286
alt-P5
WT
U136G
G150U
U136G, G150U
Rescue Factor = -1.132
P4
WT
G137C
C154G
G137C, C154G
Rescue Factor = 0.022
P4
WT
G137U
C154A
G137U, C154A
Rescue Factor = 0.201
P4
WT
U136A
A155U
U136A, A155U
Rescue Factor = -0.019
P4
WT
U136G
A155C
U136G, A155C
Rescue Factor = 0.280
P4
WT
G135C
C157G
G135C, C157G
Rescue Factor = 0.371
P4
WT
G135U
C157A
G135U, C157A
Rescue Factor = 0.183
P4
WT
G134C
C158G
G134C, C158G
Rescue Factor = 0.528
P4
WT
G134U
G38C
G134U, C158A
Rescue Factor = 0.366
P4
WT
C133G
G159C
C133G, G159C
Rescue Factor = 0.208
P4
WT
C133A
G159U
C133A, G159U
Rescue Factor = 0.425
P4
WT
A132U
U160A
A132U, U160A
Rescue Factor = 0.248
P4
WT
A132C
U160G
A132C, U160G
Rescue Factor = 0.330
pk 2-4
WT
C92G
G144C
C92G, G144C
Rescue Factor = 0.363
pk 2-4
WT
C92A
G144U
C92A, G144U
Rescue Factor = 0.242
pk 2-4
WT
U91A
A145U
U91A, A145U
Rescue Factor = 0.431
pk 2-4
WT
U91G
A145C
U91G, A145C
80
100
120
140
160
180
200
220
240
Sequence Position
Sequence Position

SI Figure S2

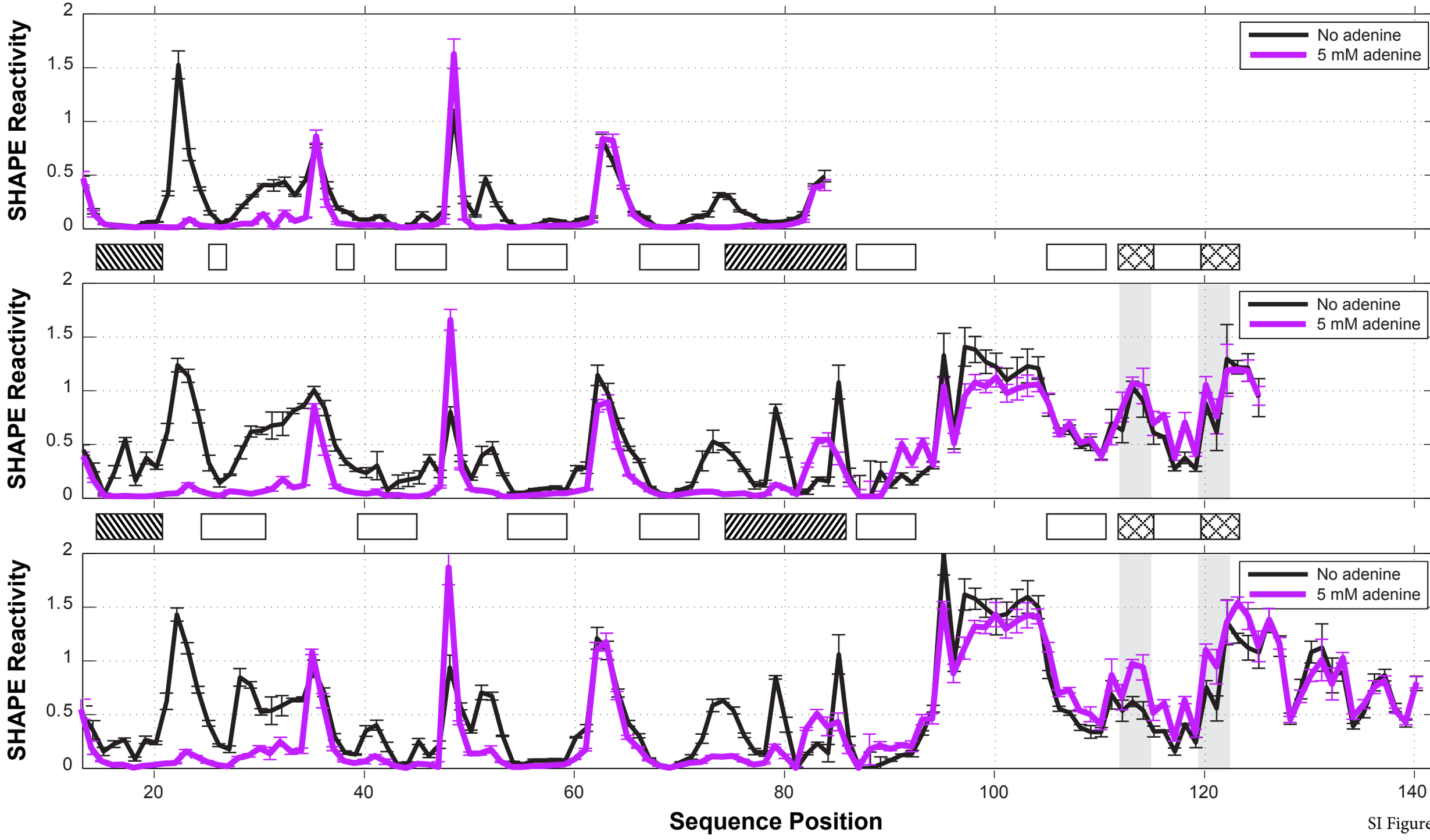
SHAPE Reactivity
No adenine
5 mM adenine
Sequence Position
0
0.5
1
1.5
2
20
40
60
80
100
120
140

SI Figure S3

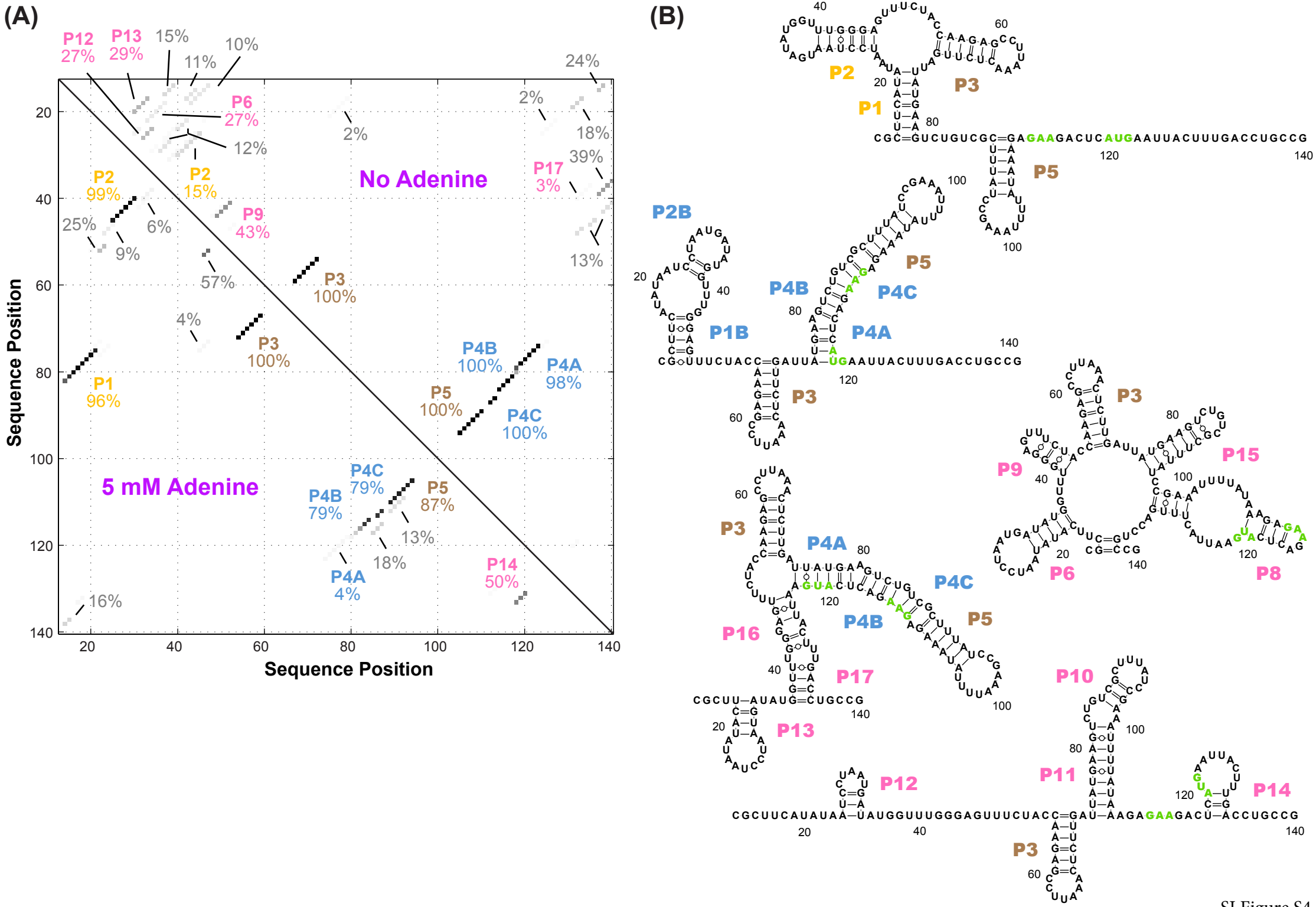
(A)
P12 27%
P13 29%
15%
11%
10%
24%
P6 27%
2%
2%
18%
12%
39%
P17 3%
P2 99%
P2 15%
No Adenine
P9 43%
25%
6%
9%
13%
57%
P3 100%
4%
P3 100%
P4B 100%
P4A 98%
P1 96%
P5 100%
P4C 100%
P4C 79%
5 mM Adenine
P4B 79%
P5 87%
13%
18%
P4A 4%
P14 50%
16%
Sequence Position
Sequence Position
(B)
P2
P3
P1
P5
P2B
P4B
P4C
P5
P1B
P4A
P3
P3
P9
P15
P6
P8
P3
P4A
P4C
P4B
P5
P16
P17
P10
P13
P12
P11
P14
P3

SI Figure S4

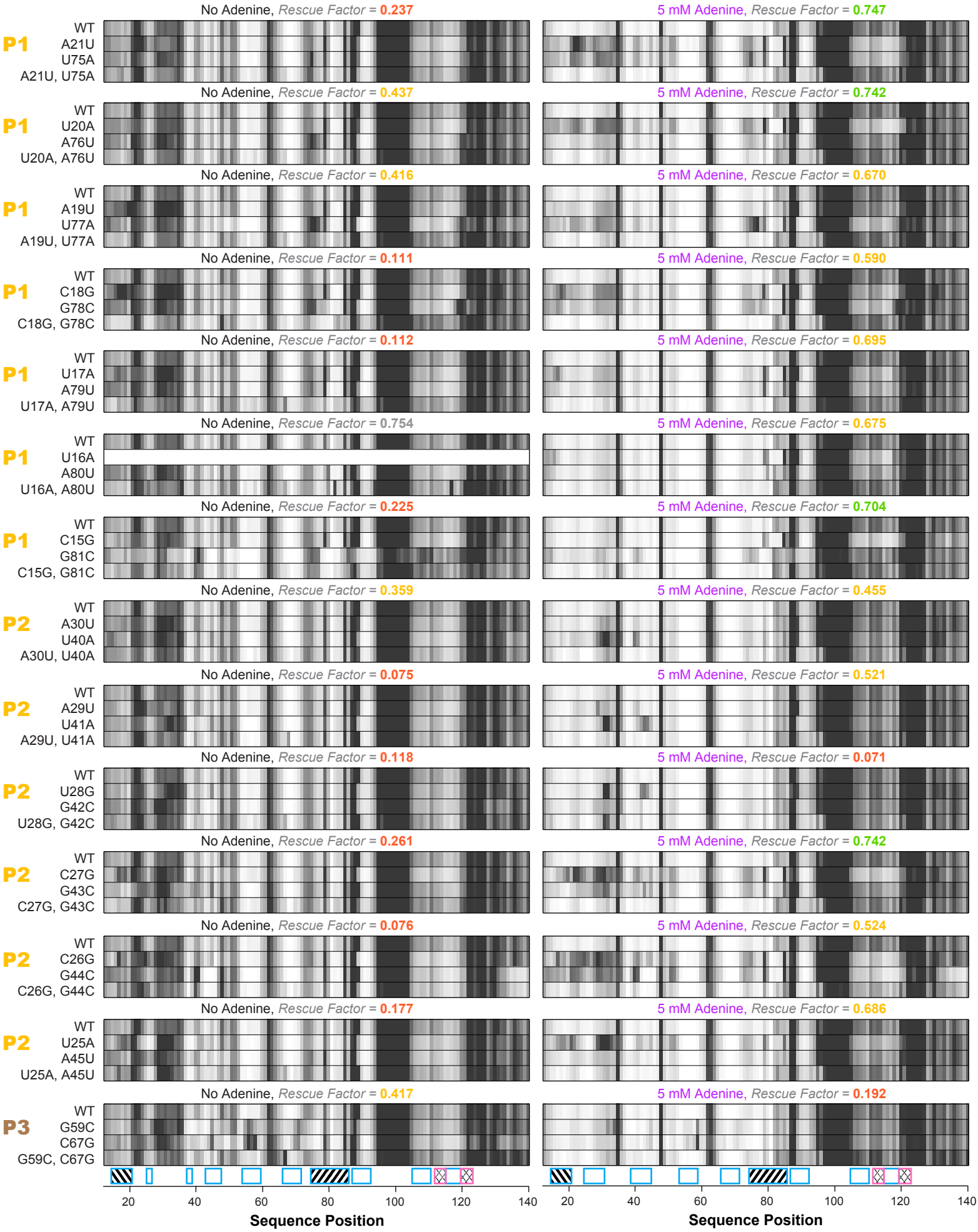
No Adenine, Rescue Factor = 0.237
5 mM Adenine, Rescue Factor = 0.747
P1
WT
A21U
U75A
A21U, U75A
No Adenine, Rescue Factor = 0.437
5 mM Adenine, Rescue Factor = 0.742
P1
WT
U20A
A76U
U20A, A76U
No Adenine, Rescue Factor = 0.416
5 mM Adenine, Rescue Factor = 0.670
P1
WT
A19U
U77A
A19U, U77A
No Adenine, Rescue Factor = 0.111
5 mM Adenine, Rescue Factor = 0.590
P1
WT
C18G
G78C
C18G, G78C
No Adenine, Rescue Factor = 0.112
5 mM Adenine, Rescue Factor = 0.695
P1
WT
U17A
A79U
U17A, A79U
No Adenine, Rescue Factor = 0.754
5 mM Adenine, Rescue Factor = 0.675
P1
WT
U16A
A80U
U16A, A80U
No Adenine, Rescue Factor = 0.225
5 mM Adenine, Rescue Factor = 0.704
P1
WT
C15G
G81C
C15G, G81C
No Adenine, Rescue Factor = 0.359
5 mM Adenine, Rescue Factor = 0.455
P2
WT
A30U
U40A
A30U, U40A
No Adenine, Rescue Factor = 0.075
5 mM Adenine, Rescue Factor = 0.521
P2
WT
A29U
U41A
A29U, U41A
No Adenine, Rescue Factor = 0.118
5 mM Adenine, Rescue Factor = 0.071
P2
WT
U28G
G42C
U28G, G42C
No Adenine, Rescue Factor = 0.261
5 mM Adenine, Rescue Factor = 0.742
P2
WT
C27G
G43C
C27G, G43C
No Adenine, Rescue Factor = 0.076
5 mM Adenine, Rescue Factor = 0.524
P2
WT
C26G
G44C
C26G, G44C
No Adenine, Rescue Factor = 0.177
5 mM Adenine, Rescue Factor = 0.686
P2
WT
U25A
A45U
U25A, A45U
No Adenine, Rescue Factor = 0.417
5 mM Adenine, Rescue Factor = 0.192
P3
WT
G59C
C67G
G59C, C67G
20
40
60
80
100
120
140
Sequence Position
Sequence Position

SI Figure S5

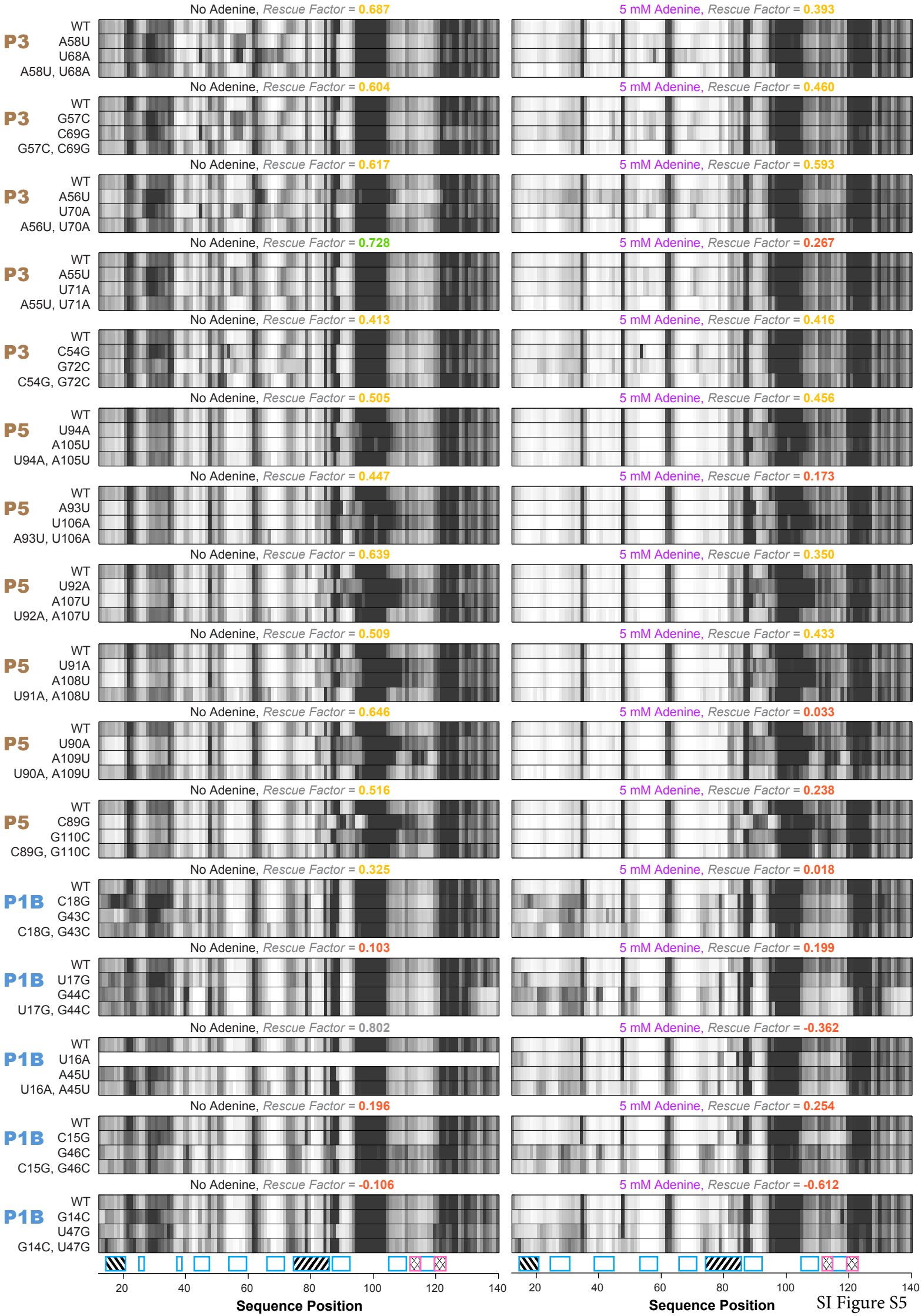
No Adenine, Rescue Factor = 0.687
5 mM Adenine, Rescue Factor = 0.393
P3
WT
A58U
U68A
A58U, U68A
No Adenine, Rescue Factor = 0.604
5 mM Adenine, Rescue Factor = 0.460
P3
WT
G57C
C69G
G57C, C69G
No Adenine, Rescue Factor = 0.617
5 mM Adenine, Rescue Factor = 0.593
P3
WT
A56U
U70A
A56U, U70A
No Adenine, Rescue Factor = 0.728
5 mM Adenine, Rescue Factor = 0.267
P3
WT
A55U
U71A
A55U, U71A
No Adenine, Rescue Factor = 0.413
5 mM Adenine, Rescue Factor = 0.416
P3
WT
C54G
G72C
C54G, G72C
No Adenine, Rescue Factor = 0.505
5 mM Adenine, Rescue Factor = 0.456
P5
WT
U94A
A105U
U94A, A105U
No Adenine, Rescue Factor = 0.447
5 mM Adenine, Rescue Factor = 0.173
P5
WT
A93U
U106A
A93U, U106A
No Adenine, Rescue Factor = 0.639
5 mM Adenine, Rescue Factor = 0.350
P5
WT
U92A
A107U
U92A, A107U
No Adenine, Rescue Factor = 0.509
5 mM Adenine, Rescue Factor = 0.433
P5
WT
U91A
A108U
U91A, A108U
No Adenine, Rescue Factor = 0.646
5 mM Adenine, Rescue Factor = 0.033
P5
WT
U90A
A109U
U90A, A109U
No Adenine, Rescue Factor = 0.516
5 mM Adenine, Rescue Factor = 0.238
P5
WT
C89G
G110C
C89G, G110C
No Adenine, Rescue Factor = 0.325
5 mM Adenine, Rescue Factor = 0.018
P1B
WT
C18G
G43C
C18G, G43C
No Adenine, Rescue Factor = 0.103
5 mM Adenine, Rescue Factor = 0.199
P1B
WT
U17G
G44C
U17G, G44C
No Adenine, Rescue Factor = 0.802
5 mM Adenine, Rescue Factor = -0.362
P1B
WT
U16A
A45U
U16A, A45U
No Adenine, Rescue Factor = 0.196
5 mM Adenine, Rescue Factor = 0.254
P1B
WT
C15G
G46C
C15G, G46C
No Adenine, Rescue Factor = -0.106
5 mM Adenine, Rescue Factor = -0.612
P1B
WT
G14C
U47G
G14C, U47G
20
40
60
80
100
120
140
Sequence Position
Sequence Position

SI Figure S5

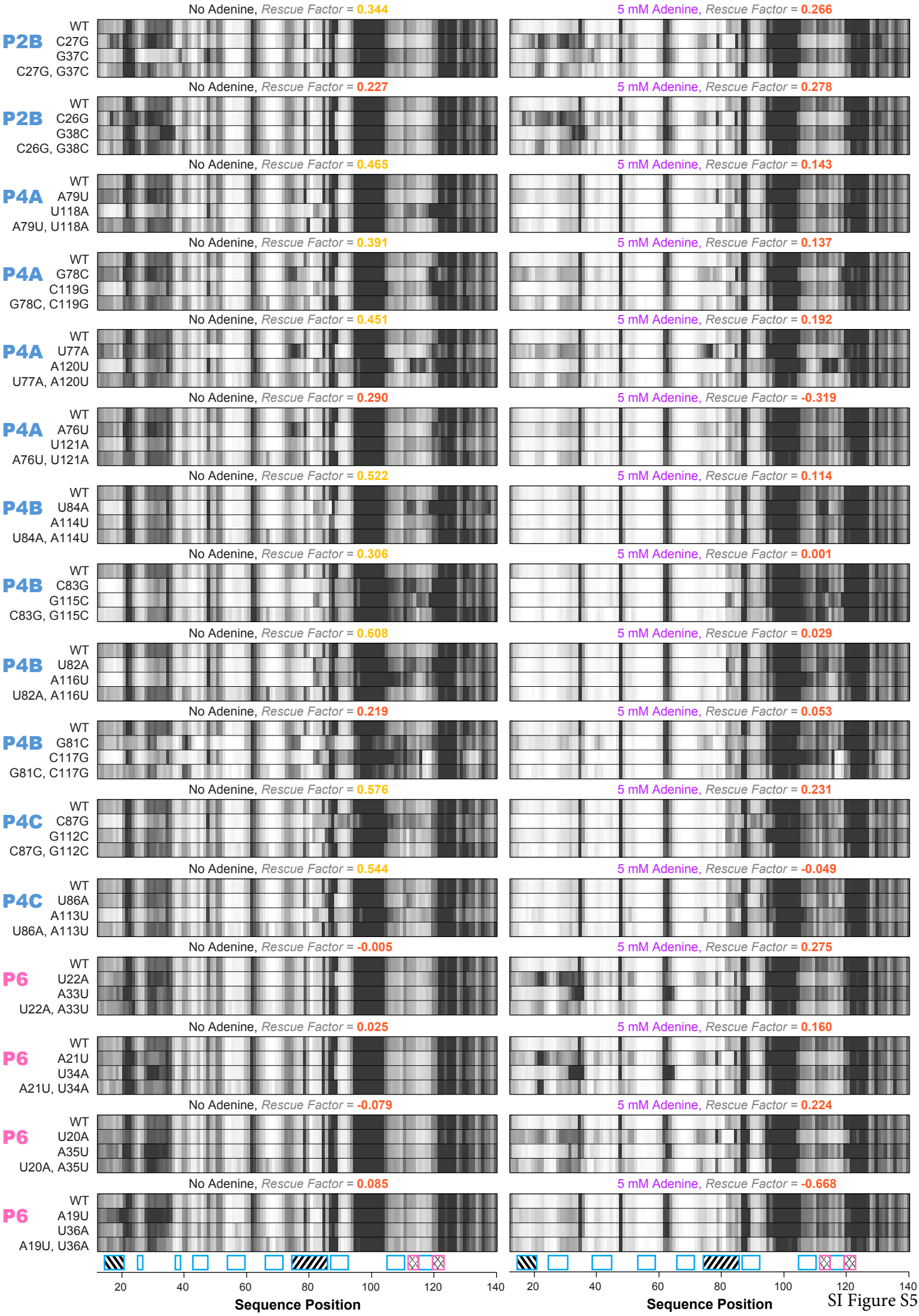
No Adenine, Rescue Factor = 0.344
5 mM Adenine, Rescue Factor = 0.266
P2B
WT
C27G
G37C
C27G, G37C
No Adenine, Rescue Factor = 0.227
5 mM Adenine, Rescue Factor = 0.278
P2B
WT
C26G
G38C
C26G, G38C
No Adenine, Rescue Factor = 0.465
5 mM Adenine, Rescue Factor = 0.143
P4A
WT
A79U
U118A
A79U, U118A
No Adenine, Rescue Factor = 0.391
5 mM Adenine, Rescue Factor = 0.137
P4A
WT
G78C
C119G
G78C, C119G
No Adenine, Rescue Factor = 0.451
5 mM Adenine, Rescue Factor = 0.192
P4A
WT
U77A
A120U
U77A, A120U
No Adenine, Rescue Factor = 0.290
5 mM Adenine, Rescue Factor = -0.319
P4A
WT
A76U
U121A
A76U, U121A
No Adenine, Rescue Factor = 0.522
5 mM Adenine, Rescue Factor = 0.114
P4B
WT
U84A
A114U
U84A, A114U
No Adenine, Rescue Factor = 0.306
5 mM Adenine, Rescue Factor = 0.001
P4B
WT
C83G
G115C
C83G, G115C
No Adenine, Rescue Factor = 0.608
5 mM Adenine, Rescue Factor = 0.029
P4B
WT
U82A
A116U
U82A, A116U
No Adenine, Rescue Factor = 0.219
5 mM Adenine, Rescue Factor = 0.053
P4B
WT
G81C
C117G
G81C, C117G
No Adenine, Rescue Factor = 0.576
5 mM Adenine, Rescue Factor = 0.231
P4C
WT
C87G
G112C
C87G, G112C
No Adenine, Rescue Factor = 0.544
5 mM Adenine, Rescue Factor = -0.049
P4C
WT
U86A
A113U
U86A, A113U
No Adenine, Rescue Factor = -0.005
5 mM Adenine, Rescue Factor = 0.275
P6
WT
U22A
A33U
U22A, A33U
No Adenine, Rescue Factor = 0.025
5 mM Adenine, Rescue Factor = 0.160
P6
WT
A21U
U34A
A21U, U34A
No Adenine, Rescue Factor = -0.079
5 mM Adenine, Rescue Factor = 0.224
P6
WT
U20A
A35U
U20A, A35U
No Adenine, Rescue Factor = 0.085
5 mM Adenine, Rescue Factor = -0.668
P6
WT
A19U
U36A
A19U, U36A
20
40
60
80
100
120
140
Sequence Position
Sequence Position

SI Figure S5

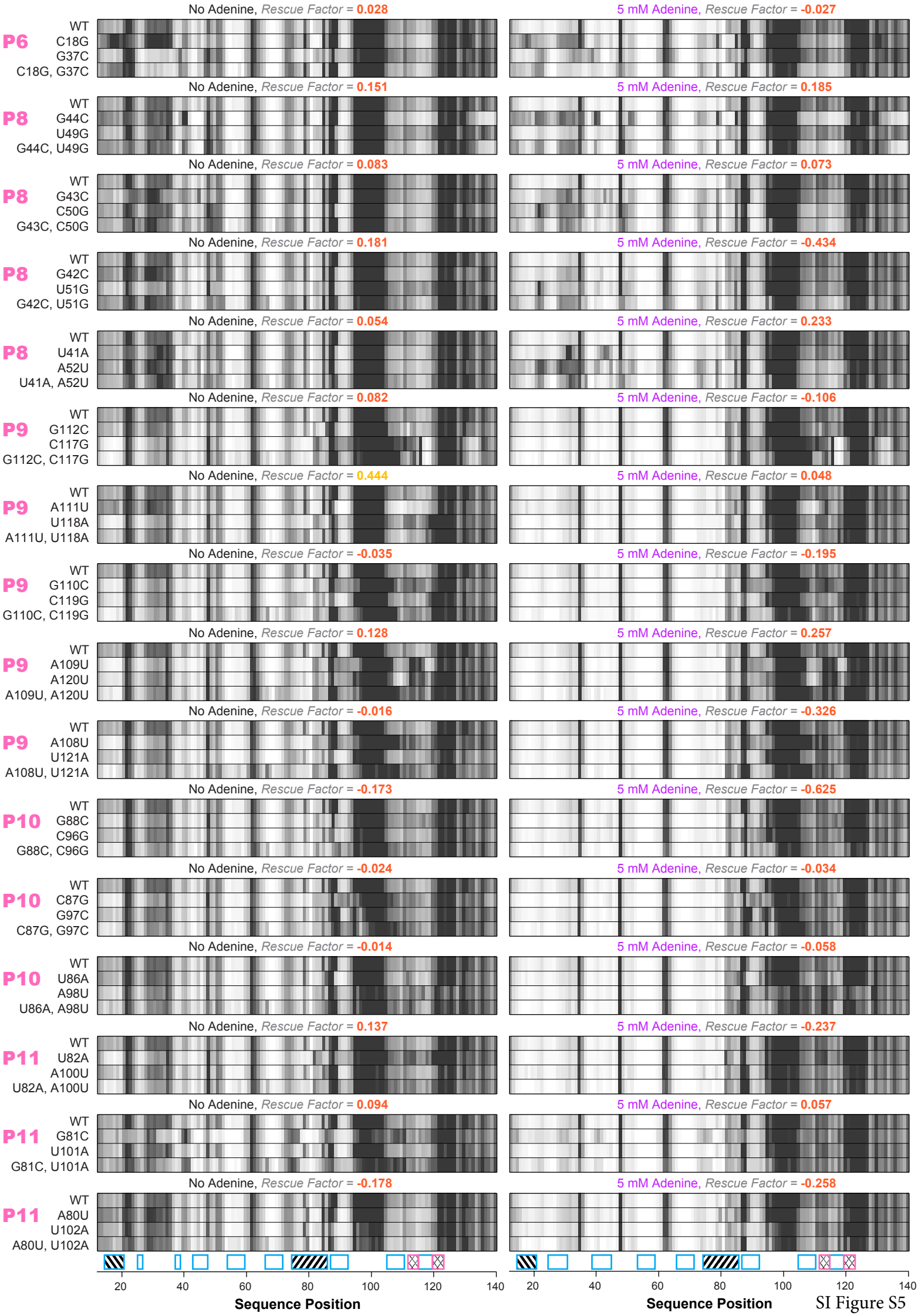
No Adenine, Rescue Factor = 0.028
5 mM Adenine, Rescue Factor = -0.027
P6
WT
C18G
G37C
C18G, G37C
No Adenine, Rescue Factor = 0.151
5 mM Adenine, Rescue Factor = 0.185
P8
WT
G44C
U49G
G44C, U49G
No Adenine, Rescue Factor = 0.083
5 mM Adenine, Rescue Factor = 0.073
P8
WT
G43C
C50G
G43C, C50G
No Adenine, Rescue Factor = 0.181
5 mM Adenine, Rescue Factor = -0.434
P8
WT
G42C
U51G
G42C, U51G
No Adenine, Rescue Factor = 0.054
5 mM Adenine, Rescue Factor = 0.233
P8
WT
U41A
A52U
U41A, A52U
No Adenine, Rescue Factor = 0.082
5 mM Adenine, Rescue Factor = -0.106
P9
WT
G112C
C117G
G112C, C117G
No Adenine, Rescue Factor = 0.444
5 mM Adenine, Rescue Factor = 0.048
P9
WT
A111U
U118A
A111U, U118A
No Adenine, Rescue Factor = -0.035
5 mM Adenine, Rescue Factor = -0.195
P9
WT
G110C
C119G
G110C, C119G
No Adenine, Rescue Factor = 0.128
5 mM Adenine, Rescue Factor = 0.257
P9
WT
A109U
A120U
A109U, A120U
No Adenine, Rescue Factor = -0.016
5 mM Adenine, Rescue Factor = -0.326
P9
WT
A108U
U121A
A108U, U121A
No Adenine, Rescue Factor = -0.173
5 mM Adenine, Rescue Factor = -0.625
P10
WT
G88C
C96G
G88C, C96G
No Adenine, Rescue Factor = -0.024
5 mM Adenine, Rescue Factor = -0.034
P10
WT
C87G
G97C
C87G, G97C
No Adenine, Rescue Factor = -0.014
5 mM Adenine, Rescue Factor = -0.058
P10
WT
U86A
A98U
U86A, A98U
No Adenine, Rescue Factor = 0.137
5 mM Adenine, Rescue Factor = -0.237
P11
WT
U82A
A100U
U82A, A100U
No Adenine, Rescue Factor = 0.094
5 mM Adenine, Rescue Factor = 0.057
P11
WT
G81C
U101A
G81C, U101A
No Adenine, Rescue Factor = -0.178
5 mM Adenine, Rescue Factor = -0.258
P11
WT
A80U
U102A
A80U, U102A
20
40
60
80
100
120
140
Sequence Position
Sequence Position

SI Figure S5

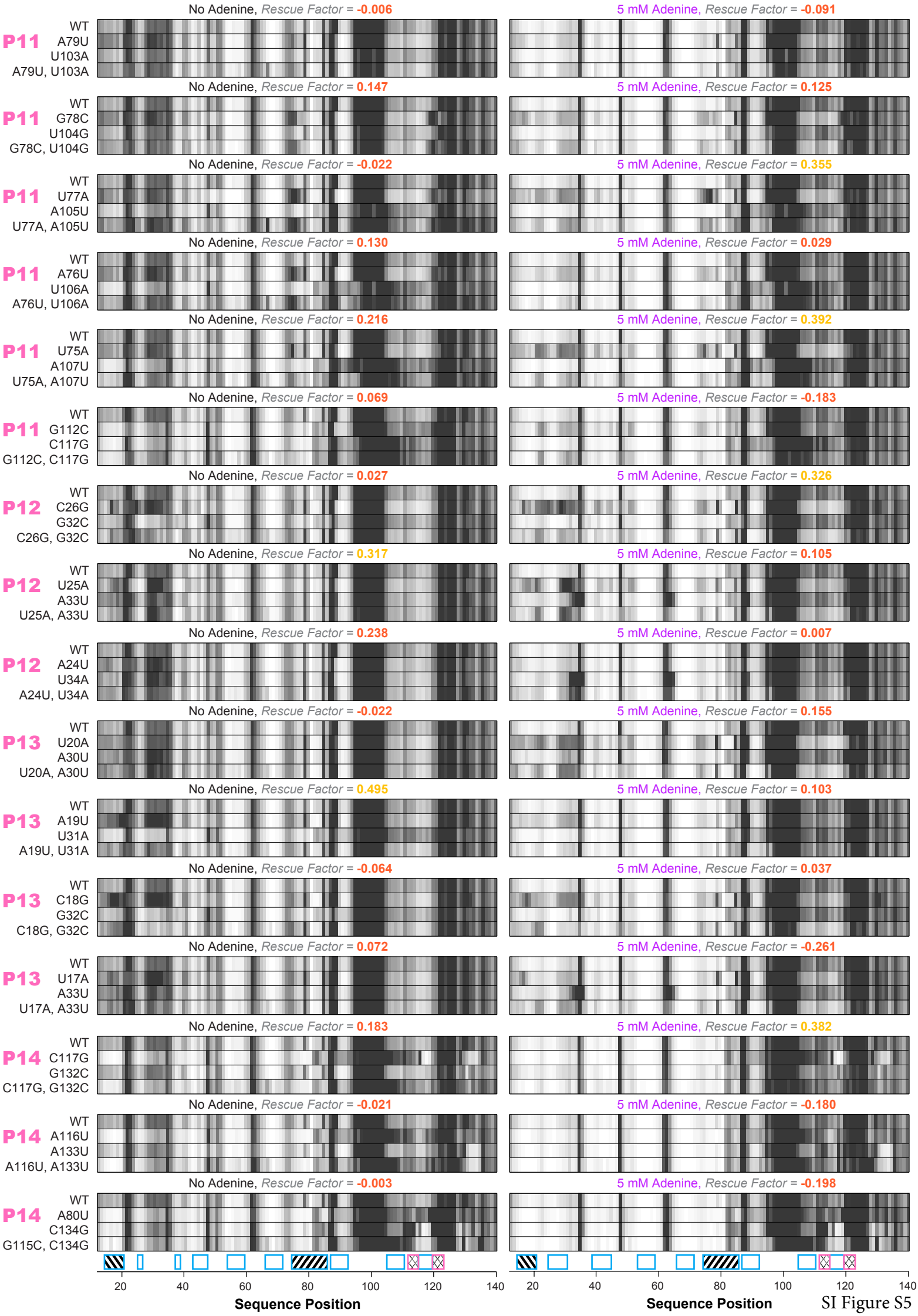
No Adenine, Rescue Factor = -0.006
5 mM Adenine, Rescue Factor = -0.091
P11 WT A79U U103A A79U, U103A
No Adenine, Rescue Factor = 0.147
5 mM Adenine, Rescue Factor = 0.125
P11 WT G78C U104G G78C, U104G
No Adenine, Rescue Factor = -0.022
5 mM Adenine, Rescue Factor = 0.355
P11 WT U77A A105U U77A, A105U
No Adenine, Rescue Factor = 0.130
5 mM Adenine, Rescue Factor = 0.029
P11 WT A76U U106A A76U, U106A
No Adenine, Rescue Factor = 0.216
5 mM Adenine, Rescue Factor = 0.392
P11 WT U75A A107U U75A, A107U
No Adenine, Rescue Factor = 0.069
5 mM Adenine, Rescue Factor = -0.183
P11 WT G112C C117G G112C, C117G
No Adenine, Rescue Factor = 0.027
5 mM Adenine, Rescue Factor = 0.326
P12 WT C26G G32C C26G, G32C
No Adenine, Rescue Factor = 0.317
5 mM Adenine, Rescue Factor = 0.105
P12 WT U25A A33U U25A, A33U
No Adenine, Rescue Factor = 0.238
5 mM Adenine, Rescue Factor = 0.007
P12 WT A24U U34A A24U, U34A
No Adenine, Rescue Factor = -0.022
5 mM Adenine, Rescue Factor = 0.155
P13 WT U20A A30U U20A, A30U
No Adenine, Rescue Factor = 0.495
5 mM Adenine, Rescue Factor = 0.103
P13 WT A19U U31A A19U, U31A
No Adenine, Rescue Factor = -0.064
5 mM Adenine, Rescue Factor = 0.037
P13 WT C18G G32C C18G, G32C
No Adenine, Rescue Factor = 0.072
5 mM Adenine, Rescue Factor = -0.261
P13 WT U17A A33U U17A, A33U
No Adenine, Rescue Factor = 0.183
5 mM Adenine, Rescue Factor = 0.382
P14 WT C117G G132C C117G, G132C
No Adenine, Rescue Factor = -0.021
5 mM Adenine, Rescue Factor = -0.180
P14 WT A116U A133U A116U, A133U
No Adenine, Rescue Factor = -0.003
5 mM Adenine, Rescue Factor = -0.198
P14 WT A80U C134G G115C, C134G
20 40 60 80 100 120 140
Sequence Position
20 40 60 80 100 120 140
Sequence Position

SI Figure S5

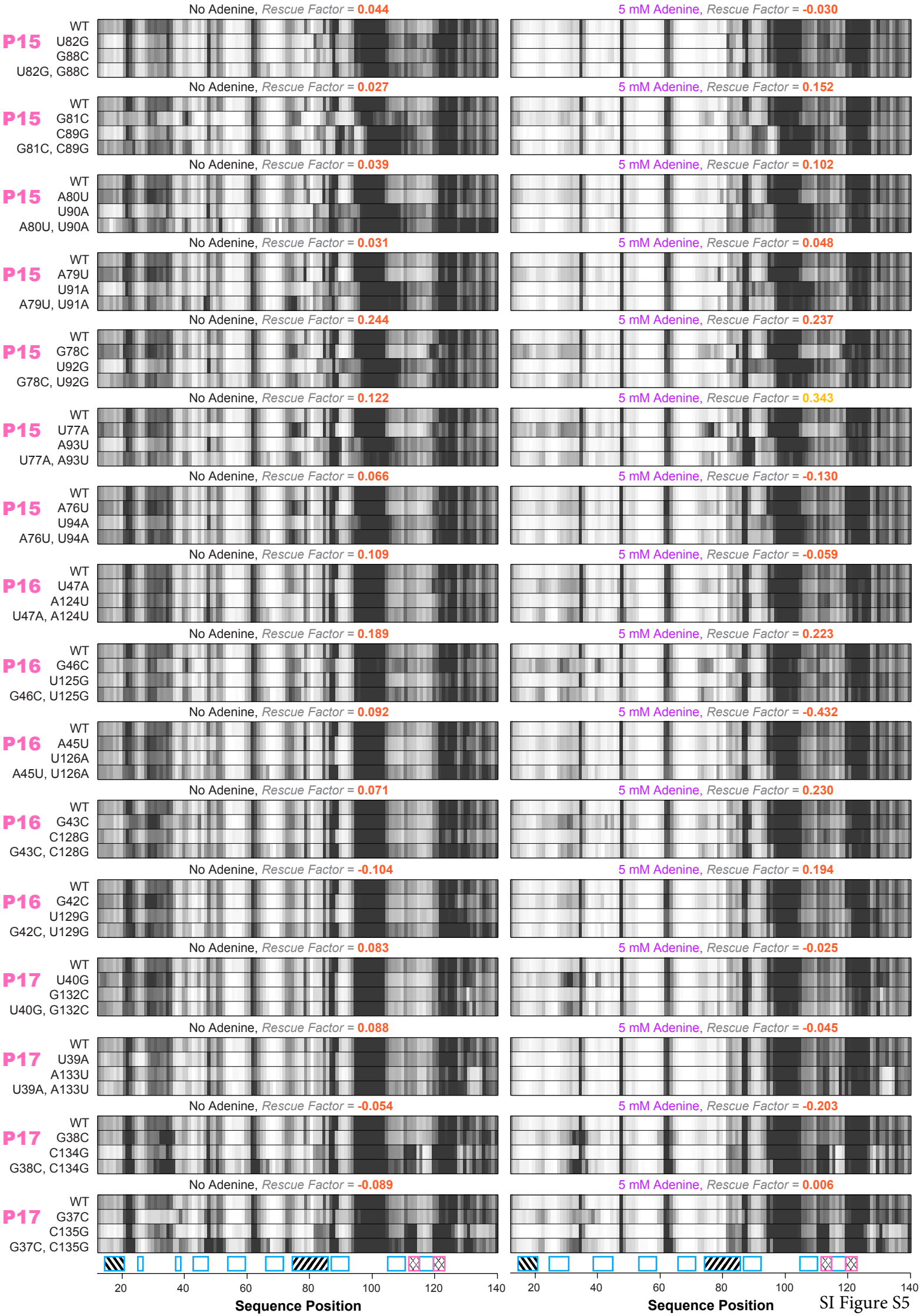
No Adenine, Rescue Factor = 0.044
5 mM Adenine, Rescue Factor = -0.030
P15
WT
U82G
G88C
U82G, G88C
No Adenine, Rescue Factor = 0.027
5 mM Adenine, Rescue Factor = 0.152
P15
WT
G81C
C89G
G81C, C89G
No Adenine, Rescue Factor = 0.039
5 mM Adenine, Rescue Factor = 0.102
P15
WT
A80U
U90A
A80U, U90A
No Adenine, Rescue Factor = 0.031
5 mM Adenine, Rescue Factor = 0.048
P15
WT
A79U
U91A
A79U, U91A
No Adenine, Rescue Factor = 0.244
5 mM Adenine, Rescue Factor = 0.237
P15
WT
G78C
U92G
G78C, U92G
No Adenine, Rescue Factor = 0.122
5 mM Adenine, Rescue Factor = 0.343
P15
WT
U77A
A93U
U77A, A93U
No Adenine, Rescue Factor = 0.066
5 mM Adenine, Rescue Factor = -0.130
P15
WT
A76U
U94A
A76U, U94A
No Adenine, Rescue Factor = 0.109
5 mM Adenine, Rescue Factor = -0.059
P16
WT
U47A
A124U
U47A, A124U
No Adenine, Rescue Factor = 0.189
5 mM Adenine, Rescue Factor = 0.223
P16
WT
G46C
U125G
G46C, U125G
No Adenine, Rescue Factor = 0.092
5 mM Adenine, Rescue Factor = -0.432
P16
WT
A45U
U126A
A45U, U126A
No Adenine, Rescue Factor = 0.071
5 mM Adenine, Rescue Factor = 0.230
P16
WT
G43C
C128G
G43C, C128G
No Adenine, Rescue Factor = -0.104
5 mM Adenine, Rescue Factor = 0.194
P16
WT
G42C
U129G
G42C, U129G
No Adenine, Rescue Factor = 0.083
5 mM Adenine, Rescue Factor = -0.025
P17
WT
U40G
G132C
U40G, G132C
No Adenine, Rescue Factor = 0.088
5 mM Adenine, Rescue Factor = -0.045
P17
WT
U39A
A133U
U39A, A133U
No Adenine, Rescue Factor = -0.054
5 mM Adenine, Rescue Factor = -0.203
P17
WT
G38C
C134G
G38C, C134G
No Adenine, Rescue Factor = -0.089
5 mM Adenine, Rescue Factor = 0.006
P17
WT
G37C
C135G
G37C, C135G
20
40
60
80
100
120
140
Sequence Position
Sequence Position

SI Figure S5

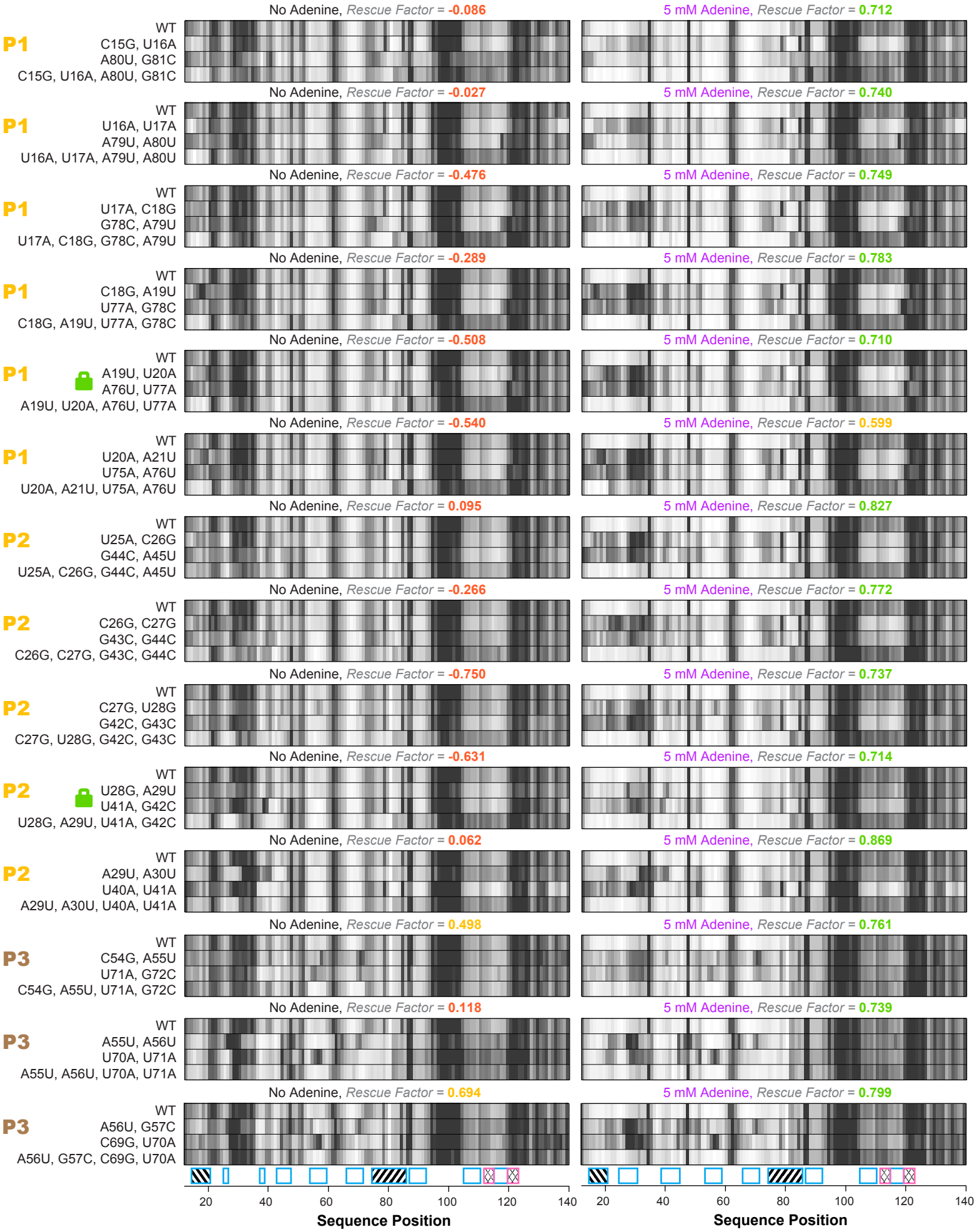
No Adenine, Rescue Factor = -0.086
5 mM Adenine, Rescue Factor = 0.712
P1
WT
C15G, U16A
A80U, G81C
C15G, U16A, A80U, G81C
No Adenine, Rescue Factor = -0.027
5 mM Adenine, Rescue Factor = 0.740
P1
WT
U16A, U17A
A79U, A80U
U16A, U17A, A79U, A80U
No Adenine, Rescue Factor = -0.476
5 mM Adenine, Rescue Factor = 0.749
P1
WT
U17A, C18G
G78C, A79U
U17A, C18G, G78C, A79U
No Adenine, Rescue Factor = -0.289
5 mM Adenine, Rescue Factor = 0.783
P1
WT
C18G, A19U
U77A, G78C
C18G, A19U, U77A, G78C
No Adenine, Rescue Factor = -0.508
5 mM Adenine, Rescue Factor = 0.710
P1
WT
A19U, U20A
A76U, U77A
A19U, U20A, A76U, U77A
No Adenine, Rescue Factor = -0.540
5 mM Adenine, Rescue Factor = 0.599
P1
WT
U20A, A21U
U75A, A76U
U20A, A21U, U75A, A76U
No Adenine, Rescue Factor = 0.095
5 mM Adenine, Rescue Factor = 0.827
P2
WT
U25A, C26G
G44C, A45U
U25A, C26G, G44C, A45U
No Adenine, Rescue Factor = -0.266
5 mM Adenine, Rescue Factor = 0.772
P2
WT
C26G, C27G
G43C, G44C
C26G, C27G, G43C, G44C
No Adenine, Rescue Factor = -0.750
5 mM Adenine, Rescue Factor = 0.737
P2
WT
C27G, U28G
G42C, G43C
C27G, U28G, G42C, G43C
No Adenine, Rescue Factor = -0.631
5 mM Adenine, Rescue Factor = 0.714
P2
WT
U28G, A29U
U41A, G42C
U28G, A29U, U41A, G42C
No Adenine, Rescue Factor = 0.062
5 mM Adenine, Rescue Factor = 0.869
P2
WT
A29U, A30U
U40A, U41A
A29U, A30U, U40A, U41A
No Adenine, Rescue Factor = 0.498
5 mM Adenine, Rescue Factor = 0.761
P3
WT
C54G, A55U
U71A, G72C
C54G, A55U, U71A, G72C
No Adenine, Rescue Factor = 0.118
5 mM Adenine, Rescue Factor = 0.739
P3
WT
A55U, A56U
U70A, U71A
A55U, A56U, U70A, U71A
No Adenine, Rescue Factor = 0.694
5 mM Adenine, Rescue Factor = 0.799
P3
WT
A56U, G57C
C69G, U70A
A56U, G57C, C69G, U70A
20
40
60
80
100
120
140
Sequence Position
Sequence Position

SI Figure S6

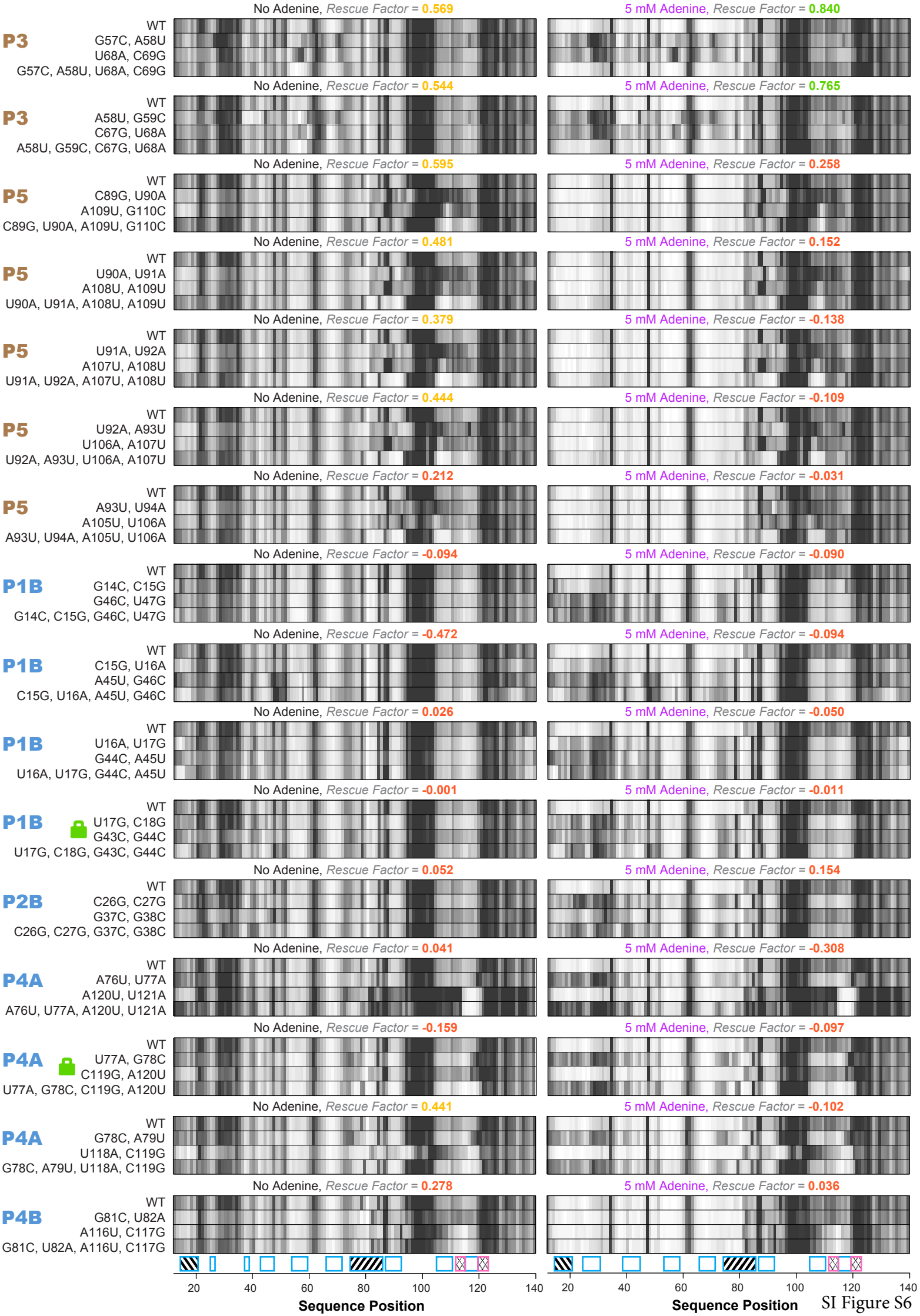
P3
WT
G57C, A58U
U68A, C69G
G57C, A58U, U68A, C69G
No Adenine, Rescue Factor = 0.569
5 mM Adenine, Rescue Factor = 0.840
P3
WT
A58U, G59C
C67G, U68A
A58U, G59C, C67G, U68A
No Adenine, Rescue Factor = 0.544
5 mM Adenine, Rescue Factor = 0.765
P5
WT
C89G, U90A
A109U, G110C
C89G, U90A, A109U, G110C
No Adenine, Rescue Factor = 0.595
5 mM Adenine, Rescue Factor = 0.258
P5
WT
U90A, U91A
A108U, A109U
U90A, U91A, A108U, A109U
No Adenine, Rescue Factor = 0.481
5 mM Adenine, Rescue Factor = 0.152
P5
WT
U91A, U92A
A107U, A108U
U91A, U92A, A107U, A108U
No Adenine, Rescue Factor = 0.379
5 mM Adenine, Rescue Factor = -0.138
P5
WT
U92A, A93U
U106A, A107U
U92A, A93U, U106A, A107U
No Adenine, Rescue Factor = 0.444
5 mM Adenine, Rescue Factor = -0.109
P5
WT
A93U, U94A
A105U, U106A
A93U, U94A, A105U, U106A
No Adenine, Rescue Factor = 0.212
5 mM Adenine, Rescue Factor = -0.031
P1B
WT
G14C, C15G
G46C, U47G
G14C, C15G, G46C, U47G
No Adenine, Rescue Factor = -0.094
5 mM Adenine, Rescue Factor = -0.090
P1B
WT
C15G, U16A
A45U, G46C
C15G, U16A, A45U, G46C
No Adenine, Rescue Factor = -0.472
5 mM Adenine, Rescue Factor = -0.094
P1B
WT
U16A, U17G
G44C, A45U
U16A, U17G, G44C, A45U
No Adenine, Rescue Factor = 0.026
5 mM Adenine, Rescue Factor = -0.050
P1B
WT
U17G, C18G
G43C, G44C
U17G, C18G, G43C, G44C
No Adenine, Rescue Factor = -0.001
5 mM Adenine, Rescue Factor = -0.011
P2B
WT
C26G, C27G
G37C, G38C
C26G, C27G, G37C, G38C
No Adenine, Rescue Factor = 0.052
5 mM Adenine, Rescue Factor = 0.154
P4A
WT
A76U, U77A
A120U, U121A
A76U, U77A, A120U, U121A
No Adenine, Rescue Factor = 0.041
5 mM Adenine, Rescue Factor = -0.308
P4A
WT
U77A, G78C
C119G, A120U
U77A, G78C, C119G, A120U
No Adenine, Rescue Factor = -0.159
5 mM Adenine, Rescue Factor = -0.097
P4A
WT
G78C, A79U
U118A, C119G
G78C, A79U, U118A, C119G
No Adenine, Rescue Factor = 0.441
5 mM Adenine, Rescue Factor = -0.102
P4B
WT
G81C, U82A
A116U, C117G
G81C, U82A, A116U, C117G
No Adenine, Rescue Factor = 0.278
5 mM Adenine, Rescue Factor = 0.036
20
40
60
80
100
120
140
Sequence Position
Sequence Position

SI Figure S6

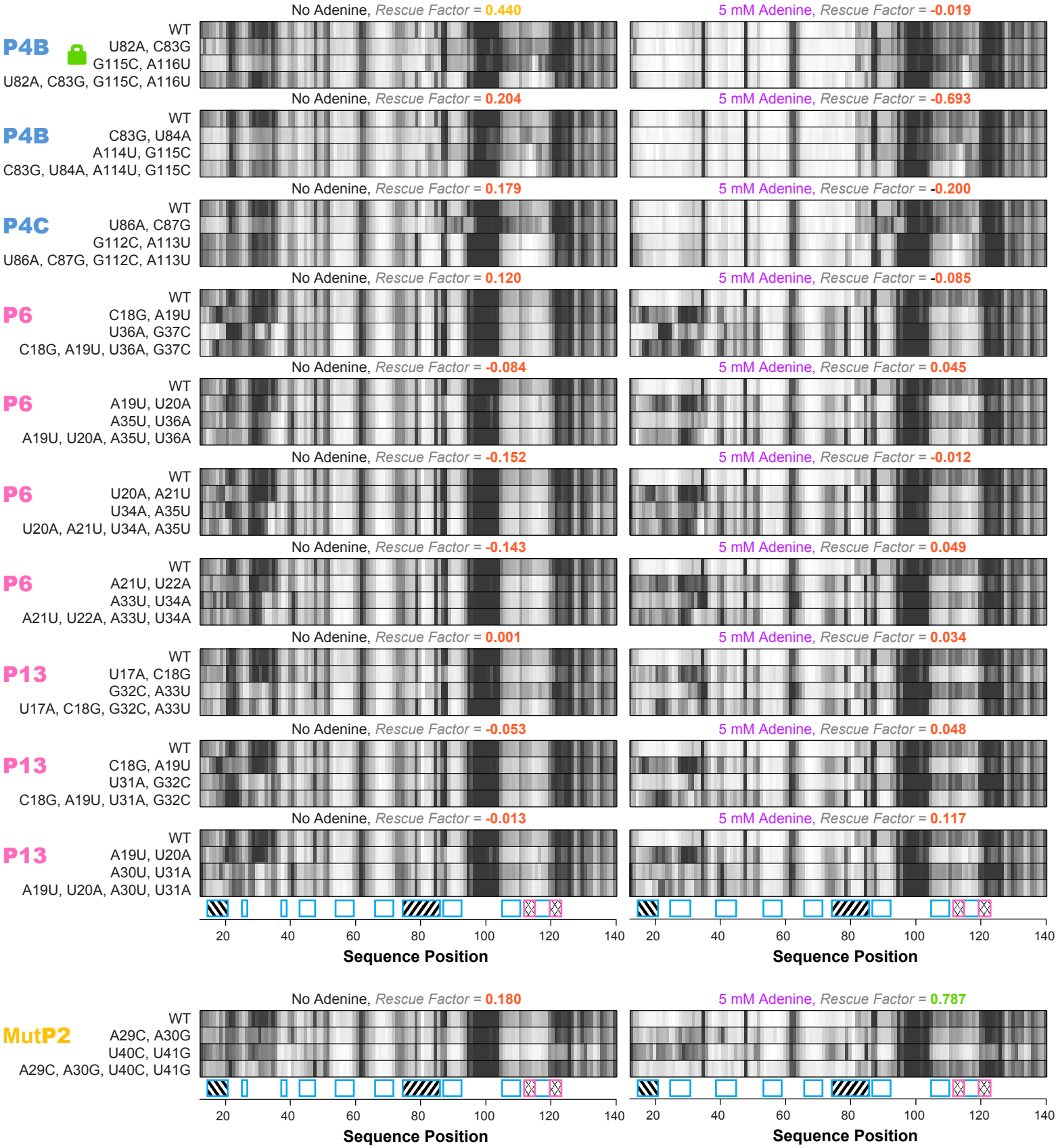
No Adenine, Rescue Factor = 0.440
5 mM Adenine, Rescue Factor = -0.019
P4B
WT
U82A, C83G
G115C, A116U
U82A, C83G, G115C, A116U
No Adenine, Rescue Factor = 0.204
5 mM Adenine, Rescue Factor = -0.693
P4B
WT
C83G, U84A
A114U, G115C
C83G, U84A, A114U, G115C
No Adenine, Rescue Factor = 0.179
5 mM Adenine, Rescue Factor = -0.200
P4C
WT
U86A, C87G
G112C, A113U
U86A, C87G, G112C, A113U
No Adenine, Rescue Factor = 0.120
5 mM Adenine, Rescue Factor = -0.085
P6
WT
C18G, A19U
U36A, G37C
C18G, A19U, U36A, G37C
No Adenine, Rescue Factor = -0.084
5 mM Adenine, Rescue Factor = 0.045
P6
WT
A19U, U20A
A35U, U36A
A19U, U20A, A35U, U36A
No Adenine, Rescue Factor = -0.152
5 mM Adenine, Rescue Factor = -0.012
P6
WT
U20A, A21U
U34A, A35U
U20A, A21U, U34A, A35U
No Adenine, Rescue Factor = -0.143
5 mM Adenine, Rescue Factor = 0.049
P6
WT
A21U, U22A
A33U, U34A
A21U, U22A, A33U, U34A
No Adenine, Rescue Factor = 0.001
5 mM Adenine, Rescue Factor = 0.034
P13
WT
U17A, C18G
G32C, A33U
U17A, C18G, G32C, A33U
No Adenine, Rescue Factor = -0.053
5 mM Adenine, Rescue Factor = 0.048
P13
WT
C18G, A19U
U31A, G32C
C18G, A19U, U31A, G32C
No Adenine, Rescue Factor = -0.013
5 mM Adenine, Rescue Factor = 0.117
P13
WT
A19U, U20A
A30U, U31A
A19U, U20A, A30U, U31A
20
40
60
80
100
120
140
Sequence Position
No Adenine, Rescue Factor = 0.180
5 mM Adenine, Rescue Factor = 0.787
MutP2
WT
A29C, A30G
U40C, U41G
A29C, A30G, U40C, U41G
Sequence Position

SI Figure S6

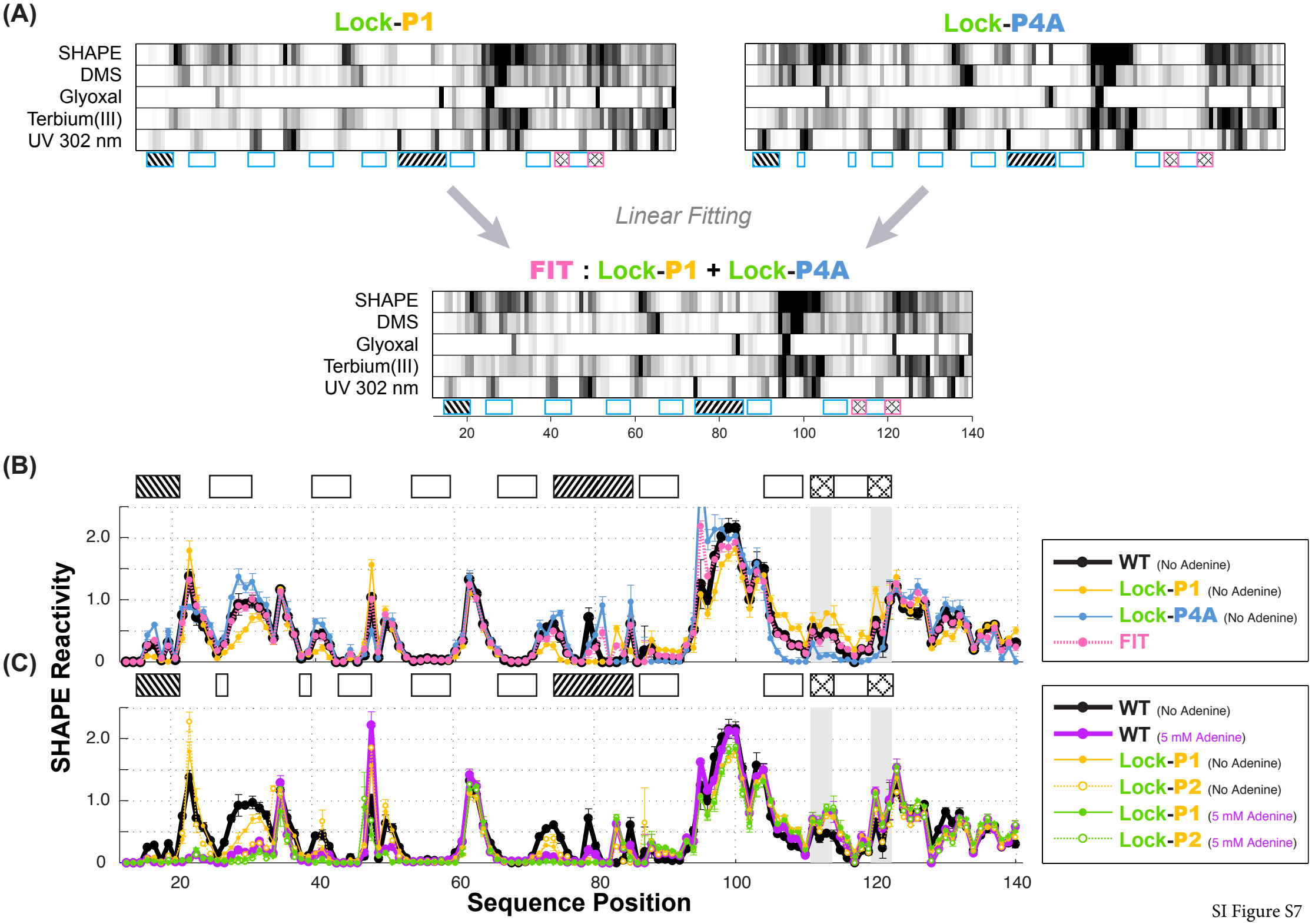
(A)
Lock-P1
Lock-P4A
SHAPE
DMS
Glyoxal
Terbium(III)
UV 302 nm
Linear Fitting
FIT : Lock-P1 + Lock-P4A
20
40
60
80
100
120
140
(B)
(C)
SHAPE Reactivity
2.0
1.0
0
WT (No Adenine)
Lock-P1 (No Adenine)
Lock-P4A (No Adenine)
FIT
WT (No Adenine)
WT (5 mM Adenine)
Lock-P1 (No Adenine)
Lock-P2 (No Adenine)
Lock-P1 (5 mM Adenine)
Lock-P2 (5 mM Adenine)
Sequence Position

SI Figure S7

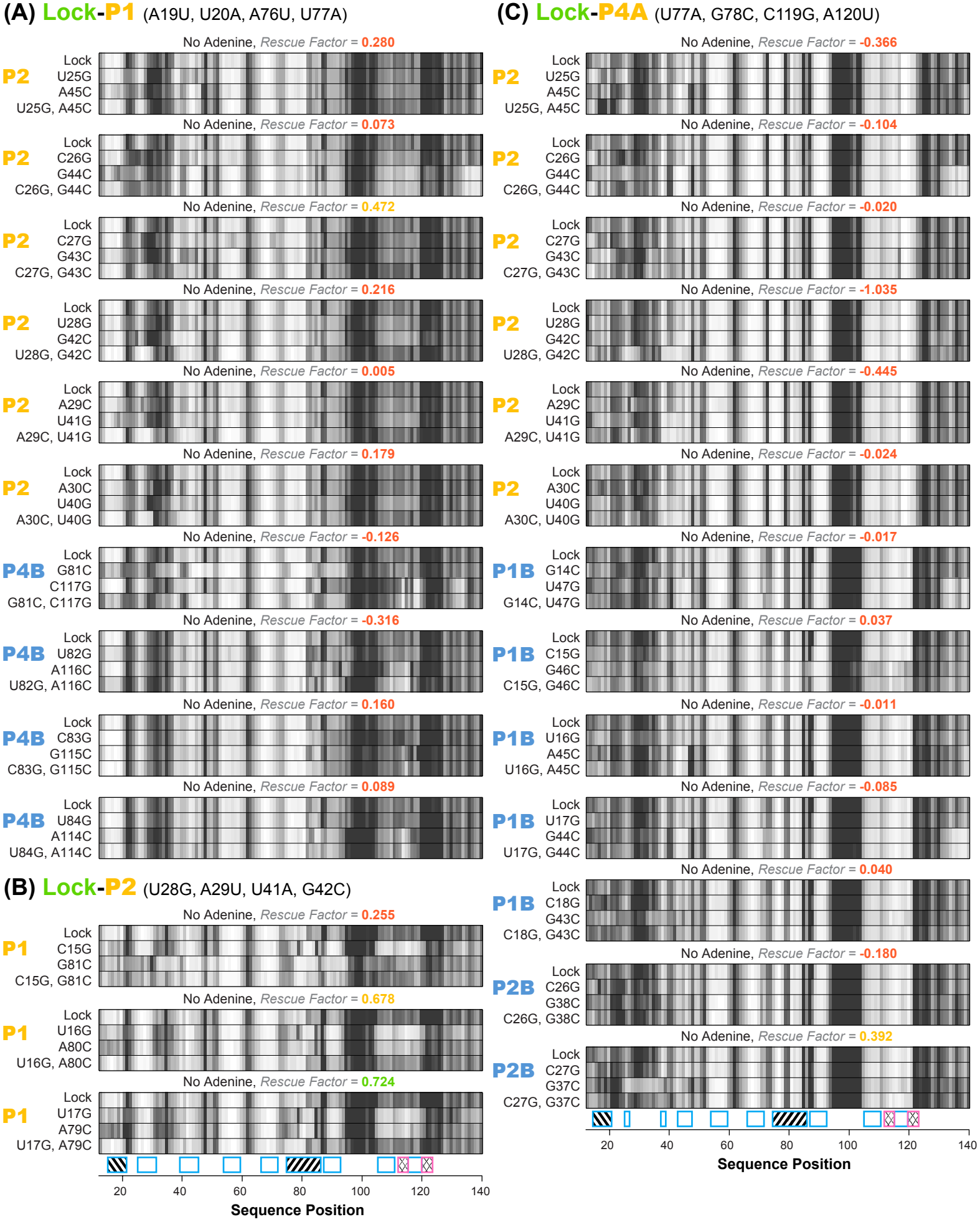
(A) Lock-P1 (A19U, U20A, A76U, U77A)
No Adenine, Rescue Factor = 0.280
P2 Lock U25G A45C U25G, A45C
No Adenine, Rescue Factor = 0.073
P2 Lock C26G G44C C26G, G44C
No Adenine, Rescue Factor = 0.472
P2 Lock C27G G43C C27G, G43C
No Adenine, Rescue Factor = 0.216
P2 Lock U28G G42C U28G, G42C
No Adenine, Rescue Factor = 0.005
P2 Lock A29C U41G A29C, U41G
No Adenine, Rescue Factor = 0.179
P2 Lock A30C U40G A30C, U40G
No Adenine, Rescue Factor = -0.126
P4B Lock G81C C117G G81C, C117G
No Adenine, Rescue Factor = -0.316
P4B Lock U82G A116C U82G, A116C
No Adenine, Rescue Factor = 0.160
P4B Lock C83G G115C C83G, G115C
No Adenine, Rescue Factor = 0.089
P4B Lock U84G A114C U84G, A114C
(B) Lock-P2 (U28G, A29U, U41A, G42C)
No Adenine, Rescue Factor = 0.255
P1 Lock C15G G81C C15G, G81C
No Adenine, Rescue Factor = 0.678
P1 Lock U16G A80C U16G, A80C
No Adenine, Rescue Factor = 0.724
P1 Lock U17G A79C U17G, A79C
20 40 60 80 100 120 140
Sequence Position
(C) Lock-P4A (U77A, G78C, C119G, A120U)
No Adenine, Rescue Factor = -0.366
P2 Lock U25G A45C U25G, A45C
No Adenine, Rescue Factor = -0.104
P2 Lock C26G G44C C26G, G44C
No Adenine, Rescue Factor = -0.020
P2 Lock C27G G43C C27G, G43C
No Adenine, Rescue Factor = -1.035
P2 Lock U28G G42C U28G, G42C
No Adenine, Rescue Factor = -0.445
P2 Lock A29C U41G A29C, U41G
No Adenine, Rescue Factor = -0.024
P2 Lock A30C U40G A30C, U40G
No Adenine, Rescue Factor = -0.017
P1B Lock G14C U47G G14C, U47G
No Adenine, Rescue Factor = 0.037
P1B Lock C15G G46C C15G, G46C
No Adenine, Rescue Factor = -0.011
P1B Lock U16G A45C U16G, A45C
No Adenine, Rescue Factor = -0.085
P1B Lock U17G G44C U17G, G44C
No Adenine, Rescue Factor = 0.040
P1B Lock C18G G43C C18G, G43C
No Adenine, Rescue Factor = -0.180
P2B Lock C26G G38C C26G, G38C
No Adenine, Rescue Factor = 0.392
P2B Lock C27G G37C C27G, G37C
20 40 60 80 100 120 140
Sequence Position

SI Figure S8

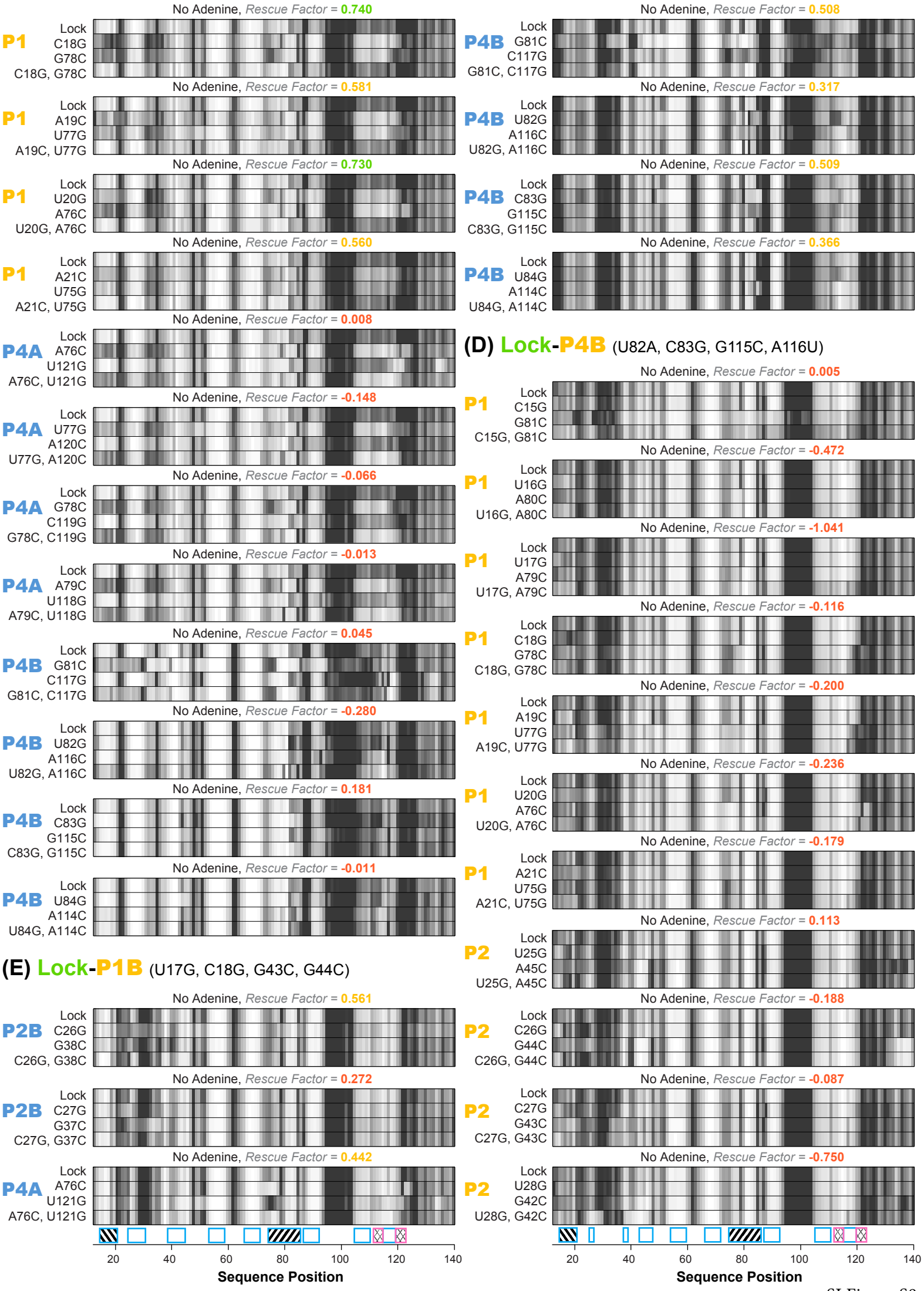
No Adenine, Rescue Factor = 0.740
P1 Lock C18G G78C C18G, G78C
No Adenine, Rescue Factor = 0.581
P1 Lock A19C U77G A19C, U77G
No Adenine, Rescue Factor = 0.730
P1 Lock U20G A76C U20G, A76C
No Adenine, Rescue Factor = 0.560
P1 Lock A21C U75G A21C, U75G
No Adenine, Rescue Factor = 0.008
P4A Lock A76C U121G A76C, U121G
No Adenine, Rescue Factor = -0.148
P4A Lock U77G A120C U77G, A120C
No Adenine, Rescue Factor = -0.066
P4A Lock G78C C119G G78C, C119G
No Adenine, Rescue Factor = -0.013
P4A Lock A79C U118G A79C, U118G
No Adenine, Rescue Factor = 0.045
P4B Lock G81C C117G G81C, C117G
No Adenine, Rescue Factor = -0.280
P4B Lock U82G A116C U82G, A116C
No Adenine, Rescue Factor = 0.181
P4B Lock C83G G115C C83G, G115C
No Adenine, Rescue Factor = -0.011
P4B Lock U84G A114C U84G, A114C
(E) Lock-P1B (U17G, C18G, G43C, G44C)
No Adenine, Rescue Factor = 0.561
P2B Lock C26G G38C C26G, G38C
No Adenine, Rescue Factor = 0.272
P2B Lock C27G G37C C27G, G37C
No Adenine, Rescue Factor = 0.442
P4A Lock A76C U121G A76C, U121G
20 40 60 80 100 120 140
Sequence Position
No Adenine, Rescue Factor = 0.508
P4B Lock G81C C117G G81C, C117G
No Adenine, Rescue Factor = 0.317
P4B Lock U82G A116C U82G, A116C
No Adenine, Rescue Factor = 0.509
P4B Lock C83G G115C C83G, G115C
No Adenine, Rescue Factor = 0.366
P4B Lock U84G A114C U84G, A114C
(D) Lock-P4B (U82A, C83G, G115C, A116U)
No Adenine, Rescue Factor = 0.005
P1 Lock C15G G81C C15G, G81C
No Adenine, Rescue Factor = -0.472
P1 Lock U16G A80C U16G, A80C
No Adenine, Rescue Factor = -1.041
P1 Lock U17G A79C U17G, A79C
No Adenine, Rescue Factor = -0.116
P1 Lock C18G G78C C18G, G78C
No Adenine, Rescue Factor = -0.200
P1 Lock A19C U77G A19C, U77G
No Adenine, Rescue Factor = -0.236
P1 Lock U20G A76C U20G, A76C
No Adenine, Rescue Factor = -0.179
P1 Lock A21C U75G A21C, U75G
No Adenine, Rescue Factor = 0.113
P2 Lock U25G A45C U25G, A45C
No Adenine, Rescue Factor = -0.188
P2 Lock C26G G44C C26G, G44C
No Adenine, Rescue Factor = -0.087
P2 Lock C27G G43C C27G, G43C
No Adenine, Rescue Factor = -0.750
P2 Lock U28G G42C U28G, G42C
20 40 60 80 100 120 140
Sequence Position

SI Figure S8

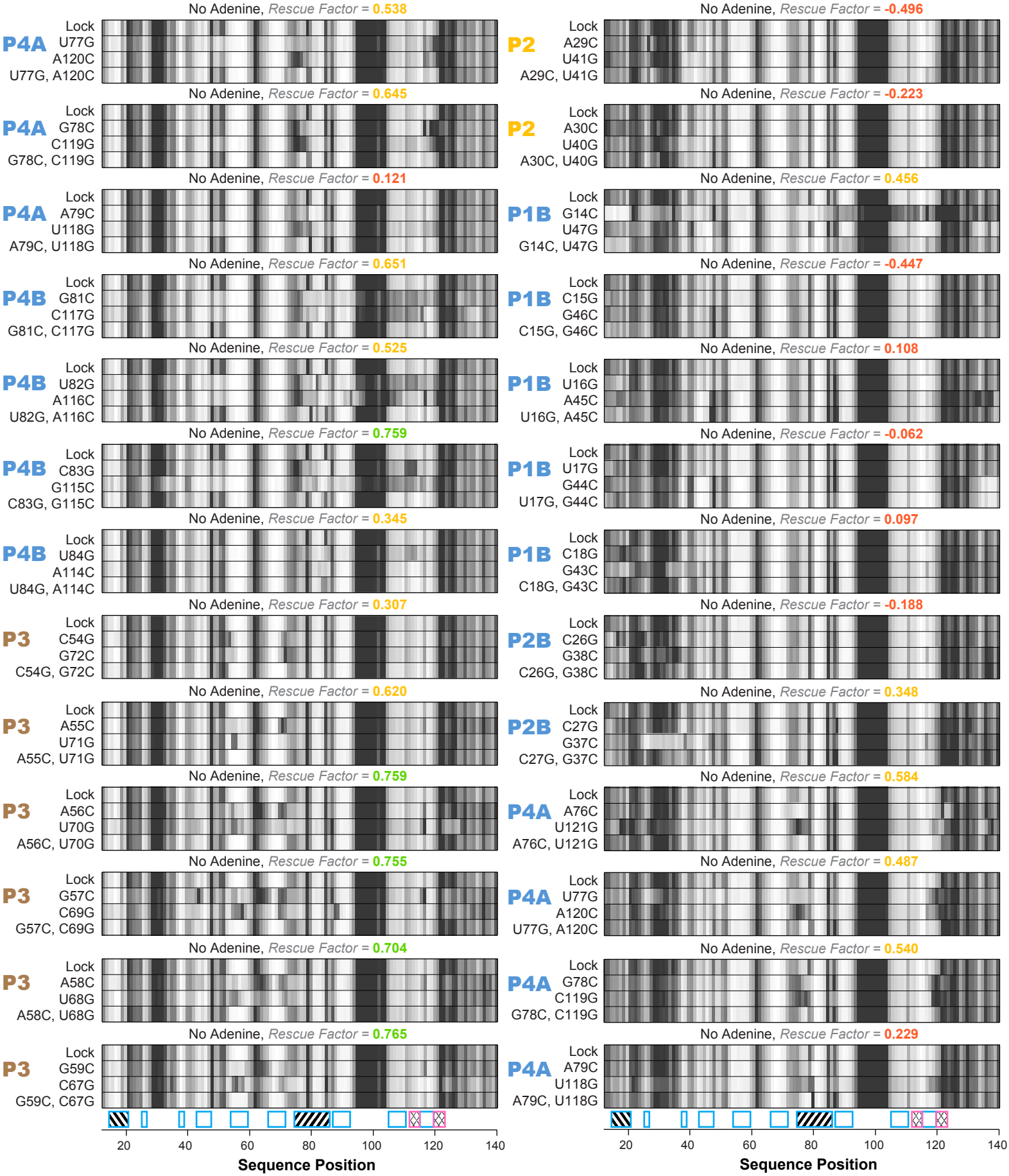
No Adenine, Rescue Factor = 0.538
P4A
Lock
U77G
A120C
U77G, A120C
No Adenine, Rescue Factor = 0.645
P4A
Lock
G78C
C119G
G78C, C119G
No Adenine, Rescue Factor = 0.121
P4A
Lock
A79C
U118G
A79C, U118G
No Adenine, Rescue Factor = 0.651
P4B
Lock
G81C
C117G
G81C, C117G
No Adenine, Rescue Factor = 0.525
P4B
Lock
U82G
A116C
U82G, A116C
No Adenine, Rescue Factor = 0.759
P4B
Lock
C83G
G115C
C83G, G115C
No Adenine, Rescue Factor = 0.345
P4B
Lock
U84G
A114C
U84G, A114C
No Adenine, Rescue Factor = 0.307
P3
Lock
C54G
G72C
C54G, G72C
No Adenine, Rescue Factor = 0.620
P3
Lock
A55C
U71G
A55C, U71G
No Adenine, Rescue Factor = 0.759
P3
Lock
A56C
U70G
A56C, U70G
No Adenine, Rescue Factor = 0.755
P3
Lock
G57C
C69G
G57C, C69G
No Adenine, Rescue Factor = 0.704
P3
Lock
A58C
U68G
A58C, U68G
No Adenine, Rescue Factor = 0.765
P3
Lock
G59C
C67G
G59C, C67G
20
40
60
80
100
120
140
Sequence Position
No Adenine, Rescue Factor = -0.496
P2
Lock
A29C
U41G
A29C, U41G
No Adenine, Rescue Factor = -0.223
P2
Lock
A30C
U40G
A30C, U40G
No Adenine, Rescue Factor = 0.456
P1B
Lock
G14C
U47G
G14C, U47G
No Adenine, Rescue Factor = -0.447
P1B
Lock
C15G
G46C
C15G, G46C
No Adenine, Rescue Factor = 0.108
P1B
Lock
U16G
A45C
U16G, A45C
No Adenine, Rescue Factor = -0.062
P1B
Lock
U17G
G44C
U17G, G44C
No Adenine, Rescue Factor = 0.097
P1B
Lock
C18G
G43C
C18G, G43C
No Adenine, Rescue Factor = -0.188
P2B
Lock
C26G
G38C
C26G, G38C
No Adenine, Rescue Factor = 0.348
P2B
Lock
C27G
G37C
C27G, G37C
No Adenine, Rescue Factor = 0.584
P4A
Lock
A76C
U121G
A76C, U121G
No Adenine, Rescue Factor = 0.487
P4A
Lock
U77G
A120C
U77G, A120C
No Adenine, Rescue Factor = 0.540
P4A
Lock
G78C
C119G
G78C, C119G
No Adenine, Rescue Factor = 0.229
P4A
Lock
A79C
U118G
A79C, U118G
20
40
60
80
100
120
140
Sequence Position

SI Figure S8

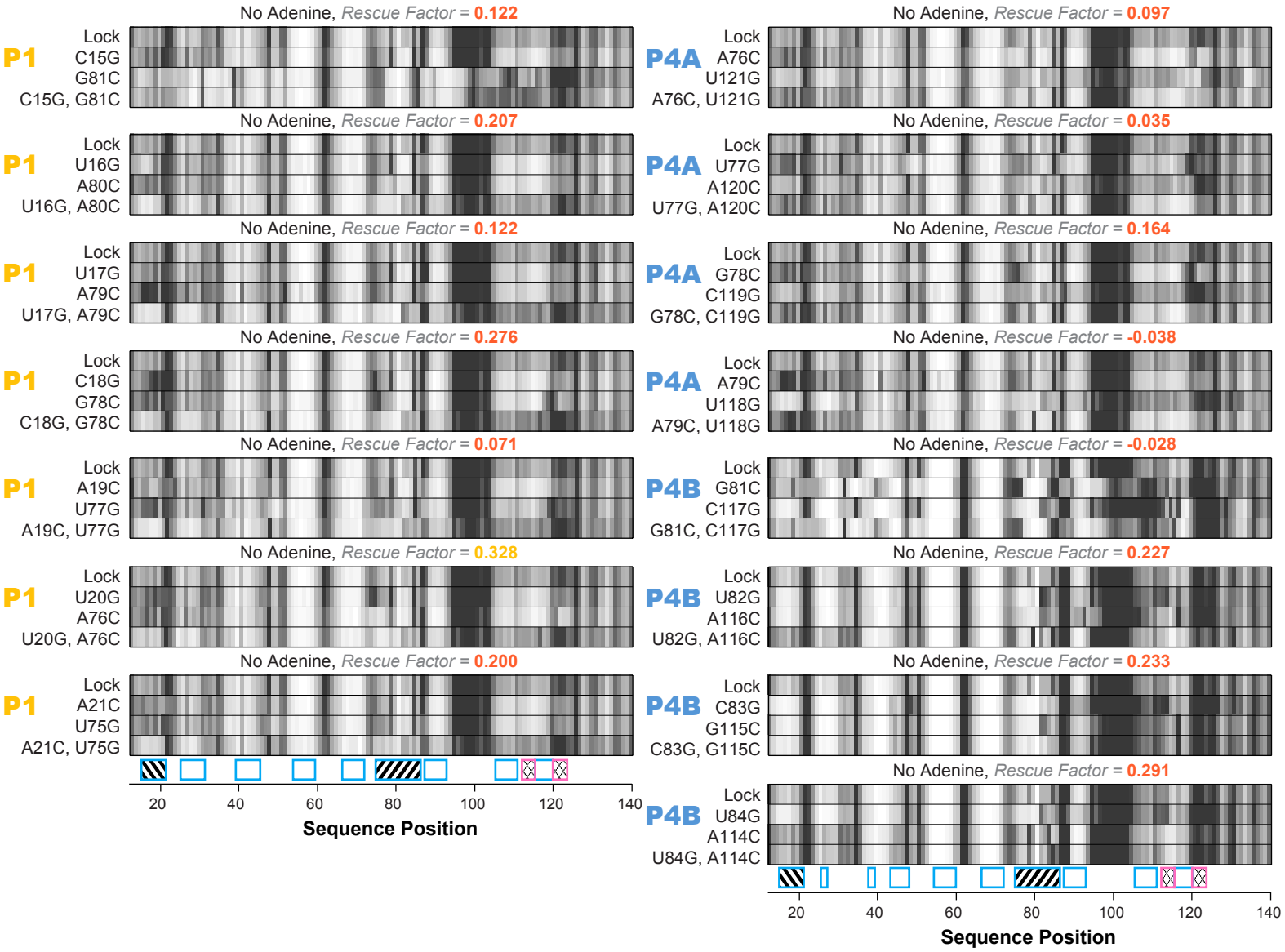
No Adenine, Rescue Factor = 0.122
P1
Lock
C15G
G81C
C15G, G81C
No Adenine, Rescue Factor = 0.207
P1
Lock
U16G
A80C
U16G, A80C
No Adenine, Rescue Factor = 0.122
P1
Lock
U17G
A79C
U17G, A79C
No Adenine, Rescue Factor = 0.276
P1
Lock
C18G
G78C
C18G, G78C
No Adenine, Rescue Factor = 0.071
P1
Lock
A19C
U77G
A19C, U77G
No Adenine, Rescue Factor = 0.328
P1
Lock
U20G
A76C
U20G, A76C
No Adenine, Rescue Factor = 0.200
P1
Lock
A21C
U75G
A21C, U75G
20
40
60
80
100
120
140
Sequence Position
No Adenine, Rescue Factor = 0.097
P4A
Lock
A76C
U121G
A76C, U121G
No Adenine, Rescue Factor = 0.035
P4A
Lock
U77G
A120C
U77G, A120C
No Adenine, Rescue Factor = 0.164
P4A
Lock
G78C
C119G
G78C, C119G
No Adenine, Rescue Factor = -0.038
P4A
Lock
A79C
U118G
A79C, U118G
No Adenine, Rescue Factor = -0.028
P4B
Lock
G81C
C117G
G81C, C117G
No Adenine, Rescue Factor = 0.227
P4B
Lock
U82G
A116C
U82G, A116C
No Adenine, Rescue Factor = 0.233
P4B
Lock
C83G
G115C
C83G, G115C
No Adenine, Rescue Factor = 0.291
P4B
Lock
U84G
A114C
U84G, A114C
20
40
60
80
100
120
140
Sequence Position

SI Figure S9

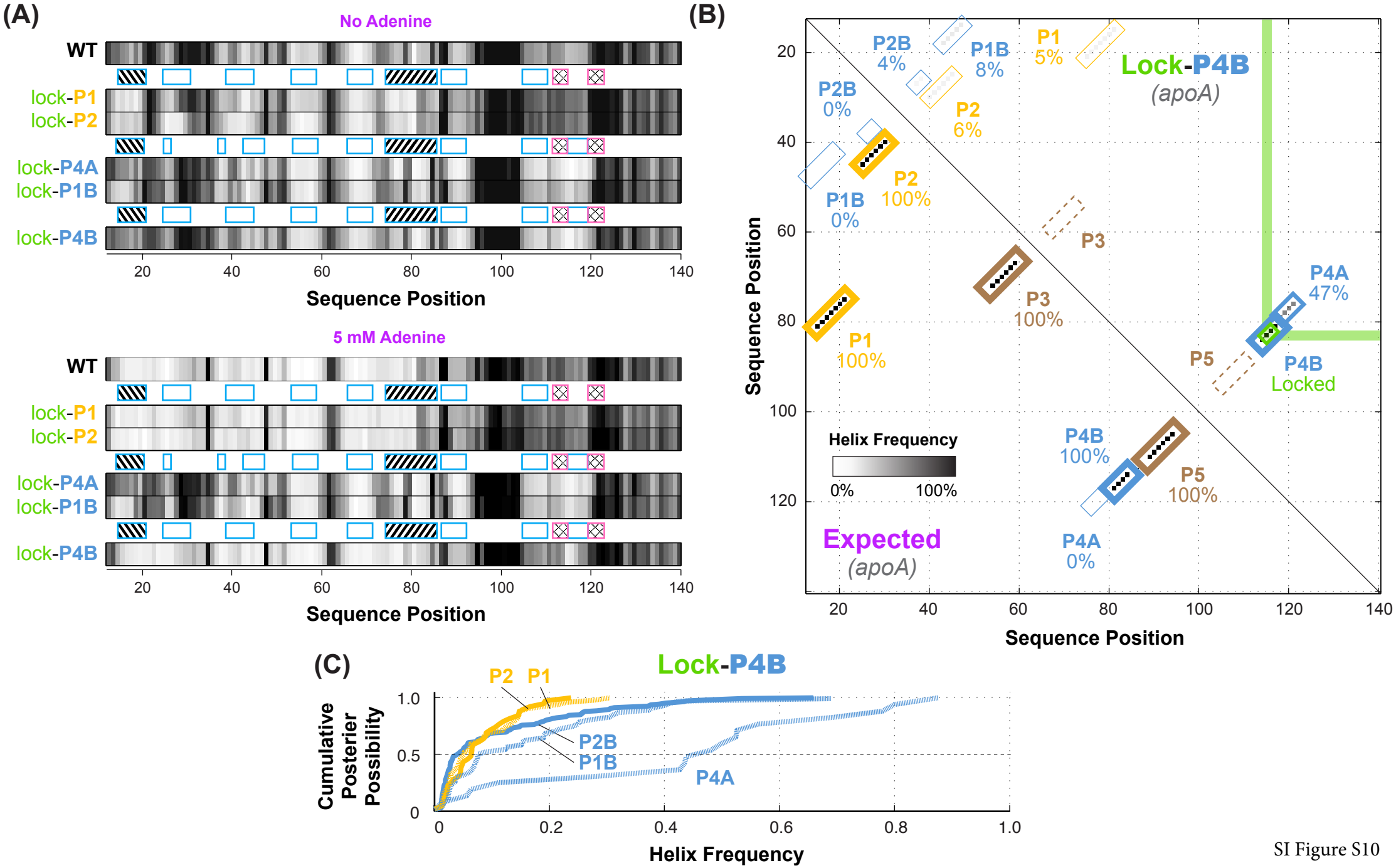

SI Figure S10

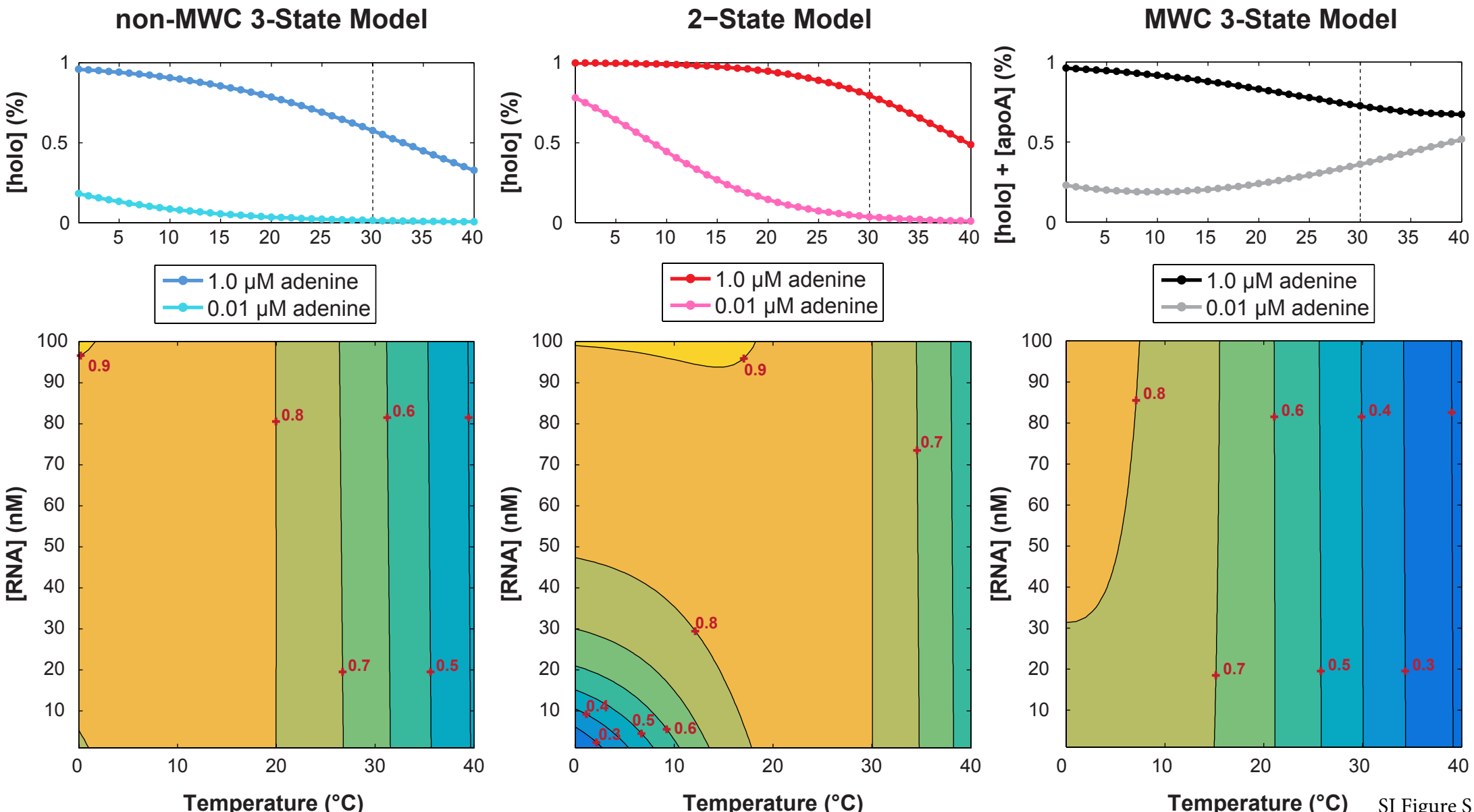

SI Figure S11

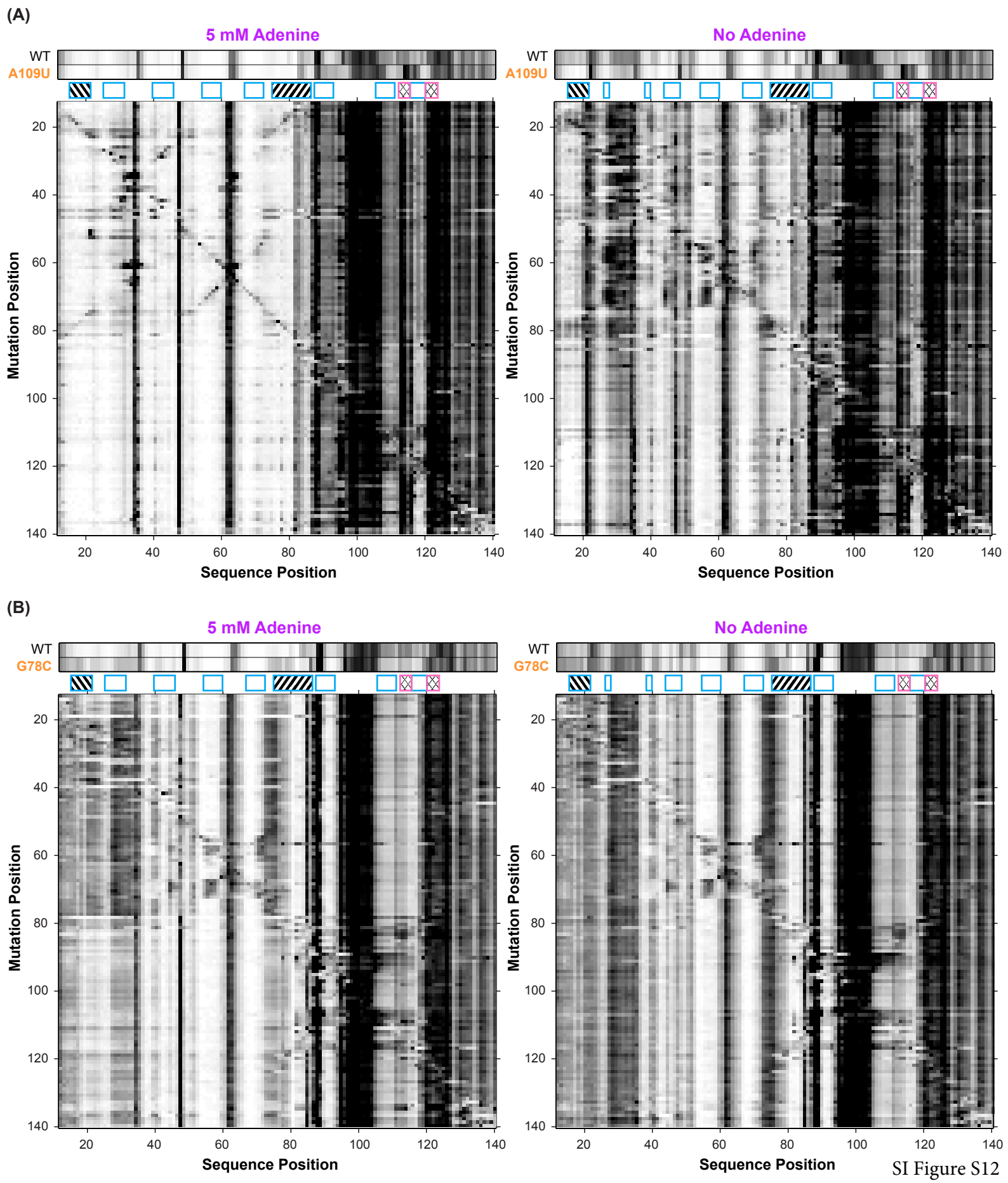

SI Figure S12

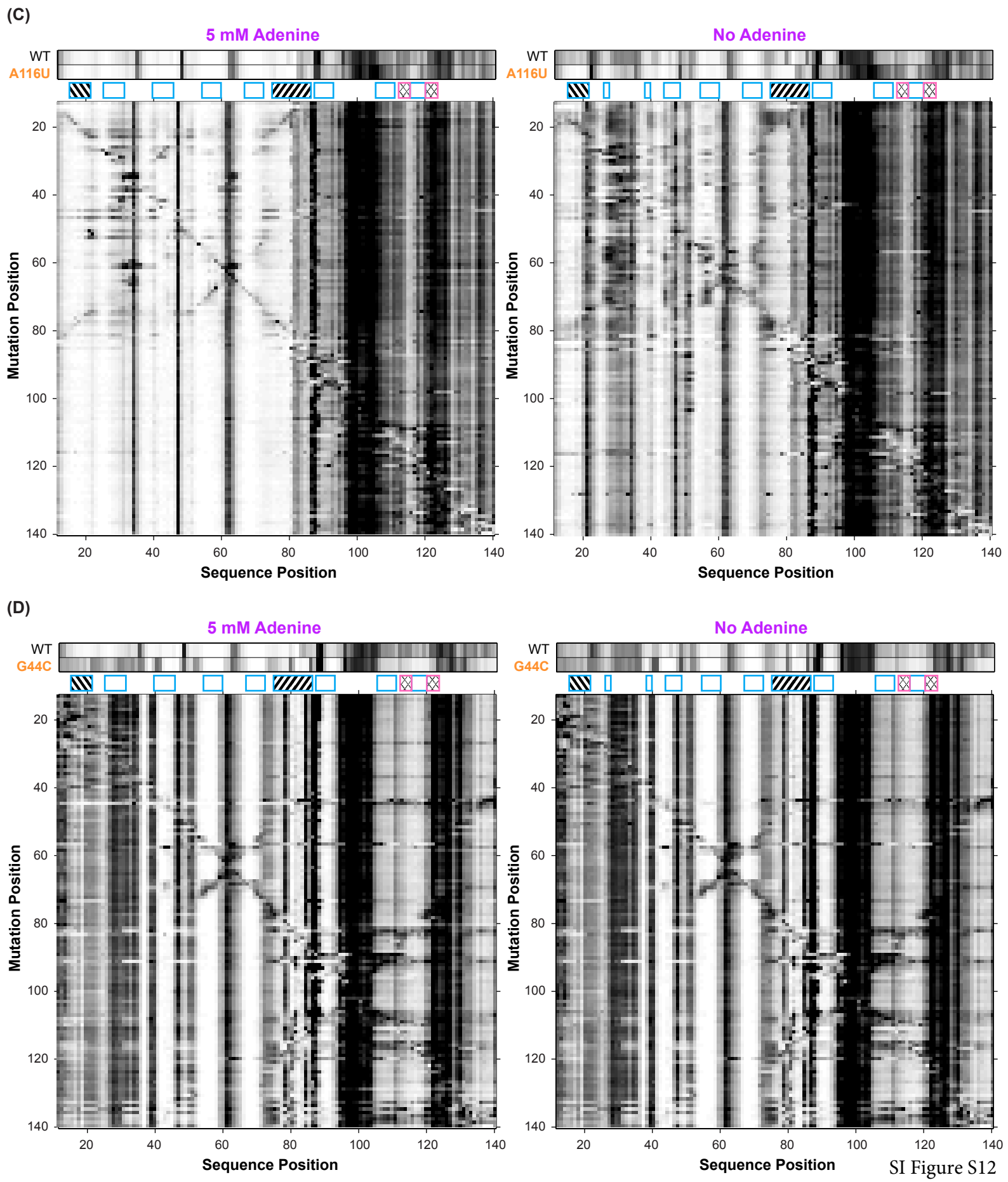

SI Figure S12

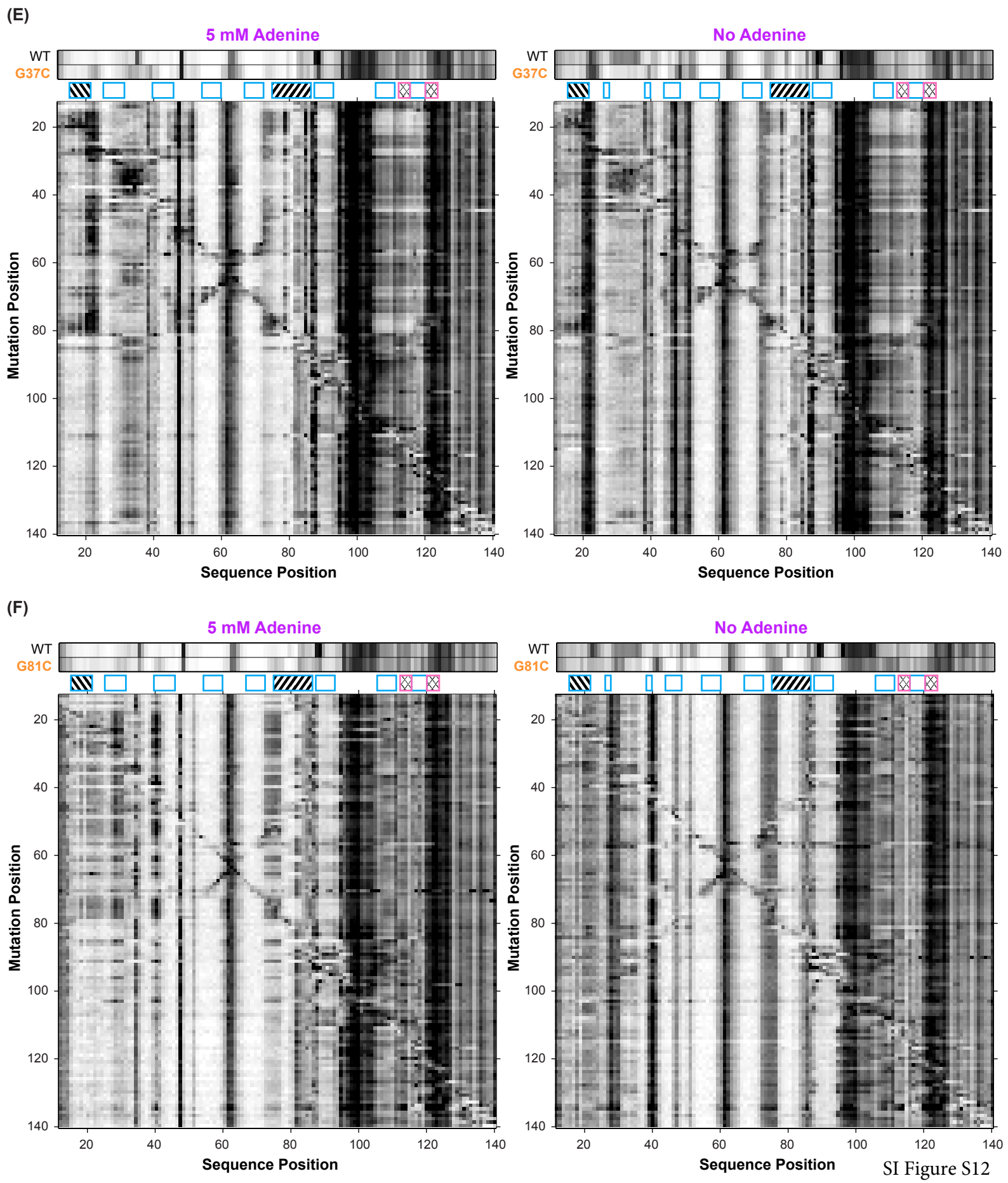

SI Figure S12

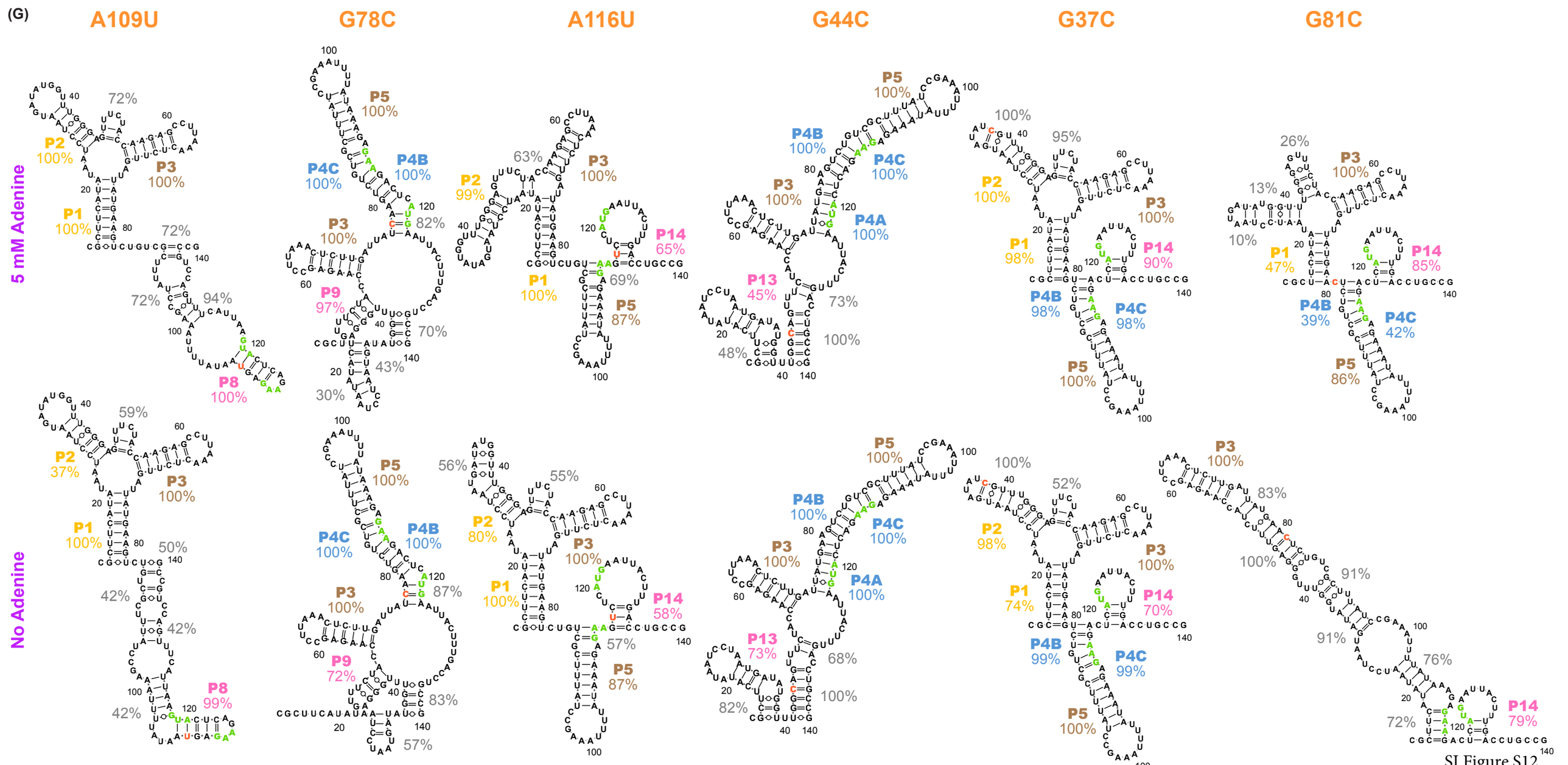

SI Figure S12

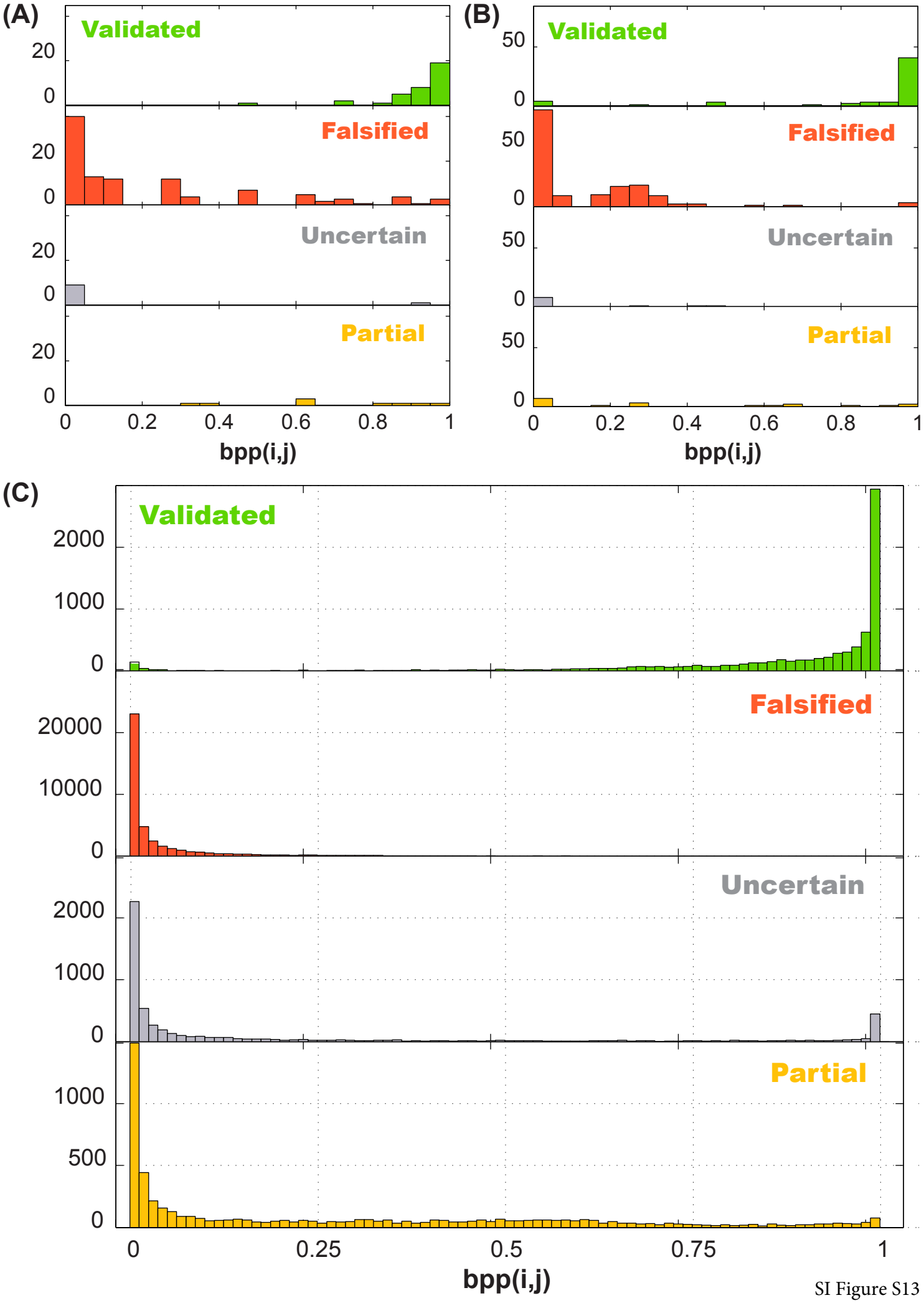

SI Figure S13

(A) M²R Single Base-Pair

	Manual Score	Auto Score
P1	? ? + + ✗ ✗ ✗	✗ + + ✗ ✗ ✓ ✗
P2	? ? ? + ✗ ✗	+ ✗ ✗ ✗ ✗ ✗
P3	+ ✓ ✓ ✓ ✓ +	+ ✓ ✓ ✓ ✓ +
P5	? + + + + +	+ + + + ✓ +
P1B	+ ✗ ✗ ✗ ✗	+ ✗ ✓ ✗ ✗
P2B	+ +	+ ✗
P4A	✓ ✓ ✓ ?	+ + + +
P4B	+ + + ✗	+ + ✓ ✗
P4C	✓ ✓	+ +
P6	? ? ? ✗ ✗ ✗	✗ ✗ ? ✗ ✗ ✗
P8	✗ ✗ ✗ ✗	✗ ✗ ✗ ✗
P9	✗ ✓ ✗ ✗ ✗	✗ + ✗ ✗ ✗
P10	✗ ✗ ?	✗ ✗ ✗
P11	✗ ✗ ? ? ? ✗ ✗ ✓ ✗	✗ ✗ ✗ ✗ ✗ ✗ ✗ ✗ ✗
P12	✗ ✗ ?	✗ + ✗
P13	? + ✗ ✗	? + ✗ ✗
P14	✗ ✗ ✗	✗ ✗ ✗
P15	✗ ✗ ✗ ✗ ✗ ✗ ✗	✗ ✗ ✗ ✗ ✗ ✗ ✗
P16	? ✗ + + +	✗ ✗ ✗ ✗ ✗
P17	+ ✗ ✗ ✗	✗ ✗ ✗ ✗

(B) M²R Double Base-Pair

	Manual Score	Auto Score
P1	✗ ✗ ✗ ✗ ✗ ✗	✗ ✗ ✗ ✗ ✗ ✗
P2	? ✗ ✗ ✗ ✗	✗ ✗ ✗ ✗ ✗
P3	✓ + ✓ ✓ ✓	+ ✗ ✓ + +
P5	+ + + + +	+ + ✗ + ✗
P1B	? ✗ ✗ +	✗ ✗ ✗ ✗
P2B	+	✗
P4A	✗ + +	✗ ✗ +
P4B	+ + +	✗ + ✗
P4C	+	✗
P6	✗ ✗ ✗ ✗ ✗	✗ ✗ ✗ ✗ ✗
P13	✗ ✗ ✗	✗ ✗ ✗

(C) LM²R

	Manual Score	Auto Score
Lock-P1		
P2	+ ✗ ✓ + + +	✗ ✗ + ✗ ✗ ✗
P4B	✗ ✗ ✗ ?	✗ ✗ ✗ ✗
Lock-P2		
P1	✗ ✓ ✓ ✓ ✓ ✓ ✓	✗ ✓ ✓ ✓ + ✓ +
P4A	✗ ✗ ✗ ✗	✗ ✗ ✗ ✗
P4B	✗ ✗ ✗ ?	✗ ✗ ✗ ✗
Lock-P4A		
P1B	✗ ? ✗ ✗ +	? ✗ ✗ ✗ ✗
P2B	? +	✗ +
P2	✗ ✗ ✗ ✗ ✗ ✗	✗ ✗ ✗ ✗ ? ?
P4B	+ + ✓ ?	+ + + +
P6	✗ ✗ ✗ ✗ ✗ ✗	✗ ✗ ✗ ? ? ?
P13	✗ ✗ ✗ ✗	? ✗ ✗ ?
Lock-P1B		
P2B	✓ ✓	+ ✗
P4A	✓ ✓ ✓ ✓	+ + ✓ ✗
P4B	✓ ✓ ✓ ?	✓ + ✓ ?
P3	✓ ✓ ✓ ✓ ✓ ✓	✗ ✓ ✓ ✓ ✓ ✓
Lock-P4B		
P1B	✓ ✓ ✗ ✗ ✗	+ ? ✗ ✗ ✗
P2B	✗ +	✗ +
P1	? ? ? ✗ ✗ ✗ ✗	✗ ? ? ✗ ✗ ✗ ?
P2	✗ ✗ ✗ ✗ ✗ ✗	✗ ✗ ✗ ? ? ?
P4A	? + ✓ ✓	+ + + ✗
Mut-P2		
P1	✗ + + + + + +	✗ ✗ ✗ ✗ ✗ + ✗
P4A	✗ ✗ ✗ ✗	✗ ✗ ✗ ✗
P4B	✗ + ✗ +	✗ ✗ ✗ ✗

Legend: ✓ Validated ✗ Falsified ? Uncertain + Partial

SI Figure S14